Studies of retinoid X receptors (Rxr) and the Rxr-signaling pathway in Atlantic cod (*Gadus morhua*) using immunochemical and *ex vivo* approaches

Emily Marie Christiansen

This thesis is submitted as a partial fulfillment for the requirements for the degree of Master of Science in molecular biology.

Department of Biological Sciences (BIO), the University of Bergen.

Thesis undertaken at the Environmental Toxicology Research Group.

Main advisor: Odd André Karlsen

Co-advisor: Anders Goksøyr

September 2023

TABLE of CONTENTS

ACKNOWLEDGEMENTS

This master thesis has been linked to the iCod 2.0 (project no. 244564) and dCod 1.0 (project no. 248840) projects, funded by the Research Council of Norway.

First and foremost, I would like to extend my gratitude towards my advisors Odd André Karlsen and Anders Goksøyr who have provided me with valuable feedback throughout this thesis. Thank you for letting me join the group meetings long before I even started my master thesis, to get a feeling of the working environment. I also truly appreciate how available you have always been throughout the work with this thesis. Thank you to Odd André for the effort and care you have spent on this thesis, and thank you Anders, for giving valuable input during the writing process.

Next, I would also like to thank Rhîan Gaenor Jacobsen for passing on your skills in the laboratory. Because of you, I feel quite confident in many of the techniques employed in this thesis. Thank you also for discussions around the experimental procedure and my results, kind guidance, humor, and particularly, for reminding me that this thesis is a marathon, not a sprint.

I would also like to thank Fekadu Yadetie for always being available in your office to answer questions regarding different procedures, and statistical tools. As well as for enduring the long hours into the night when preparing liver cultures from Atlantic cod.

I would also express my gratitude towards the environmental toxicology group and fellow master students at both the biology program and the molecular biology program. You have all made this a very pleasant time.

Lastly, I would like to send a special thank you to my family and friends for encouraging me in the process. Your contributions, both big and small, have helped me tremendously.

LIST OF ABBREVIATIONS

2D-PAGE	Two-dimensional polyacrylamide gel electrophoresis
9cDHRA	9-cis-13,14-dihydroretinoic acid
9-cis-RA	9-cis-retinoic acid
aa	amino acid
AF	Activation factor
APS	ammonium persulphate
BSA	Bovine serum albumin
CEC	Chemical of emerging concern
ChIP-seq	Chromatin immunoprecipitation-sequencing
csFBS	charcoal-stripped fetal bovine serum
DBD	DNA binding domain
DDT	Dithiothreitol
DEG	Differentially expressed gene
DHA	docosahexaenoic acid
DMSO	dimethylsulfoxide
d.w.	dry weight
ebp	3-beta-hydroxysteroid-delta(8), delta(7)-isomerase
EDCs	Endocrine disrupting chemicals
EDTA	Ethylenediaminetetraacetic acid tetrasodium salt dihydrate
ER	Estrogen receptor
FXR	Farnesoid X receptor
gmRxra/b/g	*Gadus morhua* Retinoid X receptor alpha/beta/gamma
HRE	Hormone responsive elements
IAA	Iodoacetamide
ILAB	Industrial and aquatic laboratory
IP	Immunoprecipitation
LBD	Ligand binding domain
LDH	Lactate dehydrogenase
LXR	Liver X receptor

MeOH	Methanol
MTT	3-(4,5-Dimethylthiazol-2-yl)-2,5-diphenyltetrazolium bromide
MS	Mass spectrometry
MW	Molecular weight
NR	Nuclear receptor
NTD	N-terminal domain
OTC	Organotin compound
O/N	Over night
PA	polyacrylamide
PBS	Phosphate buffered saline
PCLS	precision-cut liver slices
pI	Isoelectric point
POP	Persistent organic pollutant
PPAR –	Peroxisome proliferator-activated receptor
PTM	Post translational modification
PVC	Polyvinyl chloride
PXR	Pregnane X receptor
qPCR	quantitative polymerase chain reaction
RAR	Retinoic acid receptor
Rbp2	retinol binding protein 2
RT	Room temperature
RXR/Rxr	Retinoid X receptor
SB	Sample buffer
SDS	Sodium dodecyl sulphate
SDS-PAGE	SDS polyacrylamide gel electrophoresis
Sqlea	squalene epoxidase
SR	Steroid receptor
TB	Tissue bank
TBT	Tributyltin chloride
TEMED	N, N, N', N', Tetramethyl-ethylenediamine

TF	Transcription factor
TG buffer:	Tris glycine buffer
WB	Western blot

ABSTRACT

Nuclear receptors (NRs) comprise a large superfamily of ligand-activated transcription factors. Many NRs facilitate gene expression through heterodimeric binding to retinoid X receptor (RXR). RXR is thus part of a vast array of signaling pathways. Pollutants from anthropogenic origin are a concern as many have been found to cause endocrine disruption by acting as exogenous ligands for NRs. Organotin compounds, in particular, tributyltin (TBT) has been found to cause endocrine disruption through binding to RXR. TBT exposure remains a concern in aquatic environments due to its long half-life in sediments, giving rise to hotspots in areas of former high use such as shipyards and marinas. Atlantic cod (*Gadus morhua*) has become an important bioindicator species, however, only recently have we begun to unravel the properties of Rxr in Atlantic cod. Previously, our research group has established that there are four subtypes of Rxr in Atlantic cod, Rxra, Rxrb1, Rxrb2 and Rxrg. The focus of this thesis was to study signaling pathways governed by Rxr that may be affected by TBT exposure of Atlantic cod liver. To do so, the binding properties of custom-made antibodies, designed against a peptide sequence of gmRxra, were characterized, to determine if these antibodies could be used in downstream analysis with immunoassays, such as chromatin immunoprecipitation (ChIP). Importantly, the antibodies were found to bind Rxrb1 in liver tissues by using two-dimensional polyacrylamide gel electrophoresis in combination with immunoblotting and mass spectrometry analysis. The molecular weight (MW) of the immunoreacting band/spot identified as Rxrb1 was estimated to be 35 kDa, which is lower than its theoretical MW close to 50 kDa. This could be due to a truncation of Rxrb1 in Atlantic cod. Also, the antibodies were found to bind the Rxrb1 while denatured, but they were not able to capture this protein under the standard non-denaturing immunoprecipitation (IP) technique used in this thesis. A hydropathy plot and structural analyses revealed that there were antigenic sites on the immunogen, which would likely be exposed in the protein under native conditions. I have thus speculated that the antibodies could work if optimizing the IP technique. Precision cut liver slices and gene expression analyses were used to study modulation of Rxr signaling pathways *ex vivo* upon exposure of TBT and the endogenous Rxr ligand, 9-cis-retinoic acid (9-cis-RA). Among the genes assessed (*pparg* involved in adipogenesis, *rbp2* involved in retinol metabolism and *ebp* and *sqlea* involved in steroid biosynthesis), only *pparg* was differentially expressed after 9-cis-RA exposure and all genes were differentially expressed after TBT exposure. Overall, this thesis has given insight into the role of Rxr in Atlantic cod liver in response to TBT.

1 INTRODUCTION

1.1 Environmental Pollutants

With an increase in population sizes and growing industrialization globally, the release of chemicals has increased at an alarming rate (Rathi et al., 2021). Many compounds affect environmental processes negatively, either by occurring in excess of natural levels, hence disrupting the nature's equilibrium, or because they exert toxic effects (Rathi et al., 2021; Suzuki et al., 2020). Such compounds are commonly termed environmental pollutants. These compounds are either organic or inorganic and derive from several anthropogenic sources, including pharmaceuticals, cosmetics, antibiotics, plastics, pesticides, fire retardants, and personal care products (Rasheed et al., 2019). They originate from manufacturing plants, e.g. industrial smoke, facilities such as hospitals, agriculture, and households (Rasheed et al., 2019). Specific examples of environmental pollutants include metals, such as cadmium and mercury, polycyclic aromatic hydrocarbons (PAHs), polychlorinated biphenyls (PCBs), and polychlorinated dioxins, and dibenzofurans (PCDDs/PCDFs) (Rasheed et al., 2019; Scott & Sloman, 2004; Suzuki et al., 2020).

1.2 Persistent organic pollutants

Some chemicals are prone to persist for a longer time in the environment because they resist both biotic and abiotic degradation (Beyer et al., 2000). Such substances are commonly referred to as persistent organic pollutants (POPs) (Alharbi et al., 2018). POPs typically have lipophilic characteristics and can move into lipid phases and bioaccumulate in organisms (Alharbi et al., 2018; Chormare & Kumar, 2022). The concentrations of POPs generally increase in organisms found at higher trophic levels due to biomagnification (Windsor et al., 2020). However, several factors influence the accumulation of POPs in the food web, such as the physicochemical properties of the pollutant, its source, the environment, the diet of the organisms, and the food web in question (Borgå et al., 2004; Kelly et al., 2007). Due to their resistance towards degradation POPs can travel long distances with wind and water currents, and thus ending up in remote areas such as the Arctic (Fernández-Llamazares et al., 2020; Rasheed et al., 2019).

POPs can exert toxic effects on both humans and biota. Examples of health risks linked to exposure of POPs in humans include cancer, cardiovascular diseases, obesity, reproduction issues, and endocrine disruption (Alharbi et al., 2018). In wildlife, the effects are commonly

linked to infertility, sex ratio shifts, and cancer, potentially causing ecological disruption (Alharbi et al., 2018). Due to concerns regarding the adverse effects of POPs, national and international efforts have been implemented to identify POPs, as well as to provide restrictions and regulations on their production and use (Beyer et al., 2000). The United Nations Environmental Programme (UNEP) promoted the Stockholm Convention in 2001, which was ratified in 2004. In this convention, 12 environmental contaminants were initially classified as POPs, referred to as "the dirty dozen" (Stockholm Convention, 2019). Several other POPs have been added to the Stockholm Convention at a later stage (StockholmConvention, 2019). More pollutants may be annexed in the convention since new chemicals are constantly synthesized and the effects of them are yet to be learned. Such chemicals are often termed emerging contaminants, or chemicals of emerging concern (CECs), since their behavior, fate, and toxicological impacts are currently poorly understood (Hutchinson et al., 2013).

1.3. Endocrine Disruptors

Several physiological processes in the body, such as growth, maturation, development, and reproduction, are controlled by the endocrine system via the excretion of hormones from different glands, such as the pituitary gland, adrenal gland, and pancreas, as well as the reproductive organs (Alharbi et al., 2018). The hormones act as signals and dock to receptors on the surface or inside target cells, which initiates a cascade of biochemical processes that alter the action or activity of the cell (Hiller-Sturmhöfel & Bartke, 1998). Many POPs, but also other pollutants, function as endocrine disruptors (Alharbi et al., 2018). They do so by mimicking, blocking, or altering the actions of endogenous hormones (Gore et al., 2015). This can result in adverse reproductive, neurological, developmental, and immunological effects in humans and wildlife (Fischer and Engster, 2014; Gomes et al. 2018). Examples of endocrine related diseases in humans include obesity, type 2 diabetes, cardiovascular diseases, and certain types of cancers (Gore et al., 2015; Grün & Blumberg, 2009).

1.4 Organotin Compounds (OTCs)

Organotin compounds (OTCs) are chemicals in which several hydrocarbon chains form bonds to a central tin (Sn) atom (Martínez et al., 2020). Typically, the chemicals are represented by the formula R_nSnX_{4-n}, where R is a carbon-bonded organic group, X an inorganic substituent, and n ranges from 1 to 4 (Omae, 2003). Over 800 different OTCs have been produced (Hoch,

2001). Production of OTCs increased with the development of the plastic industry in the 1940s, as they were often used in combination with poly(vinyl)chloride (PVC) to prevent its degradation from UV radiation and heat (Hoch, 2001; Omae, 2003). Biocidal properties of trisubstituted OTCs were discovered in the 1950s and the applications of these compounds spiraled to several other areas, such as fungicides, rodent repellents, wood preservatives, and antifouling paints (Hoch, 2001; Suzuki et al., 2020).

OTCs were thought to be safe to use as antifouling paints. Firstly, because the toxicity of OTCs appeared to be dependent on the length of carbon chains, demonstrating reduced toxicity in insects and mammals with increasing alkyl length, while the opposite was observed in fungi and bacteria where the toxicity decreased with increasing numbers of alkyl length (Omae, 2003). Secondly, due to the fact that OTCs were degraded by bacteria and easily cleaved by UV radiation in direct sunlight (Omae, 2003). Lastly, because the half-life of OTCs in water, under experimental conditions, spanned only a few days (Hoch, 2001; Omae, 2003). Therefore, the leaching of OTCs into the water from antifouling paints was not a matter of concern at the time (Omae, 2003). Later it has been discovered that OTCs have lipophilic characteristics, demonstrating similar accumulation properties as many POPs (Hoch, 2001; Suzuki et al., 2020). In water, OTCs typically last between six days and a few months. In sediments, however, the half-life ranges from 1 to 9 years (Omae, 2003). This makes them readily available for filter feeders such as zooplankton and bivalves, grazing invertebrates (e.g., gastropods), and fish (Antizar-Ladislao, 2008; Borghi & Porte, 2002). OTCs have demonstrated their ability to bioaccumulate, and their toxic effects have also been linked to their role as EDCs (Mortensen & Arukwe, 2007).

1.5 Tributyltin chloride (TBT)

One of the most widely used and toxic OTCs is tributyltin (TBT) (Figure 1). Following the discovery in 1954 by van der Kerk and Luitjen, TBT became the main ingredient in antifouling paint on boats and ships, and became the primary source of trivalent OTCs generated from antifouling paints (Beyer et al., 2022; Lyssimachou et al., 2015). In the 1970's, so-called "imposex" traits was first discovered in the oyster drill (*Ocenebra* erinacea) in Arachon Bay, France (Ruiz et al., 1996). Imposex was soon also discovered in the neogastropods dogwhelk (*Nucella lapillus*) in Great Britain and the American mud snail (*Nassarius obsoletus say*) in the early 1970s (Blaber, 1970; Smith, 1971). In these snails, male sexual tissues/organs grew

superimposed over the female ones (Beyer et al., 2022). Abnormalities in shell development in mollusks such as the oyster *Crassostrea gigas* were also observed (Alzieu et al., 1986; Waldock & Thain, 1983). In the most extreme cases, the changes in snails and oysters made them unable to reproduce, consequently placing the populations at risk (Alzieu et al., 1986; Langston et al., 2015). For this reason, legislations were enacted nationally and internationally, which banned the use of antifouling paints containing OTCs on boats and ships. With the ban on TBT in antifouling paints, an increase in mollusk populations, such as that of *N. lapillus,* has increased along the coast of Norway and other European nations (Schøyen et al., 2019). However, the half-life of TBT in sediments and their continued use in some countries still cause them to be of concern, and TBT originating from both historical and recent sources are still present in the environment Beyer et al. (2022).

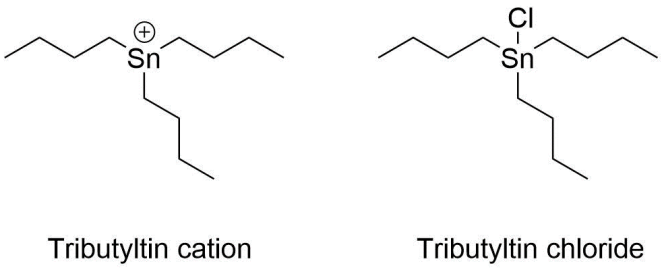

Figure 1. Structure of TBT cation from which many derivatives exist, as well as the TBT derivative used in this thesis. The structures were prepared using ChemDraw.

Chronic and acute poisonous effects of TBT are also observed in other aquatic animals such as zooplankton, algae, and certain fish species, particularly at early developmental stages (Hoch, 2001). In mammals, TBT is a known obesogen, shown in mice models (Shoucri et al., 2017) and in placentas from humans (Rantakokko et al., 2014). TBT-mediated lipid accumulation has also been observed in fish, for instance in zebrafish (*Danio rerio*) (Lyssimachou et al., 2015) and in Japanese medaka (*Oryzias* latipes) (Takai et al., 2020). Other abnormalities have also been recorded in fish after TBT exposure, such as spine deformation in juvenile Japanese medaka (K. Chen et al., 2021).

1.5.1 TBT Hotspots

Due to the half-life of TBT spanning decades in some anerobic environments, so-called hot spots have developed where the concentration of TBT in the sediments is still relatively high (Beyer et al., 2022; Sousa et al., 2014). TBT hotspots are found globally, and typically around marinas and fishing ports (Oliveira et al., 2020). In Norway, a maximum tolerable risk limit of 35 µg/kg dry weight (d.w.) in sediments has been set. However, TBT concentrations exceeding this limit have been detected in surficial sediments at 95 different locations along the Norwegian coast (Figure 2) (Beyer et al., 2022). In the top nine hot spot locations, the concentrations of TBT in the sediments are far higher than the set limit, with a mean concentration over 30 000 µg/kg d.w., and the highest concentration exceeding 100 000 µg/kg d.w., as reviewed by Beyer et al. (2022). TBT bound to sediments leak slowly back into the environment and is therefore a long-term secondary source of recontamination and raise concerns due to chronic exposure of marine organisms (Beyer et al., 2022; Sousa et al., 2014).

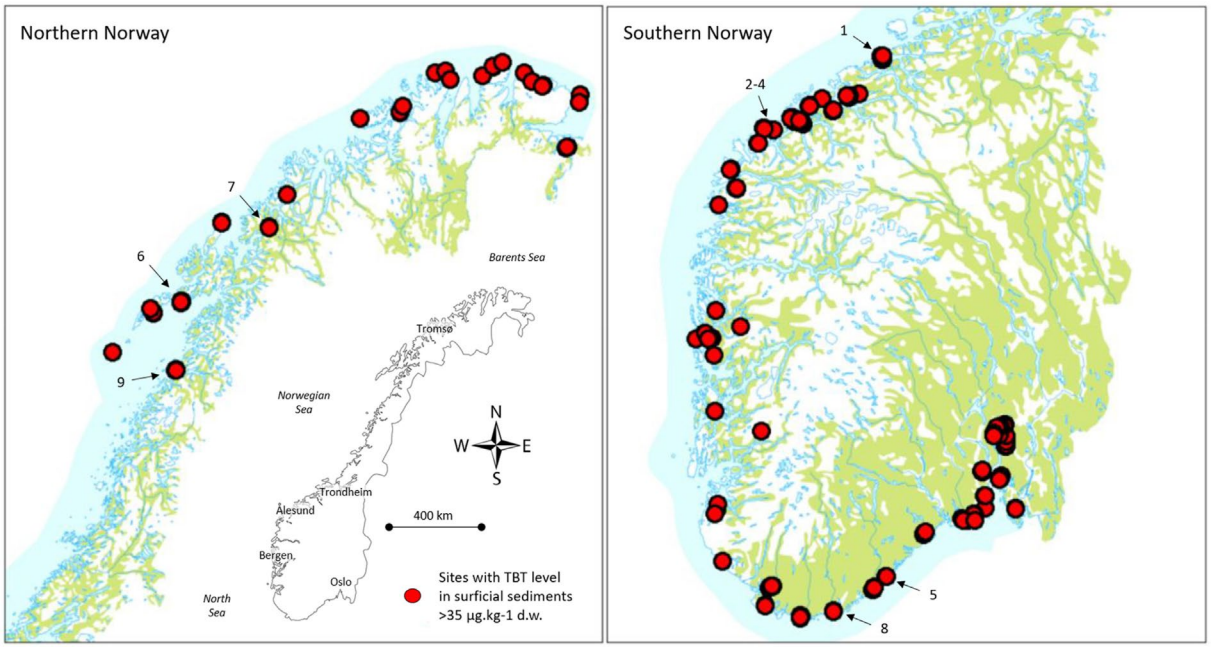

Figure 2. The geographical distribution of the 95 TBT hotspots along the Norwegian coastline. The hotspots (indicated with red dots) are in locations in which the TBT contents in superficial sediments exceed the maximum tolerance limit of 35 µg/kg dry weight (d.w.). The arrows and labels indicate the top 9 hot spots with a mean concentration exceeding 30 000 µg/kg d.w. The illustration was adapted from Beyer et al. (2022)

1.6 Nuclear Receptors

Nuclear receptors (NRs) are found in all organisms apart from fungi and plants (Frigo et al., 2021). In vertebrates, they comprise the largest family of transcription factors (Zhao et al., 2015). They regulate a vast array of cellular processes, including development, cell proliferation and metabolism, reproduction, and overall homeostasis (Sever & Glass, 2013; Zhao et al., 2015). The 48 NRs located in humans have been divided into seven subfamilies based on sequence similarity (Frigo et al., 2021). The number of NRs in different species vary (Zhao et al., 2015). Eide et al. compared the number of NRs in five toxicological model teleosts, including zebrafish (*Danio rerio*), medaka (*Oryzias latipes*), Atlantic killifish, Atlantic cod and stickleback (*Gasterosteus aculeatus*) (Eide et al., 2021). A summary of the classification of the different NRs can be seen in Figure 3, in which the NR0 group consists of atypical NRs, and the NR2 group comprises the largest subfamily (Weikum et al., 2018). Two additional subfamilies, NR7 and NR8. Have also been classified, which are not present in vertebrates (Beinsteiner et al., 2022; Huang et al., 2015).

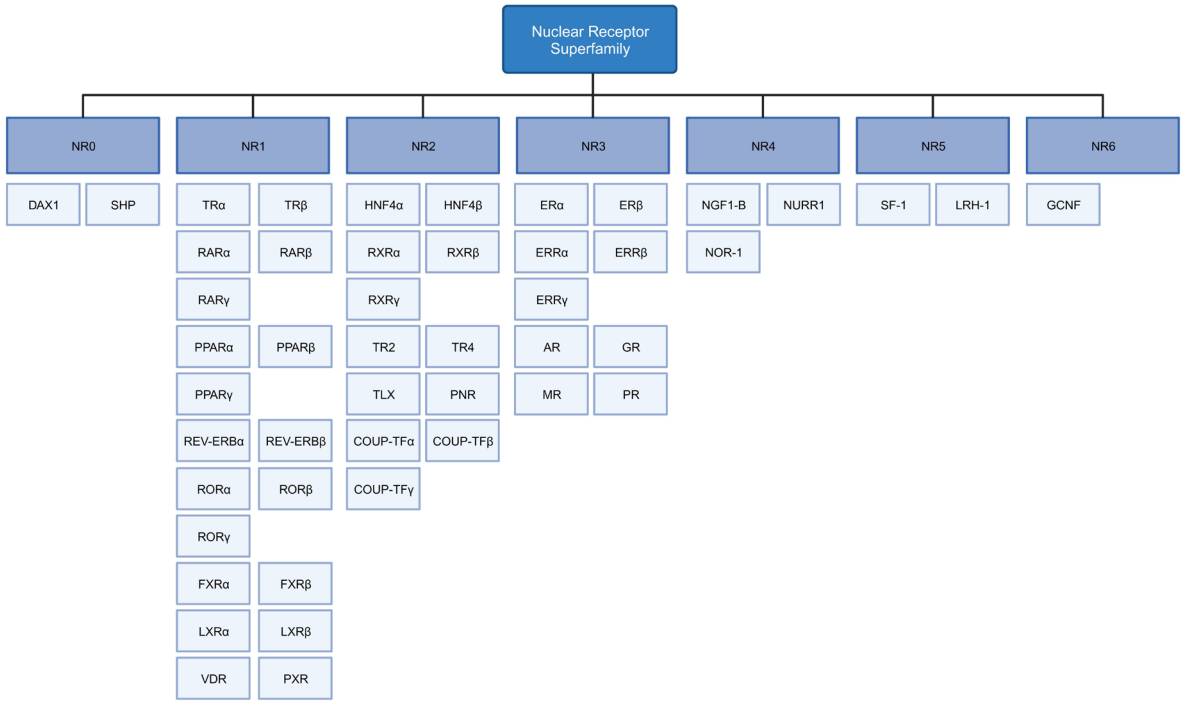

Figure 3. Schematic overview of the nuclear receptor (NR) superfamily. The classification of the 48 NRs observed in humans (*Homo* sapiens) are shown based on the list available from Weikum et al., 2018. The figure was created with BioRender.com.

All NRs share a common protein structure that is composed of a highly variable N-terminal domain (NTD), the highly conserved DNA binding domain (DBD), a hinge region, the ligand-binding domain (LBD), and the C-terminal domain (Figure 4) (Mukha et al., 2021; Weikum et

al., 2018). The DBD interacts directly with hormone responsive elements (HRE) in DNA sequences, facilitating the activation of gene transcription (Mukha et al., 2021; Sever & Glass, 2013), The LBD acts as the binding site for ligands and is crucial for ligand-mediated transcriptional activation of NRs by recruiting coregulators that activate or repress transcription of target genes (Jin & Li, 2010) Two regions, the activation factor-1 (AF-1) in the N-terminus and the activation factor-2 (AF-2) in the LBD, are also involved in transcriptional activation, in which AF1 is responsible for weak transcriptional activation when no ligand is present, and AF-2 is responsible for the ligand-dependent transcriptional activation (Mukha et al., 2021). The DBD also contains the sub-domain D-box responsible for dimerization to other NRs (Weikum et al., 2018). In some NRs there is also a C-terminal tail (Sever & Glass, 2013).

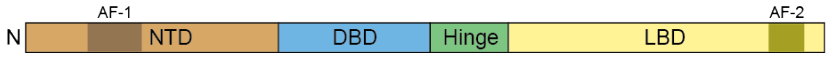

Figure 4 General structure of nuclear receptors (NRs). The domains, A/B, C, D and E are indicated in different colors. NTD is the N-terminal domain, DBD is the DNA-binding domain, LBD is the ligand binding domain, and AF-1 and AF-2 are activation factor 1 and 2, respectively.

NRs generally exist as monomers, homodimers or heterodimers (Sever & Glass, 2013). In broad terms, they are classified into two functional classes based on their mechanism of action (Khan & Okafor, 2022). Class I NRs form homodimers. Examples of this class of NRs include retinoid X receptor (RXR), as well as the steroid hormone receptors (SRs), such as the estrogen receptor (ER) (Beinsteiner et al., 2022). Class II receptors form heterodimers, usually with RXR (Beinsteiner et al., 2022; Khan & Okafor, 2022). Examples of NRs in this group includes the NR1 subfamily, for instance the retinoic acid receptor (RAR), peroxisome proliferator-activated receptor (PPAR), pregnane x receptor (PXR), and the liver X receptor (LXR) (Mangelsdorf & Evans, 1995; Toporova & Balaguer, 2020; Weikum et al., 2018). An additional class is sometimes defined with receptors that bind to DNA as monomers, although these are rare (Weikum et al., 2018). Common for most NRs is their activation or modulation through the binding of ligands, usually lipophilic molecules such as steroids (Weikum et al., 2018). Their ligands function as either agonists recruiting coactivators, or as antagonists recruiting corepressors, thus either eliciting or repressing expression of their target genes (Jin & Li, 2010). NRs are targeted unintentionally by exogenous compounds, which can cause a dysregulation of their transcriptional activity (Toporova & Balaguer, 2020). Thus, endocrine disruption can manifest in developmental, metabolic, or reproductive disorders and are of great concern, as discussed in section 1.3.

17 Retinoid X receptor

Retinoid X receptor (RXR) is a NR belonging to the NR2B subgroup of the NR superfamily (Weikum et al., 2018). RXRs are found in most metazoans apart from the demosponges (Bridgham et al., 2010). RXRs function as a co-transcription factor and heterodimerize with one third of the human NRs, such as PPAR, LXR, and PXR (Toporova & Balaguer, 2020). RXR has also been shown to function as a homodimer (Evans & Mangelsdorf, 2014). In most vertebrates, three subtypes of RXR exist, RXRalpha (RXRa), RXRbeta (RXRb) and RXRgamma (RXRg), which are encoded by three separate genes (Mangelsdorf et al., 1992; Tallafuss et al., 2006). Splice variants of RXRs have also been identified, with three variants present in humans (hRXR; b1, b2, b3) and two in mice (mRXR; g1, g2) (Mukha et al., 2021).

Binding of NRs to RXRs occurs in a permissive or non-permissive manner. Permissive heterodimers, such as those with farnesoid X receptor (FXR), LXR, PPARs, and PXR, can be activated by both their own agonist and an RXR-specific agonist, whereas non-permissive heterodimers, such as thyroid receptor (TR) heterodimers, are only activated by their own agonists prior to dimerizing with RXR (Figure 5) (Toporova & Balaguer, 2020). Permissive NR partners (PPARs, LXRs, FXRs and CAR) respond to dietary-derived lipids, and the synergistic effect of the heterodimer binding means that a robust transcriptional activity can be maintained despite low intake of lipids, achieving a profound biological response (Evans & Mangelsdorf, 2014). Non-permissive partners on the other hand, are generally hormone receptors with tight hormone control. In this way, the release of hormones is directly proportional to the transcriptional activity, which is a requirement of endocrine physiology (Shulman & Mangelsdorf, 2005).

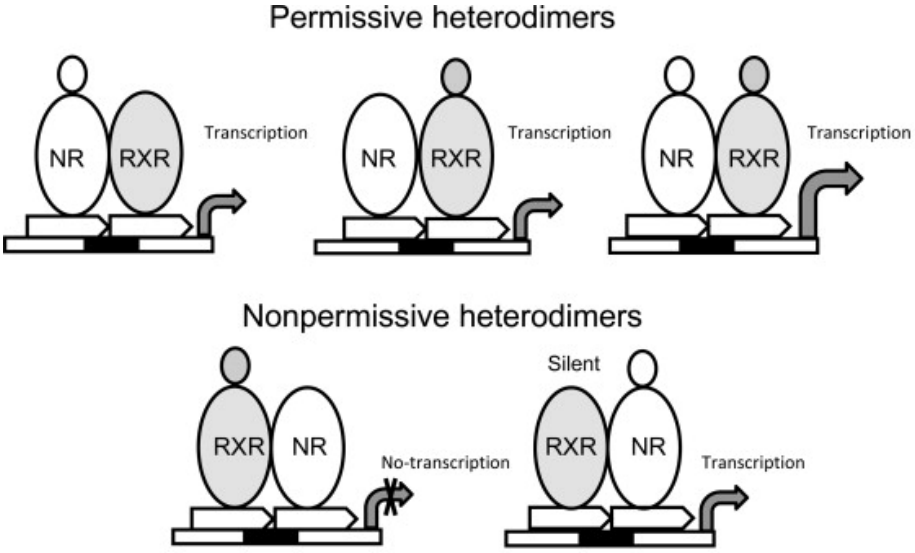

Figure 5. RXR as a permissive and non-permissive heterodimer to other Nuclear Receptors (NRs), Transcription from permissive heterodimers is activated by the ligand of either RXR or the partner NR. Binding of ligands for both NRs results in synergistic effects giving increased transcription, as indicated with a larger arrow. Non-permissive heterodimers are activated by their own ligands and the ligand for RXR does not bind. The illustration was modified from Brtko and Dvorak (2015).

1.7.1 Endogenous ligands of RXR

Despite the importance of RXR in numerous signaling pathways, endogenous ligands for these NRs are not yet well defined (le Maire et al., 2022). 9-cis-RA, a vitamin A derivative, was the first endogenous ligand to be proposed for RXR, as it had high binding affinity to all RXR subtypes (Figure 6) (Heyman et al., 1992). However, due to little or even no presence of 9-cis-RA in tissues, its role as an endogenous ligand was questioned (Arnold et al., 2012; Jones et al., 2015; Krężel et al., 2019). Other molecules have thus been suggested as endogenous RXR ligands, including free fatty acids, docosahexaenoic acid (DHA), docosatetraenoic acid, oleic acid, and arachidonic acids. However, the binding affinity of several of these are low (Krężel et al., 2019). 9-cis-13,14-dihydroretinoic acid (9cDHRA) has recently been proposed to be the new bona fide ligand for RXRs, as it binds with high affinity and is present in mammalians (de Lera et al., 2016). However its affinity to RXRs have been reported to be slightly lower than 9-cis-RA (le Maire et al., 2022). Future knowledge about the mechanisms of these ligands isis thus of interest. Until then, 9-cis-RA continues to be used as a model-ligand in research due to its high binding affinity to RXRs.

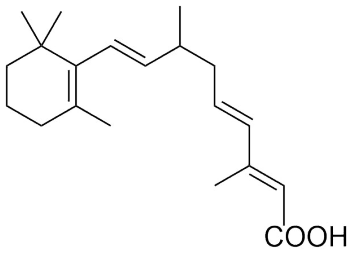

9-cis-retinoic acid

Figure 6. Structure of 9-cis-retinoic acid (9-cis-RA employed in this thesis and presumed endogenous ligand of RXR. Illustration was prepared using ChemDraw.

1.7.2 Exogenous ligands of RXR

Exogenous ligands of RXR have both a natural and synthetic origin. These are molecules that are not synthesized by the organism, but nevertheless can bind to the organism's RXR (Krężel et al., 2019). Many natural ligands have been isolated from traditional plant sources (Sharma et al., 2022). For instance, honokiol and magnolol from *Magnolia spp.* have been shown to interact with RXR:NR heterodimers and activate gene expression (Sharma et al., 2022). Synthetic ligands functioning as agonists and antagonists have been prepared based on the structure of retinoids, for instance LGD1069, 9cuAB30 and LG100754 (Krężel et al., 2019; Watanabe & Kakuta, 2018). Many of these have been found to function against carcinogenesis, and the development of ligands for RXR are considered valuable tools for treatment of signaling pathway disorders (Brtko & Dvorak, 2020).

1.7.3 TBT – an Exogenous ligand of RXR

TBT has been found to bind to RXR with high affinity, despite having no resemblance structurally or chemically to any known NR ligands (Toporova & Balaguer, 2020). This is achieved through a covalent bond between the tin atom of TBT and a sulfur atom of a conserved cysteine residue in the LBD of RXR (le Maire et al., 2009). TBT is thus thought to cause abnormal expression of genes, leading to endocrine disruption as described in Section 1.5. The binding of RXR to the RXR:PPARG heterodimer has been reported (Capitão et al., 2018; le Maire et al., 2009). The observed consequences are induction of lipogenesis and adipogenesis in mice and human mesenchymal stem cells and liver cells, as well as in zebrafish and medaka (K. Chen et al., 2021; Lyssimachou et al., 2015; Shoucri et al., 2017; Stossi et al., 2019). TBT exposure has also led to other discrepancies in normal functioning. For instance, in zebrafish embryo were cell viability and development effected, as well as the steroid metabolism

(Martínez et al., 2020). While in rare minnow disruption of the steroid biosynthesis and the retinoid metabolism were reported (Zhang et al., 2017). However, little is still known about the signaling pathways that are altered by TBT, and much research is still vital in this field.

1.8 Atlantic cod (*Gadus morhua*)

Atlantic cod (*Gadus morhua*) is a teleost with a pan-Atlantic distribution in the northern hemisphere (Figure 7) (Drinkwater, 2005). They can reside in waters ranging from -1 to 20 °C, but are typically found in waters ranging from 0 to 12 °C (Drinkwater, 2005). Atlantic cod reside in open oceans and fjords, coastal banks, and semi-enclosed bays, at 0–600 m depth (Berg & Albert, 2003). There are two distinct populations of Atlantic cod that exist; those that reside in the Northeast and those residing in the Northwest of the Atlantic (Matschiner et al., 2022). In Norway, Atlantic cod are typically divided into two ecotypes based on their migration or absence of migration (Sarvas & Fevolden, 2005). One ecotype is known as the Northeast Atlantic cod (NEA cod) and the other as the Norwegian coastal cod (NC cod). A divergence of these ecotypes is currently thought to be due to supergenes, which are clusters of genes within genomic inversions (Matschiner et al., 2022). The ecotypes spawn at overlapping coastal sites during winter and spring (March-May) (Strøm et al., 2023). However, the similarities between them stop there, as NC cod generally remain stationary in the fjords along the coastline, while the NEA cod migrate north to the Barents Sea (Berg & Albert, 2003; Strøm et al., 2023).

Figure 7. Distribution map of Atlantic Cod. The red areas indicate waters where Atlantic cod can be found. The map was collected from the Food and Agriculture organization of the United Nations (FAO, 2023) and modified using Adobe Illustrator.

Atlantic cod have an important ecological role as piscivorous top predator (Casini et al., 2009). This was unfortunately shown by the population declines in the 1980's and early 90's due to overfishing, causing a near depletion of the species (Frank et al., 2005). Consequently, the biodiversity of fish communities were affected (Ellingsen et al., 2015). For instance, "top down" effects in the food chains have been observed in the Barents Sea, in which an increase in the cod's prey fish, the planktivorous sprat (*Sprattus sprattus*) have been observed (Casini et al., 2008). This was followed by a decrease in zooplankton biomass, likely due to predation by sprat (Casini et al., 2009). Zooplankton are an important food source for cod larvae, and prolonged high populations of sprat could explain the inhibition of recovery of Atlantic cod stocks (Casini et al., 2009).

Atlantic cod are also prey for other animals such as the minke whale (*Balaenoptera acutorostrata*) and harp seals (*Pagophilus groenlandicus*) (Haug et al., 2017). They are also a valuable food source for humans, and have gained interest as a cultivated organism in cooler climates, and are thus of interest to learn more about (Morais et al., 2001). Cod are exposed to environmental stressors, for instance pollutants (Karl et al., 2016; Ono et al., 2019), In particular, the liver which is an important organ for consumption due to high vitamin D contents, is an accumulation site of fat-soluble pollutants due to its high lipid contents (Birgisdottir et al., 2012; Karl et al., 2016; Trefts et al., 2017). Atlantic cod are therefore often used as bioindicator species, in relation to both human consumption and on environmental impacts (Karl et al., 2016). The whole genome sequencing of both migratory and stationary cod has been performed (Matschiner et al., 2022; Star et al., 2011). This has led to an increase in knowledge regarding this pivotal species, in relation to how they cope with environmental stressors (Dale et al., 2020; Eide et al., 2023).

1.9 Atlantic cod Rxr[1]

Until recently, there was little information about Rxr in Atlantic cod and in teleosts in general. However, some studies have been performed recently on teleost fishes, mostly with typical model organisms such as zebrafish and Japanese medaka (Zhao et al., 2015). In contrast to mammals, which generally possess only one gene encoding each of the subtypes RXRa, RXRb and RXRg, fish may have several paralogues *rxr* genes due to the teleost-specific whole genome

[1] In this thesis, the names for proteins were capitalized for all mammals, based on the nomenclature by HGNC guidelines. Only the first letter is capitalized in protein names from fish, as described in ZFIN guidelines (Dunn, 2022)

duplication event (Philip et al., 2012). For instance, many fish species, including Atlantic cod, display paralogues genes encoding Rxrb, termed *rxrb1* and *rxrb2* (Zhao et al., 2015). Some fish, such as zebrafish and Japanese medaka, also have two copies of Rxra, i.e., Rxra1 and Rxra2 (Zhao et al., 2015). In Atlantic cod, four subtypes of Rxr have been identified, including gmRxra, gmRxrb1, gmRxrb2, and gmRxrg (Eide et al., 2018). Borge described the primary structure of their LBD and DBD, as well as the tissue-specific expression profiles of the gmRxrs (Borge, 2021). Recently, Prebensen discovered a splice variant of gmRxrb2, denoted as gmRxrb2d (2023). Furthermore, Borge and Prebensen studied ligand-activation of all the gmRxr subtypes (including the splice variant) *in vitro* with Luciferase reporter gene assays and discovered that Rxra, Rxrb2d, and Rxrg were activated by both 9-cis-RA and OTCs, with TBT demonstrating the highest potencies (Borge, 2021; Prebensen, 2023). Although we have now begun to unravel the molecular characteristics of the gmRxrs, such as their primary structures and activation by different ligands, much is still unknown about how signaling pathways are affected by activation of gmRxrs *in vivo*, as well as the adverse effects that could potentially arise in Atlantic cod from exposure to TBT and other OTCs.

1.10 Antibody Applications

Antibodies are valuable tools for studying different processes in molecular biology. Antibodies are proteins produced by B-lymphocytes known as plasma cells that reside in plasma and extracellular fluids and comprise one of the principal effectors of the immune response (Lipman et al., 2005). The function of antibodies is to recognize foreign molecules or organisms for the purpose of neutralizing or eliminating them (Lipman et al., 2005). Antibodies function by binding to recognition sites, so-called epitopes, on their targets via two Fragment antibody binding domains (Fabs) (Bass et al., 2017; Chiu et al., 2019). The binding property of antibodies has been exploited in therapeutic uses and is, for instance, important in the treatment of cancers, infections, and autoimmune diseases (Nasiri et al., 2017). In addition, antibodies are convenient research tools in molecular biology (Chiu et al., 2019). Three different types of antibodies are commonly used in research: monoclonal, polyclonal, and recombinant antibodies (Pillai-Kastoori et al., 2020). Polyclonal antibodies targeting a specific protein can be produced by injecting a protein or a peptide into laboratory animals, for instance mice or rabbits. The serum is collected from the animal at different time intervals, and the antibody towards the injected protein/peptide is purified from the serum (Yang et al., 2007). This pool of antibodies comprise of several antibodies that recognize different epitopes (Lipman et al., 2005). Monoclonal

antibodies on the other hand are synthesized by one B-lymphocyte clone and recognizes only one epitope (Zahavi & Weiner, 2020). In recent years, recombinant antibody techniques have been developed, with for instance phages (Guliy et al., 2023). However, polyclonal antibodies remain a popular choice in many applications due to lower production times and costs (Lipman et al., 2005).

Proteins of interest can be detected in immunoassays using antibodies. For instance, western blotting, a technique that employs antibodies to detect denatured proteins on a membrane, is a common tool used for protein analyses such as size determination, detecting splice variants, or post-translational modifications (PTMs) (Meftahi et al., 2021; Mishra et al., 2017). Western blotting can be coupled with immunoprecipitation (IP), a technique in which immunocomplexes between the protein and antibody are captured on solid supports and eluted for further analysis (Lal et al., 2005). Several forms of IP exist, such as chromatin IP that is often coupled with high-throughput sequencing (ChIP-seq), a valuable method for studying which genes transcription factors regulate (Ma & Zhang, 2020). The function of RXR/Rxr can be studied using immunoassays. Studies of RXR in mammals with western blotting and IP have already been reported, providing valuable information regarding these NRs (Chatagnon et al., 2015; Nam et al., 2016; Nielsen et al., 2008; Sugawara et al., 1995). However, information regarding Rxr in teleosts is still scarce, and provides a potential for future research.

1.11 Aims and Objectives

Cloning of Atlantic cod Rxr (gmRxr) subtypes, as well as their ligand-activation profiles by OTCs, has previously been described in previous MSc projects in our laboratory (Borge, 2021; Prebensen, 2023). However, this work encompassed mainly *in vitro* luciferase reporter gene assays in COS-7 cells. No studies on the effects of OTCs on the Rxr signaling pathway at a higher biological level have so far been undertaken with Atlantic cod. Understanding the effects of OTCs on cellular signaling pathways is important as this could provide knowledge about possible adverse outcomes of OTC exposure, which is still a globally prevalent environmental pollutant in many coastal hotspots.

We had previously ordered custom-made antibodies prepared against a peptide sequence of gmRxra. The aim of this thesis was to explore and confirm the binding of these antibodies to Rxrs in Atlantic cod tissue samples. This is an important step towards using antibodies in downstream analysis, such as ChIP, where antibodies are employed for studying gene

regulation networks. The second aim was to explore the effect of TBT exposure on different signaling pathways regulated by gmRxr by using *ex vivo* precision cut liver slices (PCLS) and gene expression analysis with quantitative polymerase chain reaction (qPCR). The specific objectives of this thesis are described below.

Objectives

i. Characterize antibody binding to gmRxr. With the following subobjectives:
    i. Explore *in silico* whether the custom-made antibodies produced towards gmRxra also could bind to the other Atlantic cod Rxr subtypes.
    ii. Assess whether the antibodies recognize and bind gmRxr in different Atlantic cod tissue homogenates.
    iii. Assess if the antibodies are suitable in immunoassays under both denaturing and non-denaturing conditions.

ii. Examine the activation of Rxr signaling pathways in Atlantic cod liver tissue through exposure to 9-cis-RA and TBT, with the following subobjectives:
    i. Examine the viability of liver tissues in PCLS cultures after exposure to 9-cis-RA and TBT.
    ii. Study changes in gene expression of the selected genes:
        - *pparg* – involved in lipogenesis and adipogenesis
        - *retinol binding protein 2* (*rbp2*) – involved in retinol metabolism
        - *3-beta-hydroxysteroid-delta(8), delta(7)-isomerase (ebp)* and *squalene epoxidase* (*sqlea*) – involved in steroid synthesis

2 MATERIALS

2.1 Atlantic cod

Atlantic cod were obtained from Havbruksstasjonen in Tromsø AS (Nofima, Tromsø, Norway) and kept in 500 L tanks at 10°C, 34 ppt seawater with a 12 h light/l2 h dark cycle at the Industrial and Aquatic Laboratory (Bergen, Norway). Atlantic cod of approximately 1.5 years old with a mean body weight (bw) of 1.5 kg were used for the PCLS experiments described in this thesis. The fish were fed on a commercial diet (Amber Neptune, batch no. 3343368,_Skretting, Stavanger, Norway).

Cod tissues for western blot analyses were collected from the Environmental Toxicology Research Group's tissue bank, stored at -80 °C.

2.2 Chemicals and reagents

Table 1. Chemicals and reagents used are listed in alphabetical order, with CAS numbers for chemicals and the product number for reagents.

Chemical / reagent	**CAS or Catalog Number**	**Manufacturer**
2-log DNA ladder	N0469S	New England BioLabs$_{Inc}$
3-(4,5-Dimethylthiazol-2-yl)-2,5-diphenyltetrazolium bromide (MTT)	298-93-1	Sigma-Aldrich®
6-[(3,4,5-Trimethoxybenzoyl)amino]hexanoic acid	21434-91-3	Sigma-Aldrich®
Acrylamide/bis-acrylamide 30 % solution	A3699	Sigma-Aldrich®
Agarose	9012-36-6	Sigma-Aldrich®
Ammonium persulfate (APS)	7727-54-0	Bio-Rad
Antibiotic Antimycotic Solution (100x), stabilized	A5955	Sigma-Aldrich®
Blue/Orange 6X Loading Dye	G1881	Promega
β-mercaptoethanol	60-24-2	Sigma-Aldrich®
Bovine Serum Albumin (BSA)	9048-46-8	Sigma-Aldrich®
Bromophenol blue	115-39-9	Sigma-Aldrich®
CHAPS BioChemica	75621-03-3	PanReac AppliChem ITW Reagents
Chloroform	67-66-3	Sigma-Aldrich®
Dimethyl sulfoxide	67-68-5	Sigma-Aldrich®
DL-Dithiothreitol	3483-12-3	Sigma-Aldrich®
Fetal Bovine Serum (FBS) South America, Charcoal stripped	S181F	Biowest

Formamide	75-12-7	Sigma-Aldrich®
GelRed Nucleic Acid Stain, 10,000X in water	41003	Biotium
Glycerol, 99 %	56-81-5	Sigma-Aldrich®
Glycine	56-40-6	Sigma-Aldrich®
Ethylenediaminetetraacetic acid tetrasodium salt dihydrate (EDTA)	6381-92-6	Sigma-Aldrich®
Ethanol absolute	64-17-5	VWR Chemicals
Imperial™ Protein Stain	24615	ThermoFischer Scientific
Iodoacetamide	144-48-9	Sigma-Aldrich®
IPG Buffer, pH 3-10	GE17-6000-87	GE Healthcare
Isopropanol prima	67-63-0	Antibac®
Leibovitz's (1X) L-15 Medium	21083027	Gibco™
Magnesium sulfate heptahydrate	10034-99-8	Sigma-Aldrich®
Methanol	67-56-1	Sigma-Aldrich®
N,N,N',N'-Tetramethyl-ethylenediamine (TEMED)	110-18-9	Sigma-Aldrich®
Nonidet P-40	9016-45-9	Sigma-Aldrich®
Ponceau S stain	6226-79-5	VWR International AS
Phosphate Buffered Saline, pH 7.4	806552	Sigma-Aldrich®
Pierce™ 660 nm Protein Assay Reagent	22660	ThermoFischer Scientific
PlusOne DryStrip Cover Fluid	17-1335-01	GE Healthcare Life Sciences
Potassium chloride	7447-7-40	Sigma-Aldrich®
Precision Plus Protein™ All Blue Standards	161-0373	Bio-Rad
Protease inhibitor cocktail	P8340	Merck
Protein G Agarose	11 243 233 001	Roche
Sodium chloride	7647-14-5	Sigma-Aldrich®
Sodium deoxycholate	302-95-4	Sigma-Aldrich®
Sodium dodecyl sulfate solution (SDS)	151-21-3	Sigma-Aldrich®
Sodium hydrogen carbonate	144-55-8	Sigma-Aldrich®
Sodium hydroxide	1310-73-2	Sigma-Aldrich®
Sodium phosphate dibasic dihydrate	10028-24-7	Sigma-Aldrich®
Sodium phosphate monobasic monohydrate	10049-21-5	Sigma-Aldrich®
Thiourea	28 615.231	VWR Prolabo BDH
Tributyltin chloride (TBT)	1461-22-9	Sigma-Aldrich®
TRI Reagent®	T9424	Sigma-Aldrich®
Tris base	77-86-1	Merck
Triton X-100	9036-19-5	Sigma-Aldrich®
Tween® 20 electrophoresis	9005-64-5	Sigma-Aldrich®
Urea	57-13-6	Merck
Water Nuclease Free	7732-18-5	VWR Life Science

2.3 Primers

Table 2. Primers used for qPCR analysis of gene expression

Oligonucleotide name	Sequence 5 → 3
gm_ACTB2f	CGACGGGCAGGTCATCACCATC
gm_ACTB2r	CCACGTCGCACTTCATGATGCT
gm_ebp_f	CTTTCCTGACCAACAAGCCC
gm_ebp_r	TGTGAGCATATCCATCCCGG
gm_pparg_f	CCCGGCTTTGTAGATCTGGAT
gm_pparg_r	GCACCTCTATCACGCCGTACTT
gm_rbp2_f	GGGGTGGAGTTTGACGAGTACA
gm_rbp2_r	TACCAGCTTGTCTCCATCCCAG
gm_sqlea_f	GATCTGGAGGAGGAGTCTGC
gm_sqlea_r	GATGACTTGCGTTCCCAGTG

2.4 Commercial Kits

Table 3. Commercial kits

Material / kit	Product Number (#)	Manufacturer
Cytotoxicity Detection Kit ^{PLUS} (LDH)	4744926001	Roche
SuperSignal™ West Pico PLUS Chemiluminescent Substrate	34580	Thermo Scientific
iScript	170 – 8891	BioRad
SsoAdvanced™ Universal SYBR® Green Supermix from BioRad	172-5274	BioRad

2.5 Buffers and Solutions

2.5.1 Tissue homogenization

Table 4. Tissue homogenization buffer

Component	Concentration
Sodium phosphate monobasic monohydrate ($NaH_2PO_4 \cdot H_2O$)	100 mM
Potassium chloride (KCl)	150 mM
EDTA	1.00 mM
Glycerol	10.0 %
DDT	1.00 mM
Protease inhibitor cocktail	1:10-0
Sodium hydroxide (NaOH)	Enough for pH adjusting
milliQ	-

2.5.2 SDS-PAGE

Table 5. 12 % Polyacrylamide Gel composition.

Component	12 % resolving gel	Stacking gel
Acrylamide/bis-acrylamide, 37,5:1	12 %	4.90 %
Tris pH 8.8	0.38 M	-
Tris pH 6.8	-	0.13 M
Sodium dodecylsuphate (SDS)	0.10 %	0.19 %
Ammonium persulfate (APS)	0.10 %	0.10 %
N, N, N', N', Tetramethyl-ethylenediamine (TEMED)	0.040 %	0.10 %

Table 6. 5X sample buffer

Component	Concentration
Tris-HCl, pH 6.8	250 mM
SDS	10 %
Glycerol	30 %
β-mercaptoethanol	5 %
Bromophenol blue	0.02 %

Table 7. 1X TGS Running buffer

Component	Concentration
Glycine	192 mM
Tris base	25 mM
SDS	0.1 %

2.5.3 Western Blot

Table 8. 10X Tris-glycine (TG) buffer

Component	Concentration
Tris base	250 mM
Glycine	1.90 M
MilliQ	-

Table 9. 1X Transfer Buffer

Component	Concentration
TG buffer	1x
Methanol (MeOH)	20 %
MilliQ	-

Table 10. 0.1 % TBS-Tween

Component	Concentration
Tris pH 7.5	20 mM
Sodium chloride (NaCl)	150 mM
Tween-20	0.1 %
MilliQ	-

Table 11. Blocking solution

Component	Concentration/amount
Bovine serum albumin (BSA)	5 %
0.1 % TBS-Tween	50 mL

Table 12. 2nd antibody incubation solution

Component	Concentration
BSA	2 %
Polyclonal Goat Anti-Rabbit Immunoglobulins/HRP antibody	1:2000
TBS-Tween	0.1 %

2.5.4 2D-PAGE

Table 13. Rehydration buffer.

Component	Concentration
Urea	7.0 M
Thiourea	2.0 M
CHAPS	4 % (w/v)
DTT	20 mM
Triton X-100	0.5 %
IPG buffer*	0.5 % (v/v)
ddH_20	-
*IPG buffer added to the rehydration buffer prior to use	

Table 14. 2D-PA Gel components of 12.5 % polyacrylamide gels.

Component	Concentration
Acrylamide/bisacrylamide	12.5 %
Tris-HCl, pH 8.8	0.38 M
SDS	0.10 %
APS	0.080 %
TEMED	0.080 %
ddH_20	-

Table 15. SDS equilibration solution

Component	Concentration
Tris-HCl, pH 8.8	50 mM
Urea	6.0 mM
Glycerol	30 % (v/v)
SDS	2 % (w/v)
Bromophenol blue	A few corns
ddH_20	-
2.5 mg/mL DDT or 0.045 g/mL IAA	

Table 16. Agarose

Component	Concentration
Agarose	0.4 %
TGS buffer	1X
Bromophenol blue	A few corns

Table 17. 2D Anode solution I

Component	Concentration
Tris, pH 10.4	0.3 M
Methanol (MeOH)	20 %

Table 18. 2D Anode solution II

Component	Concentration
Tris, pH 10.4	25 mM
MeOH	20 %

Table 19. 2D Cathode Solution

Component	Concentration
6-[(3,4,5-Trimethoxybenzoyl)amino]hexanoic acid	4 mM
Methanol (MeOH)	20 %

Table 20. Membrane rinse after Imperial™ Protein Stain

Component	Concentration
Acetic acid	10 %
MeOH	50 %
MilliQ	-

Table 21. Methanol rinse of membrane

Component	Concentration
MeOH	10 %
MilliQ	-

2.5.5 Immunoprecipitation

Table 22. Homogenization/Wash buffer 1

Component	Concentration
Tris-HCl, pH 7.5	50 mM
NaCl	150 mM
Nonidet P-40	1 %
Sodium deoxycholate	0.5 %
Protease inhibitor cocktail (added upon usage)	1:100
ddH_2O	-

Table 23. Wash buffer 2

Component	Concentration
Tris-HCl, pH 7.5	50 mM
NaCl	500 mM
Nonidet P-40	0.1 %
Sodium deoxycholate	0.05 %
ddH_2O	-

Table 24. Wash buffer 3

Component	Concentration
Tris-HCl, pH 7.5	50 mM
Nonidet P-40	0.1 %
Sodium deoxycholate	0.05 %
ddH_2O	-

Table 25. 1X sample buffer

Component	Concentration
5X sample buffer stock	1X
ddH_2O	-

2.5.6 PCLS

Tab6e 26. PCLS buffer, pH 8.4

Component	Concentration (mM)
Sodium chloride (NaCl)	122
Potassium chloride (KCl)	4.80
Sodium phosphate dibasic dihydrate $HNa_2O_4 – 2H_2O$	11.0
Magnesium sulfate heptahydrate (MgO_4S - $7H_2O$)	1.20
Sodium hydrogen carbonate ($NaHCO_3$)	3.70
ddH_2O	-
*For more basic solution, Sodium hydroxide (NaOH) was added. For more acidic solution, hydrogen chloride (HCl) was added.	

Table 27. PCLS culture medium

Component	Volume (mL)
L-15 Leibovitz medium	44.5
Charcoal-stripped Fetal bovine serum (csFBS)	5.0
100x antimycotic myocin, final concentration 1x.	0.5

2.5.7 RNA extraction

Table 28. Agarose gel

Component	Concentration
TAE buffer	1X (100 mL)
Agarose	1 % (w/v)
GelRed	0.5 µL

Table 29. Loading buffer for agarose gel

Component		Concentration
Blue/Orange Loading Dye	6X	1.2X
Formamide		79 %

2.6 Antibodies, immunogen, and pre-immune serum

Table 30. Antibodies and pre-immune serum used.

Antibody	Product Number (#)	Manufacturer	Stock Concentration	End concentration
Affinity purified antibody, rabbit #5789	U0864DC020-10 (#5789)	GenScript	0.542 mg/mL	1 µg/µL for WB 5 µg for IP
Affinity purified antibody, rabbit #5859	U0864DC020-10 (#5859)	GenScript	0.537 mg/mL	1 µg/µL for WB 5 µg for IP
Rxra Immunogen	UD864DC020-10	GenScript	0.670 mg/mL	Calculate
Polyclonal Goat Anti-Rabbit Immunoglobulins/HRP	P0448	Dako	-	1:2000

2.7 Equipment

Table 31. Overview of instruments and equipment, their supplier and application**.**

Instrument	Application	Supplier
C1000™ Thermal Cycler	qPCR amplification	Bio-Rad
ChemiDoc™ XRS+	Imaging Gels and membranes	Bio-Rad
CFX96™ real-Time System	qPCR	Bio-Rad
EnSpire™ 2300 Multilabel Reader	Absorbance measurements	PerkinElmer
Ettan™ IPGphor™ 3 IEF system	IEF of strips for 2D	GE Healthcare
GD100	Water bath heat shock	
Heraeus pico 21	Centrifugation	ThermoScientific
HS 501 Digital	Shaker	IKA®-Werle
MilliQ A10 advantage	MilliQ H_2O dispenser	Merck

Motor handpiece MHX/E MP220	Tissue homogenization pH measurements	XENOX Bergman
Hidex Sense Plate reader	Absorbance measurements	
Leica vibrating blade microtome VTI1200	PCLS	Leica, Wetzler, Germany
Multifuge X3R Centrifuge	Centrifugation of samples	Heraeus
NanoDrop™ One/OneC Microvolume UV-Vis Spectrophotometer	Measure concentration and purity of RNA	ThermoFischer Scientific
PowerPac™ HC	Electrophoresis power supply	Bio-Rad
T100™ Thermal Cycler	cDNA synthesis	Bio-Rad

2.8 Software

Table 32. Software Tools used

Software	Application	Supplier
Adobe illustrator	Figure preparation	Adobe Creative Cloud
BioRender 2023	Figure preparation	BioRender®
ChemDraw	Preparing structures for figures	
Clustal Omega	Multiple Sequence alignment (MSA)	EMBL-EBI https://www.ebi.ac.uk/Tools/msa/clustalo/
Excel 2020	Data processing	Microsoft
Expasy, Compute pI/Mw	Calculating pI and MW of RXR isoforms	SIB https://web.expasy.org/compute_pi/
Image Lab™ Software	Imaging gels and membranes	BIO RAD
Jalview 2.0	Annotating MSA	
protein blast (pBLAST)	Find hits matching antibody immunogen	NCBI https://blast.ncbi.nlm.nih.gov/Blast.cgi
Primer 3	Primer design	NCBI
Prism 9	Statistical analysis	GraphPad
Protein Data Bank (PDB)	Retrieving 3D structure of hRXRa	RCSB https://www.rcsb.org/
Expasy ProtScale	Hydropathy plot	SIB https://www.expasy.org/resources/protscale
PyMOL 2.5	3D visualization	Schrödinger

Word 2020	Thesis writing	Microsoft

3. METHODS

3.1 Experimental outline

Throughout this thesis, several molecular biology techniques as well as bioinformatics were employed. An experimental outline of the steps in this thesis are viewed in Figure 8.

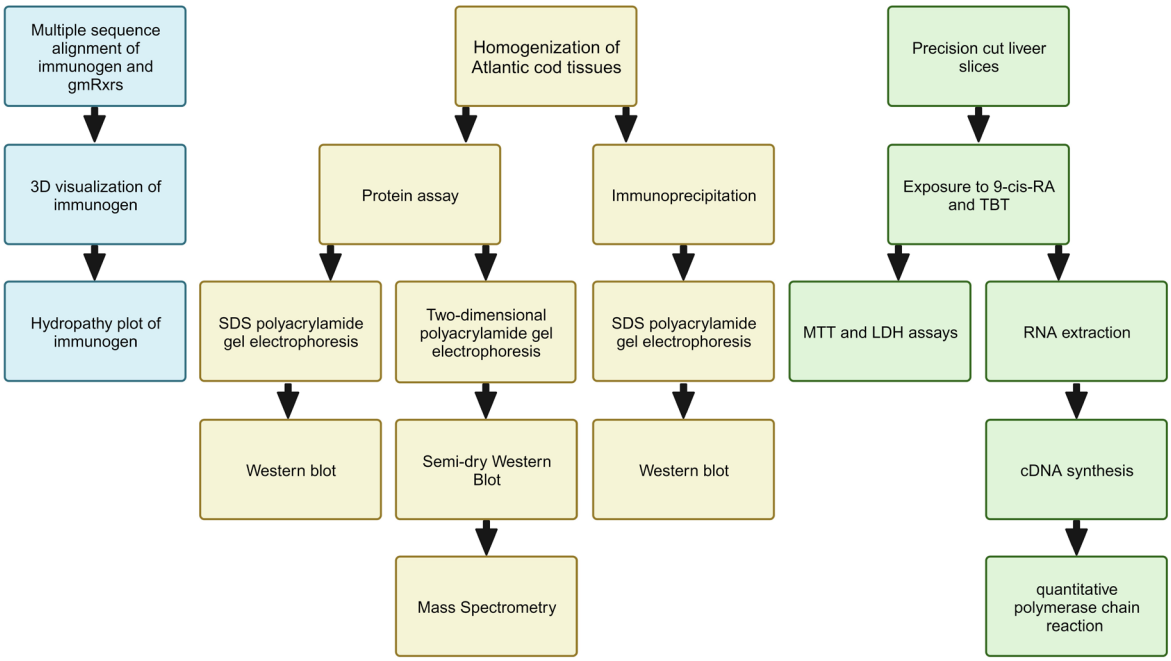

Figure 8. Experimental outline of the techniques used in this thesis. A multiple sequence alignment (MSA) was generated with the immunogen sequence, used to synthesize pAb #5789 and pAb #5859, against Atlantic cod (*Gadus* morhua) Retinoid X receptor (gmRxrs) to assess the similarity in this region. 3D visualization of the immunogen was performed using human RXRa. A hydropathy plot was generated to predict surface amino acids in the immunogen. Atlantic cod tissue was homogenized and analyzed through an SDS polyacrylamide (SDS-PAGE) gel and through western blot analysis. Western blot analysis with liver tissues was performed with pAb #5789 and pAb #5859, as well as their pre-immune serums. An immunoreactive band in the liver was identified through two-dimensional PAGE (2D-PAGE) and semi-dry western blot. 48 h exposure of liver cultures to 9-cis-RA and TBT were also performed. An MTT and an LDH assay was performed to assess the viability of the cells. RNA was extracted from the tissues and ultimately was used for gene expression analysis using quantitative polymerase chain reaction (qPCR). The figure was created with BioRender.com.

3. 2 Bioinformatics

3.2.1 Multiple sequence alignment (MSA)

The amino acid (aa) sequences of Rxra (XP_030197437.1), Rxrb1 (XP_030214648.1), Rxrb2 (XP_030202479.1) and Rxrg (XP_030228385.1) were retrieved from GenBank. Calculations of molecular weight (MW) and isoelectric point (pI) were made with the Compute pI/Mw tool (SIB). Clustal Omega (EMBL-EBI) was used to generate multiple sequence alignments (MSA) that were visualized and annotated in Jalview v2.0.

3.2.2 3D visualization of Immunogen peptide

The protein blast (pBLAST) alignment tool **(**NCBI) was used to find 3D structures with aa sequences similar to gmRxra in the Protein Data Bank (PDB) database. From the resulting hits, the 3D structure of hRXRa was downloaded from RCSB Protein Data Bank (RCSB-PDB) with the identification id: 3DZY. The structure consisted of a protein complex with hRXRa connected to PPARg, a DNA helix, as well as rosiglitazone, 9-cis Retinoic Acid and NCOA2 peptide. Using PyMOL 2.5 (Schrödinger), the immunogen sequence was identified and highlighted, and the structure visualized to fit the needs of this thesis (i.e., the DNA helix, PPARg, NCOA2 peptide, and rosiglitazone were hidden in the image generated for this thesis).

3.2.3 Hydropathy plot

A hydropathy plot was generated with the immunogen sequence using the ProtScale tool (SIB), with the window size set to 9 and the window center set to 100 %. The hydropathy plot was generated using the aa scale generated by Kyte and Doolittle (1982).

3.3 Tissue Collection

Tissues were collected from juvenile Atlantic cod, selected at random, from the Industrial and Aquatic Laboratory (ILAB), as well as from the local tissue bank (TB) at the environmental toxicology research group (stored at – 80 °C).

3.4 Tissue Homogenization

For western blot analyses, 50 mg of the following tissues, brain, skin, stomach, liver, muscle, heart, head kidneys, and ovaries were dissected from a juvenile female Atlantic cod. The tissues were rinsed in 1X phosphate buffered saline (PBS) before they were homogenized in 300 µL homogenization buffer (Table 4) containing a protease inhibitor cocktail and using an automated homogenizer tool (XENOX, MHX/E)

For the IP experiment and the 2D-PAGE procedure, liver tissue from the Atlantic cod TB was used. About 1 g and 0.5 g liver tissue was homogenized for the IP and 2D-PAGE, respectively. The tissues were briefly washed in 1X PBS before they were homogenized in 2.25 mL lysis buffer (Table 22**)** for the IP experiment, and 2 mL rehydration buffer (Table 13) for the 2D-PAGE. The IP lysis buffer contained protease inhibitor cocktail diluted 1:100.

The tissue homogenates used for western blot were shaken for 30 min at 4 °C, then centrifuged at 12 000 x *g* for 20 min at 4 °C. The IP homogenates were centrifuged at 12 000 x *g* for 10 min at 4 °C, while 2D-PAGE samples were centrifuged at 13 000 x *g* for 10 min at 4 °C. The supernatants were transferred to new tubes, avoiding the pellets and lipid layers formed at the top. Centrifugation rounds were repeated, if necessary, until no pellet or lipid layer could be detected. All homogenates were stored at –80 °C.

3.5 Colorimetric protein quantification assay

Bovine serum albumin (BSA) standards were prepared with the following concentrations in mg/mL, 2, 1, 0.5, 0.25, 0.125, 0.0625, in the buffers the tissues had been homogenized in, but without including additional protease inhibitor cocktail. 10 µL of BSA standards, buffer blanks, and samples diluted in their respective homogenization buffer were added in triplicates into a 96—well plate. The homogenates were diluted either 1:5, 1:8, 1:10, or 1:20, depending on how high their absorbance reads were in relation to the absorbances of the BSA standards. 150 µL Pierce^{TM} 660 nm Protein Assay Reagent was added into each well. The plate was shaken at 1 rpm for 1 min and incubated for 5 min in the dark at RT. The absorbances were read at 660 nm using the Perkin Elmer Enspire plate reader. The average absorbance reads of the BSA standards and their corresponding protein concentrations were used to generate a regression line in a XY-plot. The equation of the regression line and the absorbances of the homogenized tissues were used to determine the protein concentration in the samples.

3.6 Sodium dodecyl-sulphate polyacrylamide gel electrophoresis (SDS-PAGE) and western blotting (WB)

3.6.1 SDS-PAGE

1 mm PA gels were cast, consisting of a 12 % resolving gel and a 4.90 % stacking gel (Table 5). After the gels had polymerized, they were either used right away or stored at 4 °C for up to one week. Upon usage, gels were transferred from the casting unit to the electrophoresis chamber and 1X TGS Running buffer (Table 7) was poured into the tank.

Homogenate samples and the immunogen control (provided by GenScript), consisting of the part of Rxra used for immunization (Table 30), were prepared in 1X sample buffer (Table 6) and milliQ to a final volume of 20 µL. All samples were heated in a water bath at 95 °C for 5 min, before spinning them down briefly. The samples were loaded into the wells and the gels were run at 80 V for 10 min, and then at 150 V until done. The gel was stained with Imperial™ protein stain (Coomassie dye R-250) for 30 min, then rinsed 3X with distilled water, before O/N rinse in distilled water while shaking at RT. The gel image was taken using the ChemiDoc™ XRS+ imaging system from Bio-Rad.

3.6.2 Western blot procedure

Components of the blotting sandwich, including sponges, filter paper, SDS-PA gel, and nitrocellulose blotting membrane (Amersham™ Protran™ Premium 0.45 µm NC, prod. no. 10600008) were soaked in 1x transfer buffer containing 20 % methanol (MeOH) (Table 8), and then assembled and placed into the transfer cell. The chamber was filled with transfer buffer and the membrane blotted at 100 V for 1 h.

The membrane was transferred to a tray and rinsed in 0.1 % TBS-Tween (Table 10), before it was stained in Ponceau S to briefly visualize the presence of protein bands. An additional 0.1 % TBS-Tween rinse for 10 min whilst shaking at RT was done before blocking the membrane with 5 % bovine serum albumin (BSA) in 50 mL 0.1 % TBS-Tween (Table 11) for 1 h whilst shaking at RT.

The membrane was rinsed before O/N incubation with 1 µg/mL of either antibody #5759 or antibody #5859 (Table 30), or with the same volume of the pre-immune serums (concentrations not available from GenScript), prepared in 8 mL TBS-Tween at 4 °C. The membrane was rinsed in 0,1 % TBS-Tween for 10 min at RT while shaking X3 (Table 10). Then incubated with the

secondary antibody Polyclonal Goat anti-Rabbit Immunoglobulin HRP (Table 30), diluted 1:2000 in 8 mL 0.1 % TBS-Tween with 2% BSA for 1h (Table 12). The membrane was rinsed again same as above, after incubation with the secondary antibody.

To visualize immunoreactive proteins, the SuperSignal™ West Pico PLUS Chemiluminescent Substrate kit was used. A 1 mL working solution was prepared and the protocol provided by the manufacturer was followed. Images were taken using ChemiDoc™ XRS+ imaging system (BIO RAD).

3.7 Two-dimensional polyacrylamide gel electrophoresis (2D-PAGE)

3.7.1 Sample preparation

IPG buffer, pH 3 – 10 (GE Healthcare) was added to rehydration buffer to a final volume of 0.5 % to a total of 256.05 µL in two tubes (Table 13). A few corns of bromophenol blue were also added to give the solution a blue color. 750 µg Homogenate, determined by protein assay, was added to each tube, with a final volume of 540.05 µL. The samples were vortexed at low rpm, then centrifuged at 13 000 x *g* for 10 min at RT.

3.7.2 Rehydration of gel strips

The samples were carefully distributed across each of their wells in the rehydration tray, avoiding disturbing the pellet. Due to lack of 18 cm strips in our lab, 24 cm long IEF strips, pH 3 - 10 (Serva IPG *Blue*Strip, 24 cm, Lot no. IPG14162) were employed and gently submerged, face down, into the wells. 2.6 mL cover fluid was gently distributed across the strip using a pipette. The strips were left to rehydrate, with the lid of the tray placed on top, O/N for 22 h.

3.7.3. Isoelectric focusing (IEF)

108 mL cover fluid was spread evenly across the tray of the isoelectric focusing system that had been pre-cooled to 20°C, distributing the fluid into all the wells. The strips were gently transferred from the wells of the rehydration tray into wells of the IEF system, with the acidic end placed towards the anode and the basic end towards the cathode end of the system, and with the gel portion now facing upwards. Paper wicks (GE Healthcare) were hydrated with distilled water and placed at each end of the strips. The system's electrode clamps were attached right

above the paper wicks, and the machine was turned on with the steps described in Table 33). The strips were frozen at – 80 °C after the run ended.

Table 33. Iso-electric focusing steps

Step		Voltage (V)	Time (h)
1	Step	150	3
2	Step	300	3
3	Gradient	1000	6
4	Gradient	10 000	1
5	Step	12 000	4.5
Total time / duration			17.5 / ~ 52 kVh

3.7.4 Equilibration of gel strips

The IPG strips were equilibrated in the same trays as they had been frozen in, by first incubating them in 10 ml SDS equilibration solution with 2.5 mg/mL Dithiothreitol (DDT) added to it, whilst shaking at 1 rpm for 15 min, then by incubating with 10 ml SDS equilibration solution with 45 mg/mL iodoacetamide (IAA) added to it, following the same parameters (Table 15).

3.7.5 SDS-PAGE of strip

Two 12.5 % PA gel solutions were prepared in each of their 50 mL falcon tubes (Table 14). 20 cm x 20 cm large gels were cast, adding the gel mixture between the pre-cleaned glass plates, leaving 1 cm at the top of the shorter glass plate. 70 % Ethanol was poured over the gels, and the gels were left to solidify. The gels were kept at 4 °C until use.

The ends of the gel strips were cut. 5 cm of the acidic end and 2 cm of the basic end was cut off one strip, reducing the length to 17 cm, while on the other strip 4 cm of the acidic end and 2 cm of the basic end was cut off, reducing the length to 18 cm. The gel strips were rinsed in 1X TGS before placing them in between the glass plates of the 12.5 % PA gels. The acidic end was placed towards the left and the basic end towards the right, with the gel part of the strip facing outwards.

Furthermore, for one of the gels, 30 µg liver Homogenate was mixed with 1X sample buffer (Table 6) and milliQ to a final volume of 10 µL. The sample was boiled at 95 °C and spun down, before being transferred onto a 0.5 cm x 0.5 cm piece of filter paper. 10 µL of the protein ladder (Precision Plus^{TM} Standards) was also added to a paper piece of same size. The two paper

pieces were placed next to the strips on top of the gels and run as a regular SDS-PAGE alongside the second-dimension electrophoresis.

0.4 % agarose, dissolved in 1X TGS buffer with some bromophenol added, was used to seal the IPG gel strips and the paper pieces to the gels (Table 16). The cavity above the gels was filled with agarose. The glass plates, holding the gels, were transferred to the electrophoresis chamber (BIIO RAD) and the chamber was filled with 2.5 L 1X TGS Running buffer (Table 7). The gels were run at 10 mA for 2 h and then at 70 mA until done.

3.7.6 Staining of gel and visualization

One of the gels from 2D-PAGE was rinsed in MilliQ, then stained with Imperial protein stain for 2 h whilst shaking at 70 rpm at RT. The gel was rinsed over three days, in milliQ, whilst gently shaking at RT. Images were taken with ChemiDoc^{TM} XRS+ imaging system. The gel was kept in milliQ and stored at 4 °C.

Two protein spots were cut out of the gel and stored at –80 °C in Eppendorf tubes until they were sent to Mass Spectrometry (MS) analysis. The analysis was performed by the Proteomics Unit (PROBE) at UiB. There, the samples were in-gel trypsinated and the resulting peptides were analyzed with an LTQ Orbitrap MS.

3.7.7 Semi-dry western blotting of gel from 2D-PAGE

The other gel from the 2D-PAGE was used for semi-dry western blotting. The cathode and anode electrodes of the transfer apparatus were placed in milliQ water for 2 hours. Excess water was dried off the parts and the anode electrode was placed on a tray on the table. Filter paper and nitrocellulose membrane were cut to fit the size of the electrode. Six pieces of filter paper were soaked in anode solution I (Table 17) and placed on top of the anode electrode. Three filter papers were soaked in anode solution II (Table 18) and placed on top of the other filter papers. A nitrocellulose membrane was also soaked in anode solution II and placed on top of the soaked filter papers. The gel was placed on top of the membrane. The edges on the right side and the bottom of the gel were cut so the gel could fit exactly on the nitrocellulose membrane. Nine filter papers were soaked in cathode solution (Table 19) and placed on top of the gel. Air bubbles were pushed out with a roller between each step of adding filter paper or

the membrane. The cathode electrode was placed on top, the safety lid lowered, and the system was connected to a power supply. The blotting procedure was run at 250 mA for 1 h.

The membrane was blocked and incubated with pAb #5859, similarly as described in Section 6.2. However, the volumes were adjusted for the size of the membrane. Only pAb #5859 was tested, because the 2D-PAGE procedure was quite extensive and because the antibodies gave similar results in the regular WB analyses. Detection and visualization of bands were also performed similarly as described in Section 3.6.2, with adjusted volumes.

The membrane was rinsed in milliQ for 30 min on a shaker at RT. Imperial™ protein stain was added to the tray, covering the membrane. The membrane was left in the stain for 5 min at RT on a shaker. The background was reduced with 10 % acetic acid and methanol, prepared in milliQ (Table 20) O/N with the same conditions. The membrane was rinsed with 10 % methanol in milliQ (Table 21), and an image was taken using the ChemiDoc™ XRS+ imaging system from Bio-Rad (results not shown).

3.8 Immunoprecipitation

Immunoprecipitation was performed with protein G agarose beads (Roche, Ca. no. 11 243 233 001) and the protocol from Roche describing the use of these particular G-beads in IP. The antibodies pAb #5789 and pAb #5859 were tested individually (denoted as “IP eluate” further on, as it becomes the sample eluate for analysis). Two controls were also included, one in which antibody was not added to the tissue Homogenate (denoted as “IP control 1” further on), and another in which no homogenate was added (denoted as “IP control 2” further on) (Table 34).

Table 34. Composition of the samples used for immunoprecipitation.

IP eluate	IP control 1	IP control 2
Liver homogenate	Liver homogenate	Lysis buffer and protease inhibitor cocktail, diluted 1:100,
pAb #5789 or pAb #5859	Lysis buffer and protease inhibitor cocktail, diluted 1:100	pAb #5789 or pAb #5859

1 mL liver homogenate was added to two Eppendorf tubes each, for the IP eluate and IP control 1. A small amount of the homogenate was stored at -80 °C for protein assay and WB analysis and denoted the “IP homogenate” (Section 3.5 and 3.6). The Protein G agarose beadswere

mixed in their containers to homogenize the beads with the solution. 50 µL of the bead solution was added to each of the Eppendorf tubes with homogenate (IP eluate and IP control 1). The tubes were incubated while rotating at 9 rotations per minute (rpm) for 3 h at 4 °C. The agarose beads were pelleted by centrifugation at 12 000 x *g* for 20 sec, at 4 °C. The agarose beads were left behind, while the supernatants were transferred to each their own new Eppendorf tubes and carried on for the next steps of the procedure. Fractions of the supernatants were stored at -80 °C, as "Unbound fraction 1"). 1 mL lysis buffer was added to IP control 2 including protease inhibitor cocktail diluted 1:100 (Table 22, 34). 5 µg of either antibodies (pAb #5789 or pAb #5859) was added to IP eluate and to IP control 2, substituted by the same amount of lysis buffer and protease inhibitor cocktail in IP control 1. All tubes were incubated at 4 °C for 1 h whilst rotating at 9 rpm.

50 µL of vortexed beads were added to IP eluate, IP control 1 and IP control 2. They were then incubated while rotating at 9 rpm O/N, between 16 and 18 h, at 4 °C. The beads were pelleted by the same parameters as described above. Supernatants were stored at – 80 °C, as "Unbound fraction 2".

The pelleted beads were resuspended in 1 mL Wash buffer 1 (Table 22), and incubated whilst rotating at 9 rpm, for 20 min at 4 °C. The beads were pelleted again as described above. The bead wash was repeated once more with Wash buffer 1, then two times with Wash buffer 2 (Table 23), and once with Wash Buffer 3 (Table 24). Supernatants were kept as controls and stored at – 80 °C. Supernatants were denoted "Wash 1" for the first wash round, and "Wash 1.2" for the second wash with Wash buffer 1. A fraction from the first wash with Wash buffer was kept as "Wash buffer 2". The fraction from the Wash buffer 3 wash was denoted as "Wash 3". After the final wash, as much of the buffer was removed, by spinning down the tubes.

The samples were resuspended in 60 µL 1X sample buffer (SDS-PAGE) diluted in MilliQ (Table 6), then heated at 100 °C for 3 min, with flicking of the tubes now and again, to separate the beads from the antibodies and proteins. The samples were centrifuged same as before but at RT. The eluates were transferred to new tubes. The eluates were stored at – 80 °C.

Eluates and kept fractions were analyzed. The eluate samples as well as the wash samples were analyzed with SDS-PAGE and western blot analysis, following the same procedure as described in section 3.6.

.

3.9 Precision cut liver slices (PCLS)

Five juvenile cod, selected at random (two females and three males), were collected from tanks at ILAB. The fish were euthanized with a blunt force to the head and the weight and length of the fish were recorded. The fish were sterilized with 70 % ethanol before they were cut open using sterile equipment. The livers were carefully dissected out of the fish and placed in a tray containing PCLS buffer and weighed. The sex of the fish as well as the weight of the reproductive organs were recorded.

The livers were cut into blocks, approximately 3 cm long, 2 cm wide and 1-2 cm in height. The blocks were placed in petri dishes containing culture medium (Table 27) and kept on ice. One of the blocks was glued with superglue to the specimen plate of Leica Vibrating Blade Microtome VTI1200 (Leica, Wetzler, Germany). When the glue had dried, the specimen plate was placed into the buffer tray and the buffer tray was filled with cold PCLS buffer (Table 26). The surrounding ice tray was filled with ice.

The surface of the liver blocks was refined by slicing the top surface before slicing 250 µm slices used for the *ex vivo* liver culture. Slices were cut with a speed of 0.9 mm/s and an amplitude of 3mm. 250 µm slices of good quality were transferred to a petri dish containing cooled culture medium and placed on ice. The slices were further cut into squares with a scalpel, with a diameter of approximately 5 mm x 5 mm. Five liver tissue squares were placed into 9 wells (five in each well) of a 12 well plate, using one plate per fish. The plates were incubated at 10 °C whilst shaking at 50 rpm for 2 h.

3.9.1 Exposure chemicals

Stocks of 9-cis-RA and TBT were prepared in dimethyl sulfoxide (DMSO) with the following concentrations, 50 µM, 500 µM and 5 mM, made to a final volume of 500 µL. The liver tissues were exposed to 0.1 µM, 1 µM and 10 µM final exposure concentrations of either 9-cis-RA or TBT, prepared in culture medium. One control well was set up in each well, in which the liver tissues were exposed to 0.2 % DMSO. 5 pieces per fish were in each exposure well. The tissue cultures were exposed to the chemicals for 48 h at 10 °C whilst shaking at 50 rpm. After this, the tissues were snap-frozen in liquid nitrogen (N_2) and stored at -80 °C.

3.10 MTT metabolic activity assay

For the MTT assay, 12-well plates with PCLS were made as described above. However, liver slices from four instead of five fish were cultured and left to acclimatize for 1 h at 10 °C whilst shaking at 50 rpm before exposure to TBT and 9-cis-RA following the same method as described above. After 48 h exposure, the weight of the slices in each well were recorded. Afterwards, the media was removed from the wells, and replaced by 1 mL of 3-(4,5-Dimethylthiazol-2-yl)-2,5-diphenyltetrazolium bromide (MTT) solution, made by adding 2 mg per mL Leibovitz's L-15 medium, to a final volume of 40 mL. The plates were incubated at RT for 90 min whilst shaking at 70 rpm in the dark. MTT was removed completely, and the tissues washed once with 1 mL 1x PBS before 1 mL100 % DMSO was added into each well and the plates incubated for 20 min while shaking at RT. 100 µL of the DMSO from each well was pipetted in triplicates into 96-well plates, and the metabolic activity was measured at 570 and the background absorbance was measured at 650 nm using the PerkinElmer EnSpire plate reader.

3.11 LDH cytotoxicity assay

Culture medium from exposed PCLS were collected for measurements of lactate dehydrogenase activity and were pipetted in triplicates of 50 µL into 96-well plates. Fresh complete culture medium was also pipetted in triplicates of 50 µL into both plates as a blank control. The bottles from the cytotoxicity detection kit PLUS (LDH) (Roche) were thawed and mixed in a ratio of 1:45 of solution 1 and 2. 50 µL of the mixture was added to each well. The contents were mixed by gently moving the plates from side to side, before incubating the plates in the dark for 5 min. The absorbance of lactate dehydrogenase (LDH) enzymatic activity was measured at 490 nm and the background absorbance measured at 650 nm using the PerkinElmer EnSpire plate reader.

3. 12 RNA extraction from PCLS

3.12.1 RNA Extraction procedure

The lab bench and equipment were washed with 70 % ethanol. PCLS samples were kept on dry ice and weighed. The liver tissues were homogenized in 300 µL TRI Reagent (Sigma, T9424) using the manual homogenizer tool. 950 µL additional TRI reagent was added after

homogenization and the contents mixed by inverting the tubes. The tubes were placed immediately on ice.

Once all samples were homogenized, they were incubated at RT for 5 min. 250 µL chloroform (Sigma-Aldrich, 34854) was added and the tubes were shaken vigorously for 15 sec, incubated at RT for 8-9 min, and then centrifuged at 12.000 x *g* for 15 min at 4 °C. 0.4 mL of the top layers, referred to as the aqueous phases in the protocol, were transferred to new sterile tubes and equal amounts of isopropanol were added. The aqueous phase and isopropanol were mixed and incubated at RT for 8–13 min, before centrifugation at 12.000 x *g* for 10 min at 4 °C. The supernatants were discarded, and the RNA pellets were washed with 1 mL 75 % ethanol prepared in RNase free water. The samples were vortexed, then centrifuged at 7.500 x *g* for 1 min at 4 °C, and stored at -20 °C O/N.

Ethanol was removed completely by centrifuging the pellets at 7.500 x *g* for 1 min at 4 °C and by pipetting out any remaining fluid. The pellets were left to dry with the cap of the tubes open until the pellets had dried completely (35–38 min). The RNAs were dissolved in 100 µL RNAse-free water by vortexing and spinning down the tubes, then incubating them at 60 °C in a heating cabinet for 20 min. During the incubation period, the tubes were vortexed and spun down at intervals to help with dissolving RNA. The samples were then immediately placed on ice. The concentration and purity of the RNAs were measured using nanodrop**.**

3.12.2 Assessing RNA integrity with agarose gel electrophoresis

1 % agarose was dissolved in 1X TAE buffer by heating in the microwave. The agarose solution was left to acclimatize to 60 °C in the heating cabinet. 0.5 µL GelRed was added to 50 mL agarose solution and mixed before casting (Table 28). The gel was left to cast for 1 h in the casting tray, before submerging the gel in 1x TAE buffer.

RNA loading buffer was prepared with 1.2X Blue/Orange loading dye and 79 % formamide, to a final volume of 1 mL (Table 29). 9 µL of the loading buffer was mixed with 1 µL dissolved RNA. Prior to loading, the samples were vortexed and spun down, then incubated at 60 °C for 5 min before they were spun down again and placed on ice. The samples were loaded on the gels together with 5 µL 2-log DNA ladder and run at 80 V for 1 h and 30 min. BioRad's ChemiDoc^{TM} XRS+ imaging system was used for gel visualization.

3.13 Complementary DNA (cDNA) synthesis

cDNA was synthesized using extracted RNA as templates (Section 3.12) and by following the instructions in the cDNA protocol provided by iScript™. 1 µg RNA was mixed with nuclease-free water (NF-water) to a total of 10 µL and incubated at 70 °C for 5 min, followed by cooling at 4 °C in the PCR machine (Bio-Rad, T100™ Thermal Cycler). A mixture was prepared with 2x iScript reaction mix, 1 µL iScript Reverse transcriptase, and NF-water for each reaction. The volume was adjusted to match the number of reactions needed. 10 µL of this mixture was added to 1 µg RNA and the samples were spun down. One reaction was set up as a no reverse transcriptase control (NRC) and consisted of 1 µg RNA (selected at random) and iScript reverse transcriptase substituted by NF-H_2O. cDNA was produced in the PCR machine using the program described in Table 35. The cDNAs used in qPCR analyses were diluted 1:10 in NF-H_2O. cDNA used for assessing primer efficiency were pooled from 8 samples and a serial dilution was performed as required. The cDNA was stored at –20 °C until qPCR analyses were performed.

Table 35. PCR program for cDNA synthesis

Step	Temperature	Time
Priming	25 °C	5 min
Reverse transcription	46 °C	30 min
Reverse transcriptase inactivation	95 °C	1 min
Storage	4 °C	-

3. 14 quantitative Polymerase Chain Reaction (qPCR)

5 µL synthesized cDNA were pipetted in duplicates into a 96-well plate. The NRC was also pipetted in duplicates, as well as a control with NF-H_2O. A master mix was prepared with SsoAdvanced™ Universal SYBR® Green Supermix (Bio-Rad) and 2 µM forward and reverse primer for the gene of interest (Table 2). The primers were designed using the primer3 database and were specific for the following genes: *pparg*, *sqlea*, *rbp2* and *ebp*. *actb2* was included in the qPCR analyses as a housekeeping gene. 15 µL of the master mix was pipetted into the wells containing cDNA and mixed thoroughly by gently pipetting. The plate was centrifuged at 2000 x *g* for 2 min at 4 °C, before running in the qPCR machine (Bio-Rad, CFX96™ Real-Time System) according to Table 35. Each gene was tested per plate. A second plate, set up the same,

was also run in qPCR, so the Cq values obtained could be compared between the two plates. This was to make sure there were no large discrepancies due to pipetting errors.

Table 35. Cycle program for qPCR

Step	Temperature	Time	Cycles
Denaturation	95 °C	1 min	1
Denaturation	95 °C	10 sec	39
Extension/Annealing	55 °C	15 sec	
Elongation	72 °C	20 sec	
Melting curve	95 °C	10 sec	-
	65 °C	5 sec	-
	95 °C	-	-

3. 15 Data treatment and statistics

3.15.1 MTT and LDH assays

The MTT and LDH data were treated the same. The background absorbance values were subtracted from the actual absorbance reads (data obtained from the PerkinElmer EnSpire plate reader) in Excel. The average absorbance reads were calculated and divided by the weight of the tissue pieces (abs/mg). The values were normalized against the solvent control (0.2 % DMSO), adjusted to 100 %. One-way-ANOVA with Dunnett's multiple comparisons test was performed in Prism 9 (GraphPad).

3.15.2 qPCR analysis

The Cq values obtained from the qPCR machine were processed to obtain the fold change values in Excel (Microsoft, 2020) using the protocol from Schmittgen and Livak (2008). The average Cq-values of the genes tested, *pparg, rbp2, ebp* and *sqlea,* were normalized against the reference gene, *actb.2.* Change in target gene expression was then calculated as fold change to relative to the solvent control (0.2 % DMSO). Statistical analysis on the average fold change values was performed in GraphPad Prism 9, which was also used to produce graphical illustrations of the data. Mixed effects analysis and Dunnett's multiple comparisons test was performed on transformed data (y = log2(Y)). Gaussian distribution and sphericity were assumed, and the experimental design was set to matching/pairing.

4 RESULTS

4.1 Comparison of the immunogen sequence between the gmRxr subtypes

Two custom-made polyclonal antibodies (pAb), denoted as pAb #5789 and pAb #5859, were produced by GenScript by using a peptide sequence originating from gmRxra as an immunogen. As there are three additional subtypes of Rxr in Atlantic cod, i.e. gmRxrb1, gmRxrb2 and gmRxrg (Borge, 2021; Prebensen, 2023), it was of interest to assess the sequence similarity between the proteins in the region that was used for immunization. Sequence similarity was hence analyzed with a multiple sequence alignment (MSA).

The results of the MSA showed high sequence similarity among the gmRxr subtypes in the region used as an immunogen (Figure 9). The most prominent difference between the sequences in this part of the proteins were observed by 14 additional aa residues present in helix 7 of the two gmRxrb isoforms, which is not present in gmRxra or gmRxrg (Figure 9). In the region used for immunization, gmRxrg shared the highest sequence similarity to gmRxra, with only 13 substituted residues. Of the two gmRxrb subtypes, gmRxrb2 demonstrated the highest sequence identity to gmRxra (Figure 9). Thus, the order of similarity to the immunogen was as follows: gmRxrg, gmRxrb2, and gmRxrb1, with the percent identity scores of 93 %, 86 %, and 82 %, respectively.

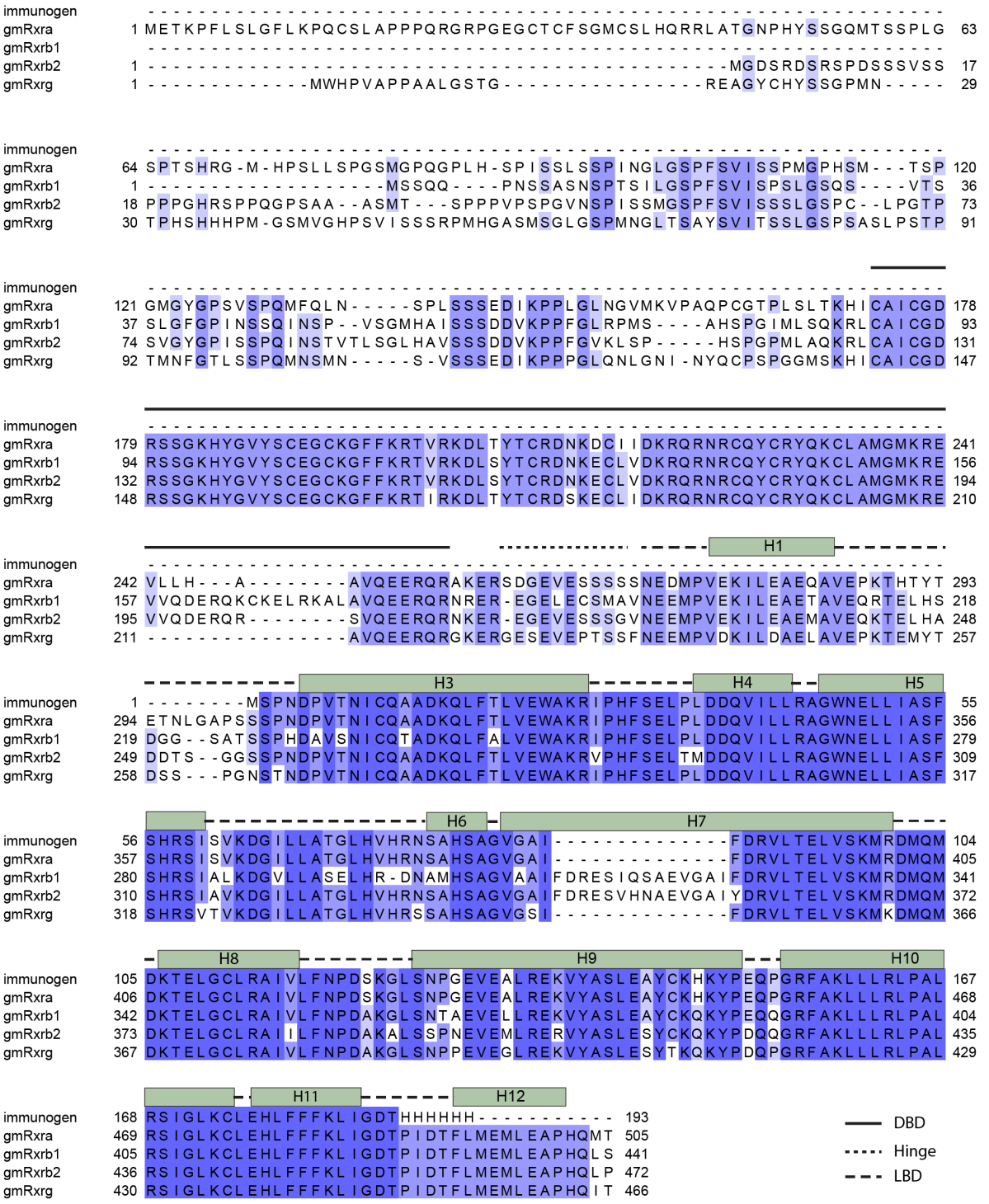

Figure 9. Multiple sequence alignment (MSA) of the retinoid X receptor (Rxr) amino acid sequences from Atlantic cod (*Gadus morhua*). The MSA covers the full sequences of gmRxra, gmRxrb1, gmRxrb2, and gmRxrg, as well as the immunogen. Percentage (%) identities between the sequences are indicated with a blue color scheme, with the darkest blue showing identical residues in all the sequences. Clustal Omega (EMBL-EBI) was used for constructing the alignment and visualization was done in Jalview. Annotation of the DNA binding domain (DBD), the hinge region, the ligand binding domain (LBD) and helices 1, 3-13 is included. The annotation was made based on the annotation by Borge (2021).

4.2 Assessment of antibody binding to proteins in Atlantic cod tissues

Since the region in Rxra that was used as an immunogen is very similar among all the subtypes (Figure 1), it was anticipated that the pAbs (pAb #5789 and pAb #5859) could also bind gmRxrb1, gmRxrb2, and gmRxrg. To determine in which tissues immunoreactive proteins would occur, WB analysis was performed on homogenized tissues of brain, skin, stomach, liver, muscle, heart, head kidney, and ovaries. These tissues were chosen based on previous data from tissue-specific gene expression analyses of Atlantic cod Rxr subtypes (Borge, 2021). Prior to WB analysis, an SDS-PA gel was stained with Coomassie dye R-250 to visualize if any tissues appeared extensively degraded after homogenization and to compare the protein pattern in the different tissues. Distinct bands were detected in all tissues, apart from some smearing in the sample derived from head kidney (Figure 10A). Overall, the SDS-PAGE analyses suggested little visible protein degradation after homogenization. An immunogen control corresponding to the gmRxra immunogen was provided by GenScript (Table 28) and included as a positive control for antibody recognition and binding.

WB analyses were performed with the two antibodies pAb #5789 and pAb #5859 individually. The immunogen control was observed as an immunoreactive band at approx. 19 kDa (Figure 10B, arrow a, Figure 10C, arrow f), estimated with a standard curve generated from the MW protein standards (Figure A1, in Appendix). This corresponded roughly with the theoretical MW provided by GenScript (20 kDa). Another band at 42 kDa was also detected in the immunogen control, which may represent a dimer of the immunogen (Figure 10B, arrow b, Figure 10C, arrow g).

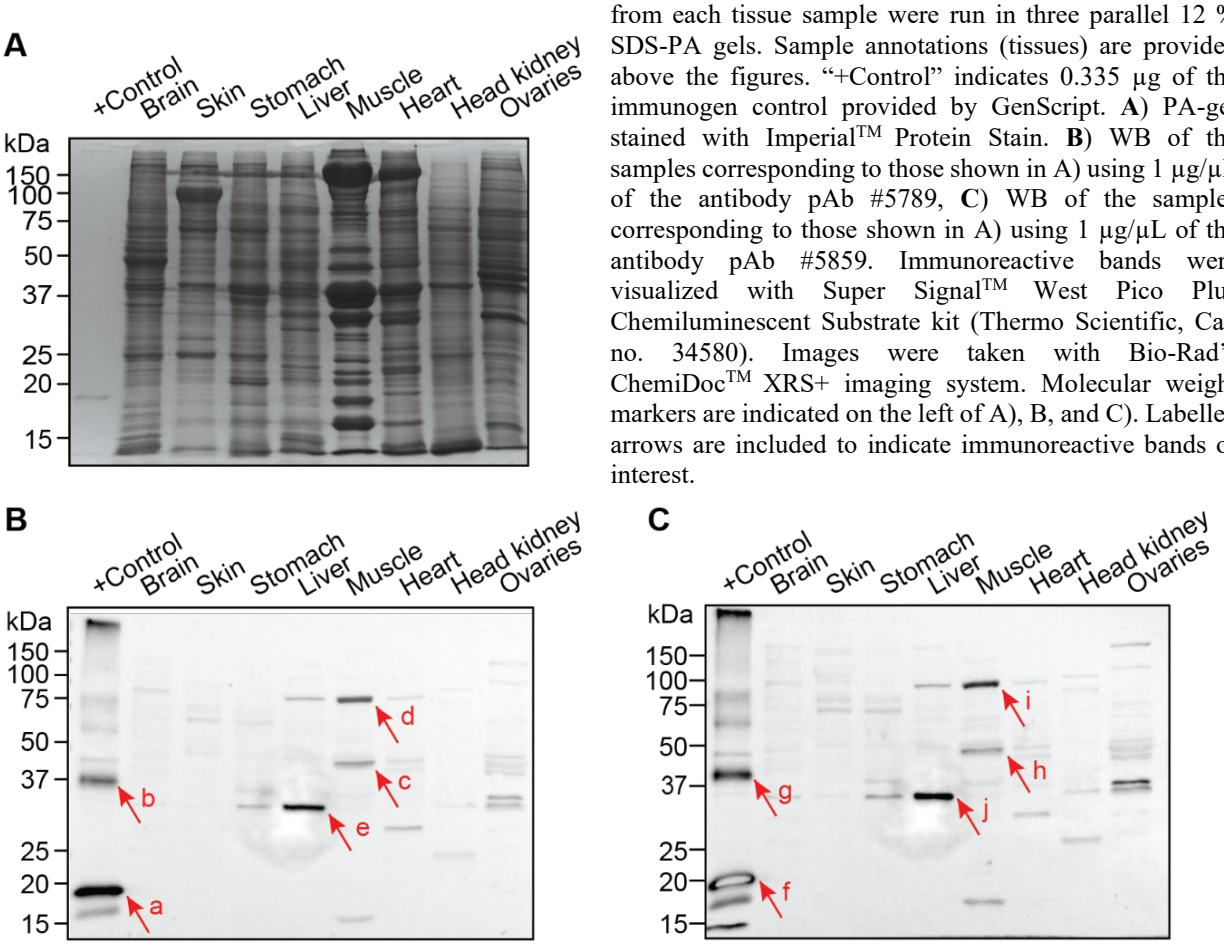

Figure 10. SDS-PAGE and WB analyses of homogenized tissues from Atlantic cod. 15 µg of protein from each tissue sample were run in three parallel 12 % SDS-PA gels. Sample annotations (tissues) are provided above the figures. "+Control" indicates 0.335 µg of the immunogen control provided by GenScript. **A**) PA-gel stained with Imperial™ Protein Stain. **B**) WB of the samples corresponding to those shown in A) using 1 µg/µL of the antibody pAb #5789, **C**) WB of the samples corresponding to those shown in A) using 1 µg/µL of the antibody pAb #5859. Immunoreactive bands were visualized with Super Signal™ West Pico Plus Chemiluminescent Substrate kit (Thermo Scientific, Cat. no. 34580). Images were taken with Bio-Rad's ChemiDoc™ XRS+ imaging system. Molecular weight markers are indicated on the left of A), B, and C). Labelled arrows are included to indicate immunoreactive bands of interest.

The resulting patterns of immunoreactive bands produced by the two antibodies were very similar (Figure 10B, 2C). Immunoreactive proteins were detected in all the tissue samples, but the patterns revealed in the various tissues differed from each other, although some bands of the same size were identified in many tissues. At the expected MWs of the canonical (full-length) gmRxr proteins (55.4 kDa Rxra, 49.1 kDa Rxrb1, 51.9 kDa Rxrb2 and 51.3 kDa Rxrg), a band with intermediate intensity was located in the muscle tissue sample, while two weaker bands were found in the heart and ovaries samples at approx. 49 kDa (Figure 10B, arrow c, Figure 10C, arrow h). Above the expected MW, a prominent band in the muscle and liver samples with a MW of approx. 82 kDa was observed, with a few fainter bands in the brain, liver, and heart samples (Figure 10B, arrow d, Figure 10C, arrow i). Below the theoretical MW of the Rxr subtypes, the most prominent immunoreactive band was detected in the liver samples, with a MW of approx. 35 kDa (Figure 10B, arrow e, Figure 10C, arrow j). Less prominent bands at approximately the same size were observed in the ovaries, particularly on the pAb #5859-incubated membrane (Figure 10C). Weaker bands at 35 MW were also detected in brain, skin, stomach, and head kidney tissues (Figure 10B, 10C).

4.3 Comparing pre-immune and immune serum in WB analyses

Although immunoreactive bands were detected in several tissues (Figure 10), the liver was chosen for further studies since precision cut liver slices (PCLS) were to be used in later experiments. The liver was also of interest due to its important role in relation to the biotransformation of xenobiotics in teleosts (Churcher et al., 2015).

To determine if any of the immunoreactive bands in the Atlantic cod liver samples originated from antibodies present in serum prior to the injection of rabbits with the Rxra immunogen, WB analyses were repeated with pre-immune serum. SDS-PAGE was performed with homogenized liver and thereafter electroblotted onto two nitrocellulose membranes. The resulting blots were briefly stained with Ponceau S and the membranes were cut in half, resulting in four membranes containing the same liver samples. One of the membranes was incubated with pre-immune serum from the rabbit in which pAb #5789 had been purified from, while the other membrane was incubated with pre-immune serum from the rabbit in which pAb #5859 had been purified from. The two remaining membranes were incubated with either pAb #5789 or pAb #5859.

The immunogen control (peptide used for immunization) was also included in these WB analyses, and as observed earlier the same band at approx. 19 kDa appeared when the membranes were incubated with either pAb #5789 or pAb #5859 (Figure 11A, 11D). Importantly, no bands were detected for the immunogen control when the membranes were incubated with either of the two pre-immune serums (Figure 11B, 11E).

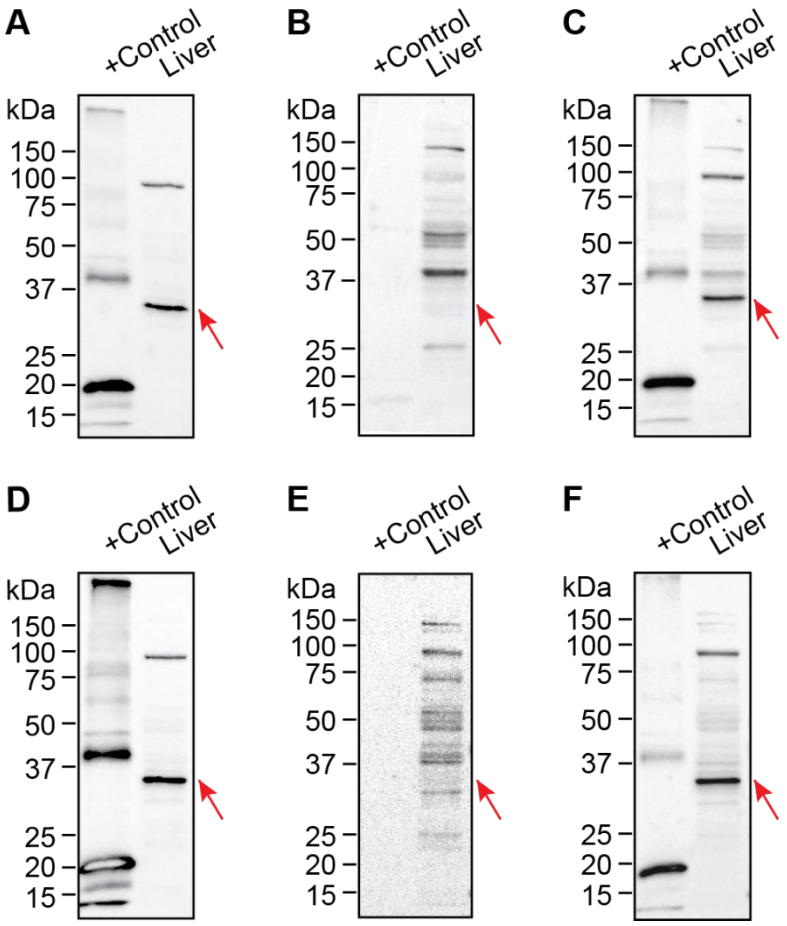

Figure 11. Comparison of immunoreactive proteins in liver by incubation with antibodies and pre-immune serum in western blot analyses. 15 µg liver tissue homogenates were separated in 12 % SDS-PA gels, as well as 0.335 µg of immunogen control (provided by GenScript), against. The nitrocellulose membranes were cut in half, to a total of 4 membranes. The membranes were incubated O/N with 1 µg/µL of **A**) pAb #5789, **B**) Pre-immune serum of pAb #5789, **C**) membrane in **B**, re-incubated with 1 µg/µL pAb #5789, **D**) 1 µg/µL pAb #5859, **E**) Pre-immune serum of pAb #5859, and **F**) membrane in **E**, re-incubated with 1 µg/µL pAb #5859. Immunoreactive bands were visualized with Super Signal™ West Pico Plus Chemiluminescent Substrate kit. Images were taken with Bio-Rad's ChemiDoc™ XRS+ imaging system. Precision Plus Protein™ All blue standards molecular weight markers are indicated on the left of each subfigure. Arrows are included to indicate the presence or absence of the band of interest at 35 kDa.

As shown previously, two immunoreactive bands were observed in the liver tissue with MWs of 82 and 35 kDa for membranes treated with both pAb #5859 and pAb #5789, in which the 35 kDa band was more prominent (Figure 11A, 11D, arrows). In the membranes incubated with pre-immune serums, no immunoreactive bands at 35 kDa were detected (Figure 11B, 11D, arrows)

The membranes treated with the pre-immune serums were also re-incubated with their corresponding antibodies to directly compare the patterns of immunoreactive proteins. Upon doing so, the band with a MW of 35 kDa appeared in both membranes (Figure 11C, 11F, arrows). This was also visualized by merging the images recorded of the membranes treated

with pre-immune serum with the membranes treated with the corresponding antibodies (Appendix, Figure A2).

4.4 Identification of the 35 kDa immunoreactive protein

An immunoreactive protein of 35 kDa was detected in the western blot analysis of liver tissue with both pAb #5789 and pAb #5859 (Figure 10), and this protein was not stained when incubating with pre-immune serums (Figure 11). It was thus of relevance to confirm the identity of the immunoreactive protein as a gmRxr subtype. To do that, 2D-PAGE was employed and followed by semi-dry western blotting and mass spectrometry (MS) analyses. 2D-PAGE has the advantage of separating proteins based on both MW and pI, and thus increasing the resolution of the protein sample.

Liver tissue homogenates were separated with 2D-PAGE as described in Section 3.7. In addition, a liver tissue homogenate sample was applied on a filter paper and run besides the MW marker as a regular 1D separation. Proteins on one of the 2D-PA gels were transferred to a nitrocellulose membrane by use of semi-dry western blotting. After the electrophoretic transfer, the membrane was stained for proteins with Ponceau S and an image was taken using the Bio-Rad's ChemiDoc^{TM} XRS+ imaging system. This was done for creating a reference map for later identifying the immunoreactive spots on a parallel gel stained with Imperial^{TM} Protein stain (Coomassie dye R-250) (Figure 12B). This procedure was performed with only one of the antibodies since the antibodies had shown similar results in the WB experiments described above. Immunoreactive spots were visualized with Super Signal^{TM} West Pico Plus Chemiluminescent Substrate kit (Figure 12A). The images recorded of the Ponceau S-stained membrane and of the PICO substrate-treated membranes (showing immunoreactive spots) were merged *in silico* to locate the immunoreactive spots in the Ponceau S-stained membrane.

In the Ponceau S-stained membrane, only the most abundant proteins were visualized, both from the liver homogenate control (1D sample) and those migrating from the IPG strip (Figure 12A). Proteins of varying MW were present and most of the protein spots were centered on the membrane around pH 6 (Figure 12A). Furthermore, several immunoreactive spots were detected on the membrane after treatment with PICO substrate, with the most abundant spot located around 35 kDa (Figure 12B, arrow a). An immunoreactive band from the homogenate control (1D sample) was also detected with a MW of 35 kDa (Figure 12B, arrow b),

corresponding to the immunoreactive protein observed in the previous WB analyses. The spot at 35 kDa was thus predicted to be the spot of interest.

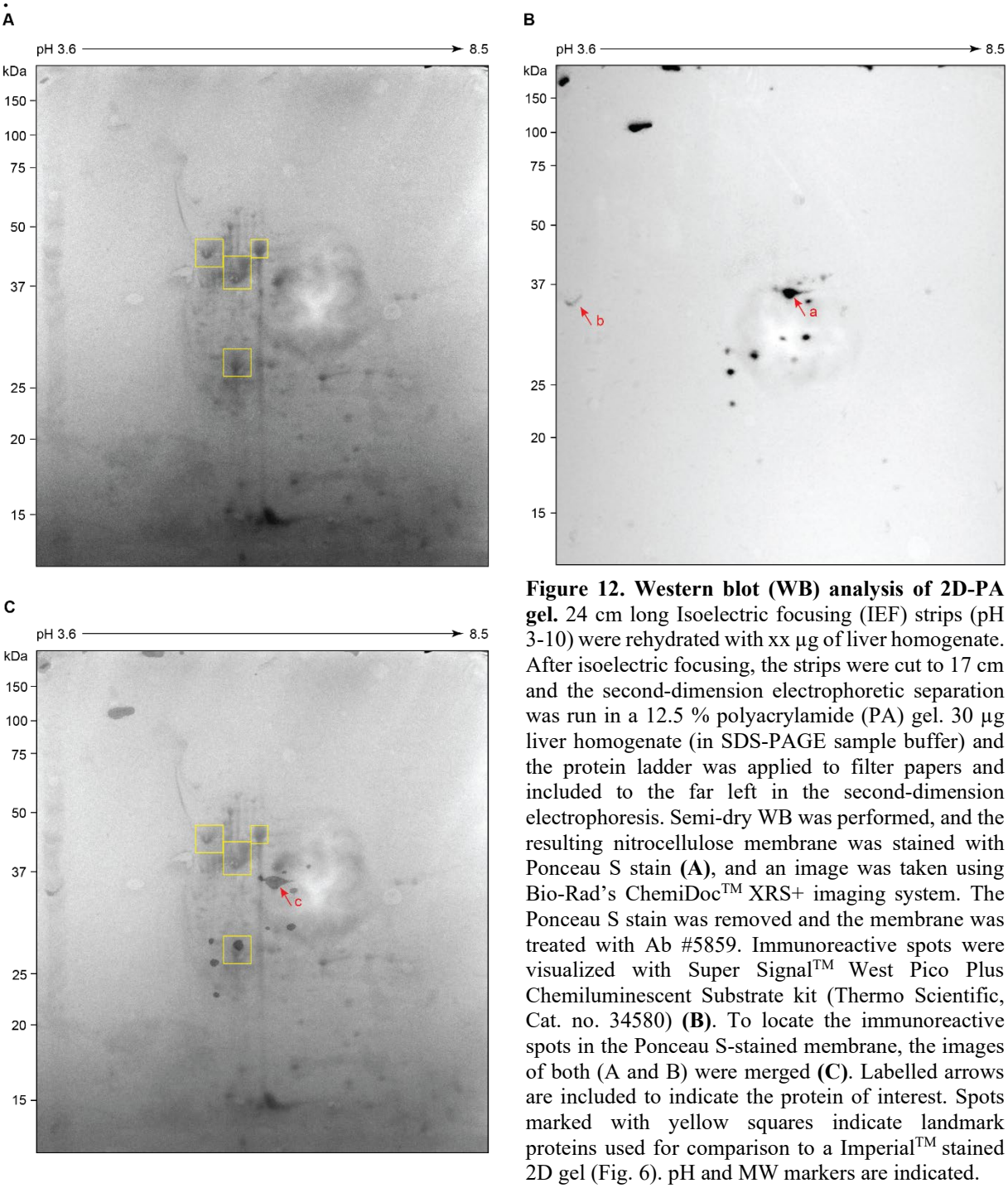

Figure 12. Western blot (WB) analysis of 2D-PA gel. 24 cm long Isoelectric focusing (IEF) strips (pH 3-10) were rehydrated with xx µg of liver homogenate. After isoelectric focusing, the strips were cut to 17 cm and the second-dimension electrophoretic separation was run in a 12.5 % polyacrylamide (PA) gel. 30 µg liver homogenate (in SDS-PAGE sample buffer) and the protein ladder was applied to filter papers and included to the far left in the second-dimension electrophoresis. Semi-dry WB was performed, and the resulting nitrocellulose membrane was stained with Ponceau S stain **(A)**, and an image was taken using Bio-Rad's ChemiDoc™ XRS+ imaging system. The Ponceau S stain was removed and the membrane was treated with Ab #5859. Immunoreactive spots were visualized with Super Signal™ West Pico Plus Chemiluminescent Substrate kit (Thermo Scientific, Cat. no. 34580) **(B)**. To locate the immunoreactive spots in the Ponceau S-stained membrane, the images of both (A and B) were merged **(C)**. Labelled arrows are included to indicate the protein of interest. Spots marked with yellow squares indicate landmark proteins used for comparison to a Imperial™ stained 2D gel (Fig. 6). pH and MW markers are indicated.

To locate the immunoreactive spot on the corresponding Imperial™ Protein -stained 2D gel, the images of the membrane after treatment with Ponceau S stain and after treatment with PICO

substrate were merged *in silico* (Figure 12C). When comparing the spot pattern adjacent to the most abundant immunoreactive spot in the merged image with the spot pattern of the Imperial™ Protein-stained gel, it was possible to locate spots of interest and it became evident that the large immunoreactive spot in the membrane covered two spots (Figure 12C, arrow c, Figure 13). pAb #5859 could hence have bound to either of these proteins, or both, as the signal from the antibody binding could have been so strong that it masked both proteins. Thus, the two spots were of interest and excised from the Imperial™ -stained 2D-PA gel and sent to the proteomics core facility (PROBE) at the University of Bergen for protein identification with mass spectrometry (MS) analysis.

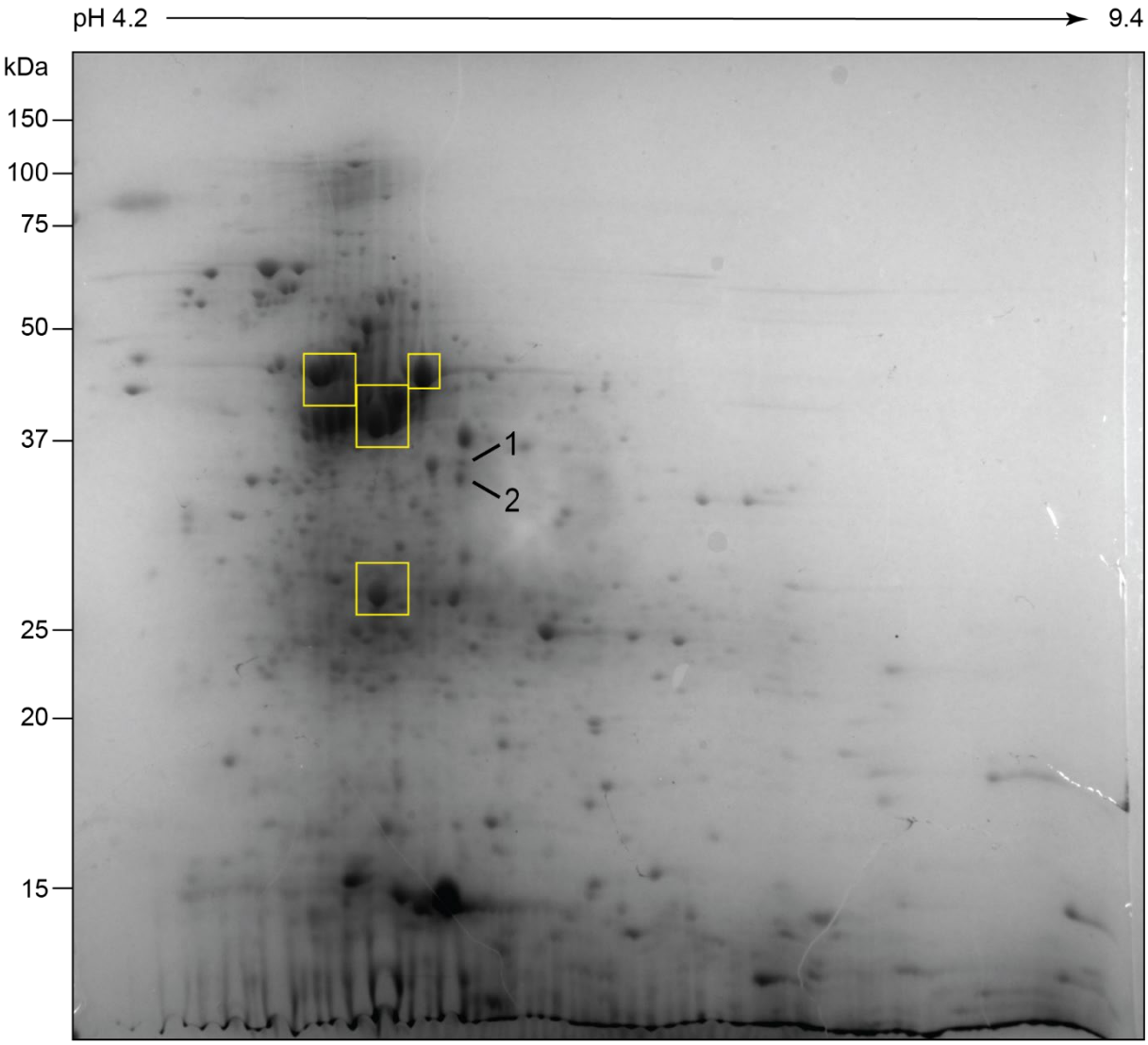

Figure 13. Locating the immunoreactive proteins in a Coomassie stained 2D-PA gel. A 24 cm long isoelectric focusing (IEF) gel strips (pH 3–10) were rehydrated with 750 µg liver homogenate prepared in rehydration prior to IEF. The IPG strip was cut to 18 cm, and the second-dimension electrophoresis was run in a 12.5 % polyacrylamide (PA) gel. Precision Plus Protein™ All Blue Standards Molecular weight markers are indicated to the left and pH above the gel. The gel was stained with Imperial Protein™ stain (Coomassie dye R-250). The image was taken with the Bio-Rad ChemiDoc™ XRS+ imaging system. The membrane from Figure 12 was used to locate the proteins of interest in the gel, here denoted as spot 1 and 2.

4.4.1 Protein identification by mass spectrometry (MS) analysis

The results of the MS analysis revealed that each spot contained numerous different proteins. However, no peptides belonging to any Rxr subtype was detected in spot 1, while in spot 2 there were four peptide hits that matched with high significance to parts of the gmRxrb1 aa sequence (Figure 14). The combination of these four sequences could only be found in the LBD of gmRxrb1.

Figure 14. Mass spectrometry peptide identifications displayed in the gmRxrb1 protein sequence. Two protein spots from a 2D PA gel (Figure 13) were sent to MS analysis at the PROBE unit at the University of Bergen (UiB). Of the protein hits that were retrieved in gel spot 2, one hit consisted of four peptides identical to those found in gmRxrb1. The four peptide sequences have been indicated in the sequence of gmRxrb1 in green, blue, purple, and yellow. The protein sequence was prepared in Jalview and annotated in Adobe Illustrator. The DNA-binding domain (DBD), hinge region, ligand-binding domain (LBD) and helix 1 and 3-12 are also shown, based on the annotation by Borge (2021).

4.6 Immunoprecipitation

After confirming that pAb #5859 recognizes and binds to gmRxrb1, it was of interest to use the antibodies in immunoprecipitation (IP) experiments to assess whether they were able to bind to the gmRxrb1 protein when it is in its native state. IP was performed in two rounds and testing the antibodies individually. IP fractions were then analyzed in WB and the resulting membranes were incubated with either pAb #5789 or pAb #5859, depending on which pAb had been used in the IP.

The immunogen control and the immunoreactive protein in liver homogenates were stained at their expected locations at 19 and 35 kDa in the WB analyses (Figure 15) (Ponceau S stains can be found in Appendix, Figure A3). As expected, the IP liver homogenates prior to IP treatment were found to have the same immunoreactive band as in the homogenate control (located at 35 kDa in both membranes (Figure 15A, arrow a, Figure 15B, arrow d). Bands of the same size

were also observed in the Wash 1 fraction. There seemed to be little to no immunoreactive protein in the Wash 2 and Wash 3 wells (Figure 15).

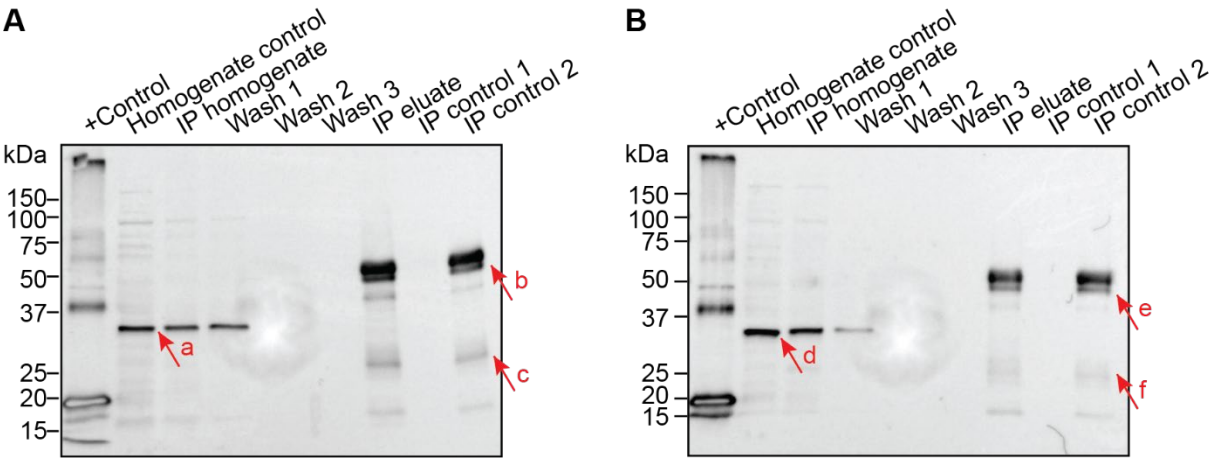

Figure 15. Immunoprecipitated (IP) liver homogenates analyzed with western blotting (WB). 1 mL liver homogenates were immunoprecipitated with Protein G agarose beads (Roche, Ca. no. 11 243 233 001). Immunoprecipitation was performed with both pAb #5789 and pAb #5859. Two IP controls were included, one consisting of beads and homogenate, but no antibody added ("IP control 1"), and one consisting of beads and antibody, but no homogenate ("IP control 2"). Western blot analysis was performed with the IP eluates and the IP controls, 0.335 µg immunogen control, 15 µg liver homogenates tested previously ("Homogenate control"), as well as against the homogenate used in IP ("IP homogenate") and wash fractions ("Wash 1/2/3"). **A)** Membrane incubated with 1 µg/µL pAb #5789 with the IP procedure tested with pAb #5789. **B)** Membrane incubated with 1 µg/µL pAb #5859 with the IP procedure tested with pAb #5859. Immunoreactive bands were visualized with Super Signal™ West Pico Plus Chemiluminescent Substrate kit. Images were taken with Bio-Rads ChemiDoc™ XRS+ imaging system. Molecular weight markers are indicated on the left of A) and B). Labelled arrows are included to present the immunoreactive band at 35 kDa, and the heavy and light chains belonging to IgG. bands at different MWs.

No immunoreactive band at 35 kDa were detected in the IP eluates, nor in IP control 1 and 2 (Figure 15). Instead, abundant bands were observed slightly above 50 kDa and some weaker bands at approx. 26 kDa in the IP eluate and in IP control 2, which only contained beads and antibodies, and no liver homogenate (Figure 15A, arrow b and c, Figure 15B, arrow e and f). These bands reflect the polypeptide chains of the IgG antibodies, which have expected MWs of about 55 and 25 kDa for the heavy chains and the light chains, respectively (Lal et al., 2005). These results indicated that a gmRxr specific band was not retained in the IP eluates, and thus had been removed during the washing steps. In addition, no immunoreactive bands could be observed in IP control 1, consisting of homogenate and beads and no antibody (Figure 15A, 15B). This showed that there was no unspecific binding of immunoreactive bands from gmRxr to the agarose beads.

4.6.1 Verification of gmRxrb1 in the Wash fractions of Immunoprecipitation

Since the band of interest was not detected in the IP eluates (Figure 15), WB analysis was performed with unbound fraction 1 and 2 of the IP procedure, as well as with the second wash with Wash buffer 1 (Table 22), to see if there were any remaining bands of interest after the first wash (Figure 15). If any bands were present in these wash fractions, it could indicate that the antibodies did not bind the immunoreactive protein during the IP.

Treatment with the two antibodies gave similar results this time as well (Figure 16). In the unbound fractions, the band of interest was detected at 35 kDa, and had approximately the same intensity as the control IP homogenate from before starting IP (Figure 16).

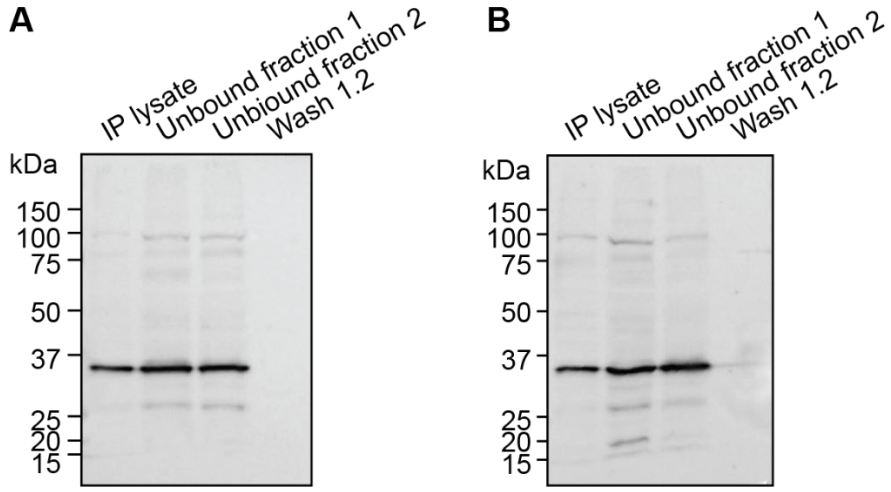

Figure 16. Western blot analysis of unbound fractions from immunoprecipitation. Immunoprecipitation was performed with 1 mL liver homogenate and using either pAb #5789 or pAb #5859 attached to agarose G beads (Roche, Ca. no. 11 243 233 001) and the protocol from Roche (described in section 3.8). Western blot analysis was performed with fractions of the liver homogenate prior to starting IP, pre- and clearings, as well as a fraction of the second wash in Wash buffer 1. The resulting nitrocellulose membranes were incubated O/N with 1 µg/µL of **A**) pAb #5789 and **B**) pAb #5859. Immunoreactive bands were visualized with Super Signal™ West Pico Plus Chemiluminescent Substrate kit (Thermo Scientific, Cat. no. 34580). Images were taken with Bio-Rad's ChemiDoc™ XRS+ imaging system. Molecular weight markers are indicated on the left of A) and B).

The band of interest was prominent in the unbound fractions at 35 kDa (Figure 16). No visible bands were observed in the well containing a sample from the second wash with wash buffer 1 (Table 22) of the homogenate treated with pAb #5789 (Wash 1.2) (Figure 16A). However, in the "wash 1.2" well for the pAb #5859-treated sample it was a weak band in this region, suggesting some immunoreactive protein was still present during this wash step (Figure 16B).

In summary, the results showed that there were no bands of interest in the IP eluate samples (Figure 15). Instead, they were present in the primary wash fractions, as well as the clearings (Figure 16). This suggests that the antibodies pAb #5789 and pAb #5859, did not bind to the

immunoreactive protein detected in the WB analyses under the non-denaturing conditions used in this IP assay.

4.7 3D visualization of the topology of the peptide sequence used to immunize rabbits

A 3D crystal structure of hRXRa was modified in PyMOL to visualize potential binding sites for antibodies in the native structure of gmRxrs. To date, there are no structures for Rxr from Atlantic cod that exists. However, structures of RXR from other species with similar sequences exist. Thus, the gmRxra sequence was run in pBLAST against the RCSB Protein Data Bank (RCSB-PDB database). The structure of the top hit from human RXRa (hRXRa) was retrieved with the PDB id 3DZY. The structure was downloaded into PyMol and modified so that only hRXRa and the protein sequence corresponding to the region in gmRxra that was used for immunization were visualized.

To assess the similarity between hRXRa and gmRxra, particularly in the region of gmRxra used for immunization, the aa sequences were aligned in an MSA using Clustal Omega. The region of hRXRa corresponding to the region in gmRxra used for immunization, differed by only two aa residues, substituting glycine in gmRxra with alanine in hRXRa (Figure 17A). The percentage identity (%) between the two sequences was 99 %. Due to this strong sequence identity, the human version of the RXRa protein was a good candidate for visualizing the 3D structure of the immunogen.

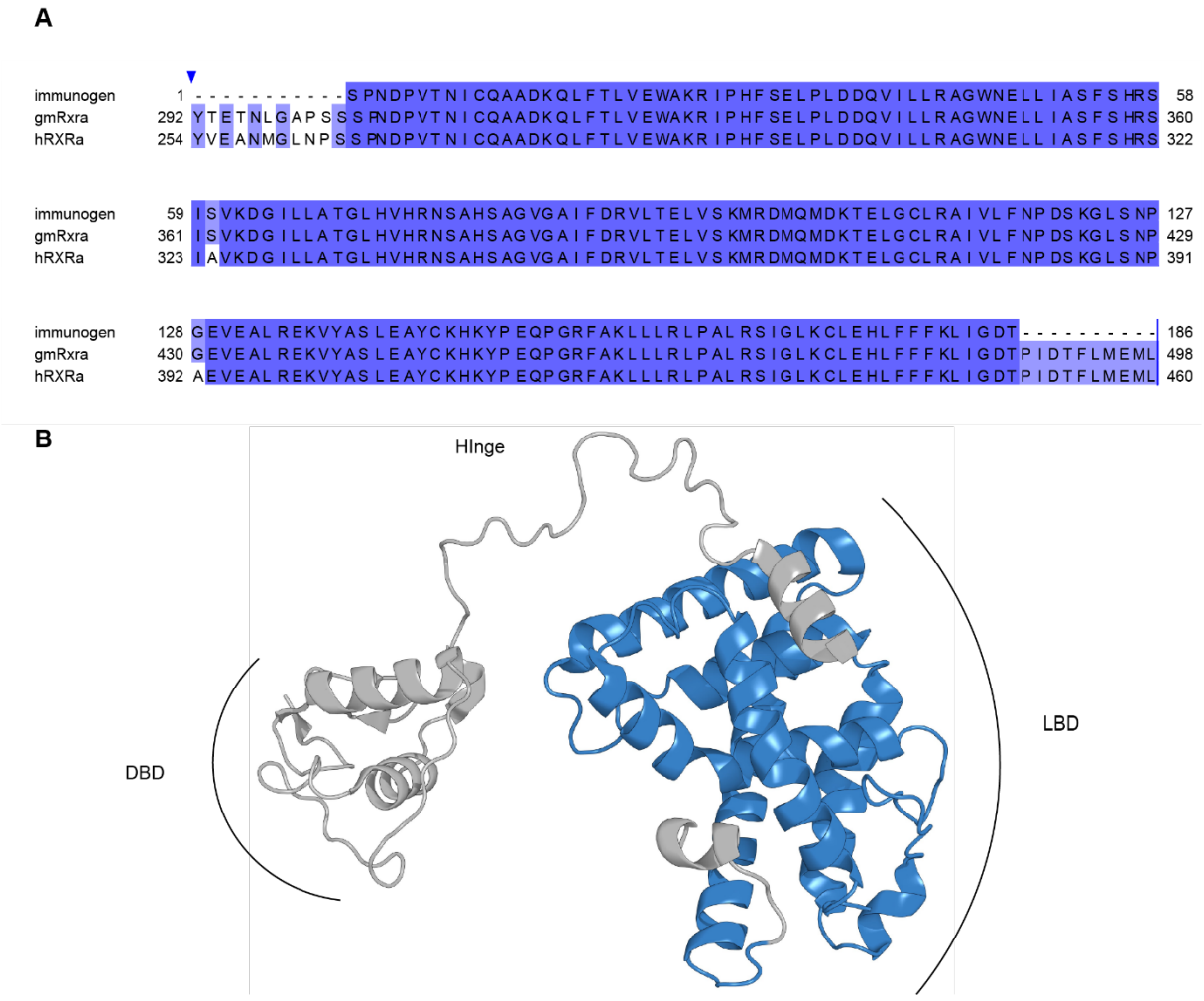

Figure 17. 3D visualization of the peptide sequence used for immunization. (A) The MSA covers the region in gmRxra used for immunization and corresponding regions in hRXRa**.** The immunogen is included in the alignment as well as a few flanking residues on each side of hRXRa and gmRxra. Percentage (%) identity between the sequences is indicated with a blue color scheme, with the darkest blue showing identical residues in all the sequences. Clustal Omega was used for constructing the alignment and visualization was done in Jalview. **(B)** 3D visualization of hRXRa with the immunogen sequence colored in blue, and the remaining protein shown in grey. The structure was created using the PyMol software and was modified from the structure obtained in PDB with the id: 3DZY. The DNA-binding domain (DBD), the hinge region and the ligand-binding domain (LBD) are annotated.

From the final structure prepared in PyMol, it was shown that hRXRa consisted of the DBD and the LBD linked together by the hinge region (Figure 17B). The immunogen sequence comprised most of the LBD, and thus covered a large area of the protein (Figure 17B). Many of the helices in the immunogen sequence are exposed to the outside of this domain. The epitopes would therefore be assumed to be accessible for some of the antibodies.

4.8 Hydropathy plot

To predict if any epitopes were accessible for antibody binding, a hydropathy plot was generated. These plots can provide knowledge on hydrophobic and hydrophilic properties of segments in proteins. They can thus help predict which parts of the peptide are more likely to be found at the core and which parts are more likely to be found at the surface of the protein. Generally, hydrophobic segments are found on the inside of water-soluble globular proteins, while hydrophilic segments are found on the outside of the protein.

Positive scores in a hydropathy plot indicate hydrophobic residues while negative scores indicate hydrophilic residues. The hydrophilic regions were of particular interest, as they are more likely to be accessible for antigen binding. The resulting plot of the gmRxra-based immunogen peptide showed a mixture of both hydrophobic and hydrophilic regions (Figure 18). The first aas, 4 – 36, displayed short stretches of both hydrophilic and hydrophobic residues (Figure 18). The region with the longest stretches of hydrophobic and hydrophilic segments occurred between the 37th aa and onwards. For the hydrophilic aas, three regions of the peptide were of interest, due to their length, from 96 to 107 aa, 119 to 129 aa and 143 to 156 aa. The last one of these consisted of the longest stretch of hydrophilic residues (14 aas). These regions were thus presumed to be possible antigenic sites.

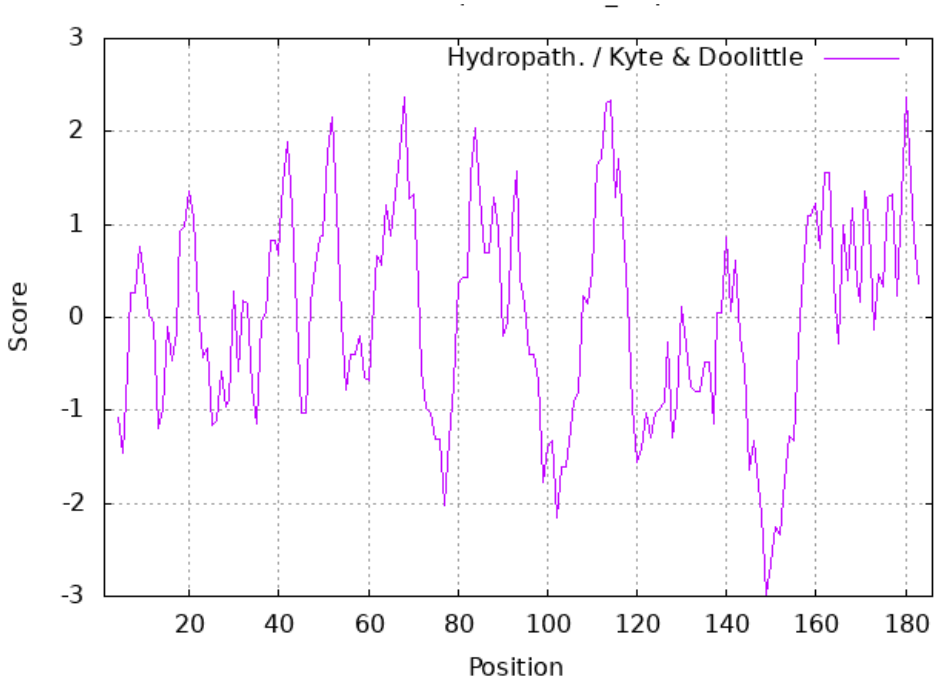

Figure 18. Hydropathy plot of the immunogen sequence. The plot was generated with ProtScale from Expasy, with a window size of 9 and with the Kyte and Doolittle amino acid (aa) scale (Kyte & Doolittle, 1982). The plot displays the aa residues on the X-axis, and the hydropathy score on the Y-axis. A positive score indicates a hydrophobic aa and a negative score indicates a hydrophilic aa.

4.9 Modulation of Rxr-signaling pathways by 9-cis-RA and TBT

To learn more about the possible effects of 9-cis-RA and TBT on Rxr signaling pathways, an *ex vivo* approach was used to mimic an *in vivo* situation of the Atlantic cod liver. PCLS cultures were used for this purpose to study the effects of different concentrations of 9-cis-RA and TBT on selected genes belonging to cellular signaling pathways where Rxr is involved in modulating their expression.

4.9.1 Cell viability and Cytotoxicity determination

To assess that the concentrations used of TBT and 9-cis-RA were not cytotoxic for the PCLS, an MTT assay and a LDH assay were used to monitor the metabolic activity and structural integrity of the cells within the liver tissues.

The MTT assay displayed no significant changes in the metabolic activity when tissues were exposed to increasing concentrations of either 9-cis-RA or TBT in comparison to the solvent control (Figure 19). However, a non-significant trend of reduced metabolic activity was observed at higher TBT concentrations. Like the MTT assay, the LDH assay resulted in some variations between the different exposure groups and the solvent control (Figure 20). However, these variations were not statistically significant. In this assay, no trend in reduced cellular integrity was observed when increasing the exposure concentrations of TBT, as was observed in the MTT assay (Figure 19, 20).

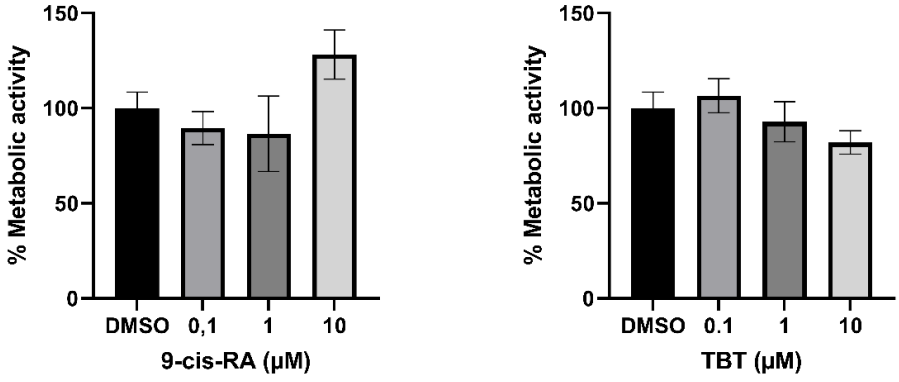

Figure 19. MTT viability assay performed on Atlantic cod precision cut liver slices. PCLS were prepared in four replicates from four individual Atlantic cod livers. The liver cultures were exposed to 0.2 % DMSO as a solvent control, and 0.1, 1 and 10 µM of the exposure chemicals 9-cis-RA and tributyltin (TBT) for 48 h. The MTT assay was performed in triplicates and the absorbance measurement reads were recorded. Mean values in absorbance at 570 nm are presented here as percent change in metabolic activity ± SEM in comparison to the solvent control (DMSO) (n = 4) plotted in GraphPad Prism. One-way Anova with Dunnett's multiple comparisons test was performed and gave no significant differences between the DMSO control and the exposure groups.

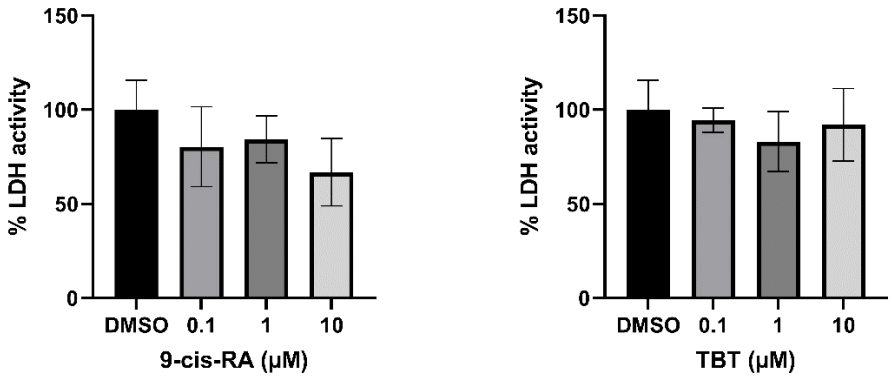

Figure 20. LDH cytotoxicity assay performed on Atlantic cod precision cut liver slices. PCLS were prepared in five replicates from five individual Atlantic cod livers. The liver cultures were exposed to 0.2 % DMSO as a solvent control, and 0.1, 1 and 10 µM of the exposure chemicals 9-cis-RA and tributyltin (TBT) for 48 h. The LDH assay was performed in triplicates and the absorbance measurement reads were recorded. Mean values in absorbance at 490 nm are presented here as percent change in cytotoxicity ± SEM in comparison to the solvent control (DMSO (n = 5) plotted in GraphPad Prism. One-way Anova with Dunnett's multiple comparisons test was performed and gave no significant differences between the DMSO control and the exposure groups.

4.9.2 RNA Quality Assessment

After the 48 h exposure of the PCLS cultures to 9-cis-RA and TBT, the tissues were homogenized, and RNA was extracted. Prior to cDNA synthesis and subsequent qPCR analyses the RNA purity was assessed through spectrophotometric measurements with Nanodrop One/One^{c} instrument, while the integrity of the RNA was assessed with agarose gel electrophoresis.

The spectrophotometric measurements demonstrated that most of the RNA samples had an $A_{260nm/280nm}$ absorbance ratio of 1.9, suggesting that there was little protein contamination in the samples (presented in Table A1 in the Appendix). The $A_{260nm/230nm}$ ratios, which provide an indication of solvent impurities, showed some more variations with most values occurring below 2.0. This could indicate some impurities resulting from the reagents used during the RNA extraction procedure. When assessing the RNA integrity with agarose gel electrophoresis, two abundant bands were detected between 3.0 and 1.0 kilobase pairs (kbp), representing the 28S and 18S ribosomal RNAs, respectively (Figure 21). The presence of these bands indicates that the RNA integrity was maintained during the isolation. The RNA samples were used further for cDNA synthesis and qPCR analyses.

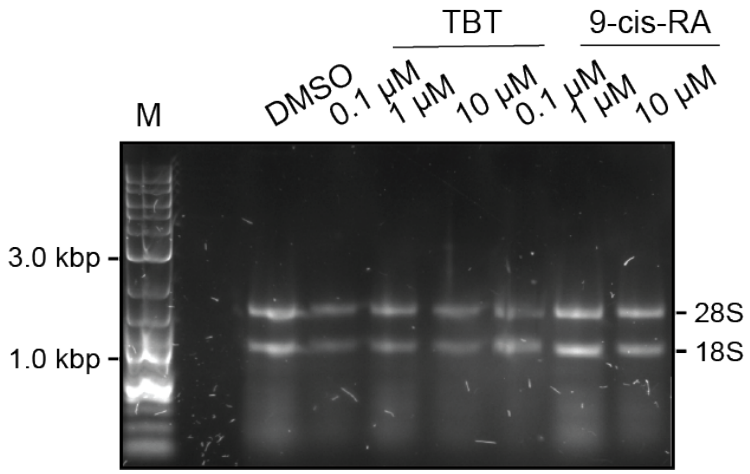

Figure 21. Assessment of RNA integrity with agarose gel electrophoresis. RNAs were extracted from Atlantic cod liver tissues derived from PCLS cultures. PCLS from five Atlantic cod were exposed to a solvent control (0.2 % DMSO) and three concentrations (0.1, 1 and 10 µM) of the two chemicals, 9-cis-RA, and TBT. RNA samples were separated in a 1 % agarose gel and visualized with GelRed. The figure displays only a small selection of representative samples isolated from liver tissues. 2-log DNA ladder, denoted by M, is indicated in the figure.

4.9.3 9-cis-RA and TBT-mediated changes in the expression of genes linked to Rxr-signaling pathways

The expression of four genes associated to different Rxr-signaling pathways, including *pparg, rbp2, ebp,* and *sqlea,* were analyzed using qPCR. The cycle threshold (Ct) values obtained from these analyses were used to calculate the fold changes in gene expression in PCLS exposed to 0.1, 1 and 10 µM of either TBT or 9-cis-RA relative to the solvent control (0.2 % DMSO).

Among the PCLS exposed to 9-cis-RA, only the *pparg* demonstrated a significant differential expression (Figure 22). Here, an upregulation with a mean of 1.67-fold change in comparison to the solvent control was revealed. The fold change in the expression of *rbp2*, *ebp* and *sqlea* decreased slightly with increasing concentrations of 9-cis-RA, but these were not statistically significant changes (Figure 22).

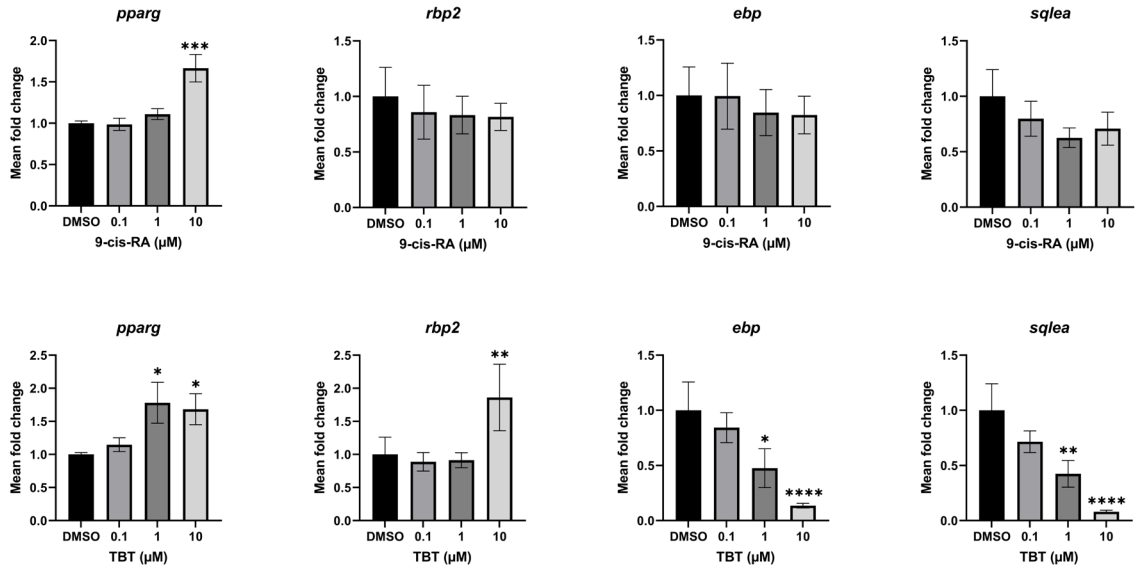

Figure 22. Gene expression data of *pparg, rbp2, ebp* and *sqlea* after exposure of PCLS to 9-cis-retinoic acid (9-cis-RA) and tributyltin (TBT). PCLS were prepared from five Atlantic cod and exposed to 0.1, 1 and 10 µM of 9-cis-RA, TBT, or a solvent control (0.2% DMSO) for 48 h at 10 °C. The graphs display the mean fold change in gene expression relative to the solvent control with the standard error of the mean (SEM) (n = 5 for all samples except the 1 µM TBT exposure where n = 4). Statistical significance was calculated with log2-transformed data, using a mixed effects model and Dunnett's post hoc test. The following significance levels are denoted as follows: * $p < 0.05$, ** $p < 0.01$, *** $p < 0.001$ and **** $p < 0.0001$.

TBT exposure of PCLS resulted in significant differential expression of all the genes assessed (Figure 22). An increased expression of both *pparg* and *rbp2* were observed (Figure 22). For *pparg*, a significant upregulation was found at 1 µM and 10 µM TBT exposure, with a mean fold change of 1.78 and 1.68, respectively. For *rbp2*, a significant upregulation occurred with 10 µM TBT exposure, with a mean fold-change of 1.86.

Notably, the expression levels of *ebp* and *sqlea* were downregulated in a dose-dependent manner when the concentrations of TBT were increased (Figure 22). For both genes, exposure to 0.1 µM TBT did not yield any significant changes to the gene expression. On the other hand, exposure to 1 µM and 10 µM TBT produced significant downregulation, with mean fold changes of 0.48 and 0.14 for *ebp,* and 0.42 and 0.08 for *sqlea*, respectively.

5 DISCUSSION

In our research group, much focus has been placed on characterizing the Rxr subtypes in Atlantic cod, including studying their ligand-activation properties by the endogenous ligand 9-cis-RA, as well as by exogenous OTCs (Borge, 2021; Prebensen, 2023). However, these studies dealt with cloned gmRxr subtypes expressed transiently in a COS-7 cell line and did not examine Rxr in Atlantic cod cells and tissues. This master thesis was thus a continuation of the mentioned projects, in which effects of 9-cis-RA and TBT exposure to liver tissues and the consequent effect on the Rxr signaling pathway were in focus. There were two overall aims in this thesis. First, the aim was to characterize the binding of the antibodies to gmRxr, by determining, *in silico,* if the antibodies could bind to other gmRxrs than gmRxra they were produced towards, assessing if the antibodies bind gmRxrs in different Atlantic cod tissues and finally to determine if the antibodies are suitable for immunoassays under denaturing and non-denaturing conditions. The second aim was to examine the activation of gmRxr signaling pathways in liver tissue cultures through exposure to 9-cis-RA and TBT, by first examining the viability of liver tissues in PCLS after exposure, then studying alterations in gene expression of the selected genes *pparg, rbp2, ebp* and *sqlea.* To achieve this, it was important to determine if the available custom-made polyclonal antibodies produced against a 184-aa sequence in Atlantic cod Rxra could recognize and bind to Rxr. It was observed in WB analyses that the pAbs bound to a protein in cod liver with a MW of 35 kDa, and by using 2D-PAGE in combination with mass spectrometry it was shown that this band was indeed Rxrb1. However, the antibodies were not successfully used for IP in this thesis, which would enable downstream analyses such as ChIP. Studies of gene expression with PCLS was also performed in which the four genes *ebp*, *pparg, rbp2* and *sqlea* were differentially expressed after TBT exposure, indicating a pronounced effect of TBT *ex vivo* on three pathways where Rxr is involved.

5.1 Multiple sequence alignment of gmRxr subtypes revealed similar antigen sequences

The sequence alignment of the different subtypes of gmRxr showed high sequence similarity between the gmRxr variants, particularly in the region used for immunization. Fourteen additional residues were observed in H7 in gmRxrb1 and gmRxrb2 in comparison to gmRxra. It has previously been shown that these additional residues prevent ligand binding to gmRxrb2 (Prebensen, 2023). A possible consequence of these 14 additional residues could also be a

structural change of the gmRxrb proteins that renders epitopes near this region inaccessible. However, polyclonal antibodies are comprised of antibodies recognizing different epitopes on the antigen, and although if epitopes in this region were affected, other epitopes would still be intact (Lipman et al., 2005; Nasiri et al., 2017). The length of the region used for immunization also strengthens this claim, as it provides a template for many epitopes. Even though epitopes close to these 14 amino acids could be altered by the structural changes, others were likely unaffected (Lipman et al., 2005). Hence, it was anticipated that the antibodies constructed towards Rxra also could bind to the other subtypes of Rxr, which we also observed through the identification of Rxrb1 as the immunoreactive band in liver tissue, as discussed further below.

A gmRxra-based polypeptide was used for immunization when the custom antibodies were made. However, based on previous studies on tissue specific expression of the Rxr subtypes in Atlantic cod, Rxra appears to be the least dominant subtype in most tissues (Borge, 2021). A cross reaction of the pAbs with the other Rxr subtypes could therefore be an advantage in downstream analyses when aiming to study the signal pathways affected by all gmRxrs. However, it proposes a disadvantage if wanting to study the different and specific roles the Rxr subtypes may have in cellular signaling pathways. Different roles for different subtypes have previously been hypothesized due to their different tissue localizations. RXRb is ubiquitously expressed in most tissues of vertebrates, including teleosts (Borge, 2021; Mangelsdorf et al., 1992). In mammals, RXRa and RXRg show a more tissue specific expression, where RXRa is abundant in liver, kidneys, spleen, and visceral tissues, while RXRg is detected primarily in muscles and the brain (Mangelsdorf et al., 1992). In teleosts, the expression of Rxra is significantly lower than in mammals, and a divergence of RXRa/Rxra roles has been proposed by Tallafuss et al. (2006). RXRs are thought to play a critical role in several developmental processes as well as in the regulation of physiology and metabolism due to their function as the main dimerization partner for many NRs, and because they are abundant in most tissues (Szanto et al., 2004). Using studies with knock-out animals, both general and specific effects have been observed for the different subtypes. Specific tissue effects of RXRa occurred in the adipocyte tissue, causing perturbed differentiation and resistance to obesity. RXRb knockout resulted in alopecia and dermal cyst formation, while RXRg knockout resulted in disturbed lipid metabolism and impaired regenerative capacity in the liver and multifocal hyperplasia in the prostate in mouse models, as reviewed by Szanto et al. (2004). Little knowledge exists regarding knockout effects of Rxr in teleosts. In addition, the expression pattern of many Rxr subtypes differ from that of the mammalian counterparts. Thus, there is still much to learn

regarding the Rxr subtype functions in Atlantic cod and other fish species. It would certainly be advantageous to be able to study the different roles of the Rxr subtypes by using subtype-specific antibodies. However, due to the little knowledge regarding Rxr signaling in Atlantic cod, knowledge of the Rxr signaling as a whole still provides valuable information.

5.2 Identification of Rxrb1 in liver tissues

WB analyses with pAb #5789 and pAb #5859 consistently revealed an immunoreactive band at 35 kDa in liver homogenates. WB with pre-immune serum was performed to assess occurrence of immunoreactive bands deriving from unspecific binding to proteins by antibodies present in the pre-immune serum (MacPhee, 2010). Importantly, these analyses showed that the band corresponding to the immunogen control appeared on the WB only when exposed to the antibodies and not when exposed to the pre-immune serum. Hence, this supports that there were no other antibodies in the affinity purified antibody solutions that could bind to the antigen. Similarly, the 35 kDa immunoreactive band was not detectable in WB of liver samples when the pre-immune serum was used. Thus, it was established that the staining of the immunoreactive band at 35 kDa was due to binding of pAb #5789 and pAb#5859. The exact identities of all the immunoreactive bands observed in the liver and other tissues could not be determined in this thesis. However, as there were several immunoreactive bands appearing in the pre-immune serum-incubated membranes that migrated with the same MW as immunoreactive bands observed in the membranes incubated with the antibodies, it can be assumed that several of these were likely due to unspecific binding by antibodies already present in rabbit serum prior to the immunization. The identity of the immunoreactive 35 kDa band as Rxrb1 was confirmed by using 2D-PAGE and western blotting in combination with mass spectrometry analyses. Two protein gel spots were sent to analysis and in the second of these, four peptide sequences belonging to the LBD of Rxrb1 were identified. This confirmed that the polyclonal antibodies that were prepared specifically against a region in gmRxra could also recognize and bind to other gmRxr subtypes, which also was suggested from the high sequence identities between these proteins.

Borge has previously established that mRNA levels of gmRxr subtypes varies in the different tissues of Atlantic cod (Borge, 2021). Interestingly, the initial WB analyses with several different tissues also revealed a 35 kDa immunoreactive band that appears to correspond to the one identified as gmRxrb1 in the brain, skin, stomach, head kidney and ovary tissue samples. From the expression data from Borge, it was found that the expression of Rxrb1 was higher than the expression of the other subtypes in ovaries, head kidney, stomach and liver (Borge, 2021). The results of the western blot in this thesis agree with the expression data from Borge, as these bands are detected in the blots. The brain and skin tissues differed in this respect, as the levels of gmRxrb1 were not higher than the level of other gmRxrs. (ibid.). A comparison of gene expression and protein levels is a difficult task. However, it is interesting that the same levels were found in the tissues as in Borge's gene expression results. This could indicate that the immunoreactive bands observed in the other tissues could also be from gmRxrb1. However, this needs to be confirmed by additional analyses such as mass spectrometry.

5.3 Is the lower MW of gmRxrb1 than expected due to proteolytic cleavages?

As noted in the results, the theoretical MW for gmRxrb1 was 49.1 kDa, whereas the WB results consistently showed a band corresponding to a protein of ~35 kDa in liver. The difference between observed and expected MW could be due to proteolytic cleavages, or cleavage of an unknown signal peptide (Pillai-Kastoori et al., 2020). Although few reports on truncation of RXRb have been published, some information on this topic exists for RXRa (Casas et al., 2003; Cho et al., 2010; Di Martino et al., 2022; Nagaya et al., 1998). Of particular interest are the results published by Casas et al., in which truncated RXRa with a MW of 44 kDa was identified in the mitochondria of rat liver, differing from the full length size of the protein at 54 kDa (Casas et al., 2003). They found that RXRa was cleaved into the truncated form by m-calpain and that the N-terminal end product from this cleavage was degraded (Casas et al., 2003). Later, Cho et al. established the presence of a 30 kDa LBD fragment of RXRa in human cancer cell lines, including Hep62 hepatocarcinoma cells, also due to proteolytic cleavage, with cathepsin L-type protease as another proposed lysosomal enzyme functioning on RXRa (Cho et al., 2010; Nagaya et al., 1998). The reduction in MW of RXRa in human and rat agrees with a smaller protein band observed for Rxrb1 in this thesis. In addition, the MS analysis of gmRxrb1 retrieved four peptide sequences that belonged solely to the LBD. The LBD region has also been reported as part of the truncated forms of RXRa. Nagaya et al. reported that the truncated RXRa lacked the N-terminus, and they suspected that the cleavage by Cathepsin L-type

protease was a mechanism for modulating thyroid hormone action (Nagaya et al., 1998). Casas et al. reported that the hinge region and the LBD remained after cleavage and reported an involvement of the truncated RXRa in mitochondrial activity (Casas et al., 2003). Finally Cho et al. reported that a 30 kDa RXRa truncation in SiHa cell lines consisting of the LBD remained after cleavage and inhibited radiosensitization by retinoic acid (Cho et al., 2010). Thus, it could be that the protein band observed here is a truncated form of Rxrb1 resulting from a controlled proteolytic cleavage. As there is little gmRxra present in Atlantic cod, particularly in the liver, it could be speculated that Rxrb1 acquired the role of RXRa in mammals (Borge, 2021). This should be studied further as the mechanism of such a truncation and its functional implication are very interesting.

5.4 The unsuccessful immunoprecipitation using conventional techniques was surprising

In the IP experiments conducted in this thesis the antibodies were not able to bind and capture gmRxrb1 when using non-denaturing conditions. The IP results were a bit surprising as the antibodies were expected to bind natively folded gmRxrs due to several reasons. The first being that the manufacturer had tested the Ab-binding to the immunogen through indirect ELISA. ELISA is an immunoassay that generally employs native proteins (Lechtzier et al., 2002). Secondly, the region of Rxra used for antibody generation comprised quite a large part of the protein. 3D visualization of hRXRa, which shared 99 % sequence identity to gmRxra, revealed that the region of the protein used for immunization contained many exposed stretches. This was also suggested in the hydropathy plot, which showed several regions with hydrophilic properties. Thirdly, the polyclonal nature of the antibodies suggest that they should recognize several epitopes in the antigen and thus increasing the likelihood of binding to a native protein (Lipman et al., 2005). Employing IP techniques with RXR has been done before by others. Sugawara et al. produced pAbs against peptides of each of the known mouse RXR subtypes present in the pituitary gland (Sugawara et al., 1995). ChIP assays has also been performed using pAbs designed for RXRa from Santa Cruz Biotechnology (Chatagnon et al., 2015) in adipocyte cell cultures prepared from 3T3-LI fibroblasts (Nielsen et al., 2008) and in mouse brain tissue and embryonic stem cells (Nam et al., 2016). To my knowledge, no results have been published with IP techniques for Rxr in teleosts, although studies on transcriptional regulation in liver of teleost fish have been performed using ChIP and antibodies towards other transcription factors (Q. Chen et al., 2021; Xu et al., 2023). It can also be mentioned that it has

been noted by others that IP has not worked as reported by manufacturers of antibodies. For instance, Trivedi et al. were also not able to perform IP from liver homogenates when using a commercial antibody towards the transcription factor HSF1 from Proteintech. However, the antibody was successful in IP with homogenates from heat-shocked HeLaS3 cells (Trivedi et al., 2021). In their case, they overcame the issue by discarding the use of their antibodies and instead employing an oligonucleotide which was specific for HSF1 coupled to magnetic beads for IP (ibid.).

According to Lechtzier et al., antibodies generally recognize either linear or conformational epitopes, although in some cases they can recognize both types (Lechtzier et al., 2002). The WB results in this thesis have shown that the antibodies did bind gmRxrb1 while the protein was denatured. Thus, it is concluded that pAb #5789 and pAb #5859 recognize denatured linear epitopes. In addition, our samples derive from tissues consisting of complex protein environments with competing proteins (Pillai-Kastoori et al., 2020). When dealing with homogenates consisting of complex protein interactions, analyte-dependent interference can occur in which the results can be quite different (Tate & Ward, 2004) This is important as the total avidity, i.e. the total binding strength, could have been altered (Oostindie et al., 2022). The binding affinity between the antibodies and the antigens might not have been strong enough for immunochemical methods using native conditions (Weller, 2018). This seems likely, as the proteins were located in the wash fraction, thus assuming that they did bind to the antibodies, but that they were easily washed off during the wash steps. The Rxr proteins might thus not have been readily accessible in the homogenate mixture in classical IP procedures.

For the IP experiment undertaken in this thesis, the procedure might have been able to work if optimizations were performed. For instance, changes to the protocol could have been made to reduce possible interferences in the sample from the buffers used during the IP procedure (Tate & Ward, 2004), Other antibodies could have been used in conjunction with the antibodies designed for gmRxra, such as has been done by Nielsen et al.(2008) and Chatagnon et al. (2015). However, in these two studies, they focused on RXR as a heterodimer partner. Thus, including more antibodies might restrict the study of the RXR signaling pathway. Furthermore, many of the studies mentioned above employed commercial antibodies. This might have been a better approach in this thesis, as the antibodies are already validated by others, This can, as stated by Weller, increase the likelihood of successful immunoassays (Weller, 2018). However, few such antibodies exist for gmRxr, and it might thus not have been possible to use previously validated antibodies for this purpose. Nevertheless, antibodies that function in one assay are not

necessarily good for other assays, and antibody specificity and selectivity for different assays can be difficult to predict (Pillai-Kastoori et al., 2020). A final option could be to discard the use of antibodies and instead use oligonucleotides as done by Trivedi et al. (2021). However, due to the time restrictions in a master thesis it was deemed more important to move on to addressing the second aim of the thesis.

5.5 Modulation of Rxr-signaling pathways through exposure to TBT and 9-cis-RA

The LDH and MTT assays showed that the concentrations of TBT and 9-cis-RA used in this thesis did not yield any significant cytotoxic effects on the PCLS, which may be a concern when acquiring gene expression data. Similar results have also been reported previously in our lab with COS-7 cells, although significant decreases in structural integrity was observed from 0.25 µM TBT (Borge, 2021; Prebensen, 2023). Four genes were chosen for studying their transcriptional response in *ex vivo* liver tissue to different concentrations of the endogenous ligand 9-cis-RA and the OTC TBT. These genes include *pparg*, *sqlea*, *ebp,* and *rbp2,* which are connected to different signaling pathways that involves Rxr.

Exposure to both 9-cis-RA and TBT resulted in similar trends in how they affected the gene expression, in particular for *pparg*, *ebp* and *sqlea*. However, TBT exposure resulted in larger and more significant changes. This is of particular interest as 9-cis-RA is classified as an endogenous ligand for RXR/Rxr due to its high binding affinity (Heyman et al., 1992). From the results provided in this thesis, it could be speculated that TBT is a more potent ligand than 9-cis-RA. This is of particular interest as TBT does not bind to the whole ligand binding pocket in the LBD, but only binds covalently to a sulfur atom of a conserved cysteine residue (le Maire et al., 2009). Potent binding of TBT to LBD in gmRxr subtypes have also been recorded *in vitro* by Borge and Prebensen for gmRxra, gmRxrb2d and gmRxrg (Borge, 2021; Prebensen, 2023). Similar results have also been observed by others. For instance, Grün et al. reported that TBT was just as potent as 9-cis-RA in gene expression induction, but less potent than the RXR specific synthetic ligands LG100268 and AGN195203 (Grun & Blumberg, 2006). This is an area for important future studies, in particular also for the understanding of 9-cis-RA as an endogenous ligand (Krężel et al., 2019).

5.6 Upregulation of *pparg* in PCLS

The effect of TBT on the PPARg:RXR / Pparg:Rxr heterodimer is one of the most studied pathways in relation to TBT exposure and alterations of gene expression. Pparg is found in most vertebrates so the consequent effects of TBT exposure can affect many organisms (Capitão et al., 2018). TBT exposure is related to lipogenesis and adipogenesis in both mammals and fish, and is thought to induce lipogenesis by binding to the PPARg:RXR / Ppar:Rxr heterodimer (Lyssimachou et al., 2015; Shoucri et al., 2017; Stossi et al., 2019). In mammals, TBT has already been classified as an obesogen since it contributes to metabolic imbalance and obesity, particularly during exposure in early development (Grun et al., 2006). In this thesis, an upregulation of *pparg* mRNA was observed with increased concentrations of both 9-cis-RA and TBT. 9-cis-RA gave the most significant effect at 10 µM with the other concentrations not differing from the solvent control. TBT exposure on the other hand, caused the same significant changes in *pparg* expression at 1 and 10 µM exposures. An upregulation of *pparg* agrees with the findings of previous studies, also displaying an upregulation of this gene from TBT exposure. For instance, exposure of zebrafish to 10 ng/L TBT before hatching resulted in significant upregulation of *pparg* in the liver (Lyssimachou et al., 2015). Lyssimachou et al. observed the strongest upregulation of *pparg* at 10 ng/L and lower upregulation at 50 ng/L. In human mesenchymal cells, upregulation of *pparg* was observed during exposure to both TBT and the rexinoid IRX4204 (Shoucri et al., 2017). Here, the highest upregulation of *pparg* was from 100 nM IRX204, followed by 5 nM TBT, and finally 50 nM TBT (Shoucri et al., 2017). Similar results were observed in this thesis, with the highest upregulation of *pparg* from TBT exposure occurring from 1 µM TBT and not 10 µM TBT.

Interestingly, TBT has been found to function as an agonist also for PPARg (in addition to RXR) in several vertebrates, demonstrating significant upregulation of PPARg target genes in humans (mammals), African clawed frog (*X. tropicalis)*, spotted gar (*L. oculatus*), and little skate (*L. erinacea*), when exposed to 100–250 nM TBT (Capitão et al., 2018). However, in zebrafish, no significant changes in Ppar-target genes were observed, and it is speculated that the function of TBT as a Pparg agonist is lost in teleosts (Capitão et al., 2018). From this perspective, we can assume that the increase in expression found here could be due to the binding of TBT to Rxr and not Pparg. However, this needs to be further investigated in Atlantic cod and in general in more detail, to verify this claim.

5.7 Upregulation of *rbp2* mRNA from TBT exposure

Retinol binding proteins (RBPs) are members of the family of intracellular lipid binding proteins (Parmar et al., 2013). RBP was first discovered in mammals, residing in the intestines, and is thought to be involved in the uptake of retinols (Blaner et al., 2020). In fish, such as zebrafish and medaka, *rbp2a*, which is the ortholog of the gene tested in this thesis, is dominant in the intestines but also resides in the liver (Parmar et al., 2013). The results in this thesis also show the expression of *rbp2* in the Atlantic cod. RBP2 is involved in the uptake of retinols by binding to them and are at present hypothesized to be a part of the metabolism of retinols (Napoli, 2016). Thus, the results presented here, in which 10 µM TBT resulted in upregulation of *rbp2*, could illustrate an upregulation of this metabolism pathway. This is interesting, as it defies the results shown by Zhang et al., which indicated a TBT-mediated downregulation in expression of the genes involved in this pathway (Zhang et al., 2017). However, changes in the expression of one gene do not necessarily give an indication of the entire pathway and more genes should thus be tested to make a firm conclusion.

The RXR:PPARa transcriptional complex has been proposed to facilitate the transcription of *Rbp2* in mammals (Blaner et al., 2020). Although little data are published regarding the effect of TBT exposure on retinol uptake and metabolism, these suggestions match with the upregulation of *rbp2* observed in this thesis, and likely as a result of TBT binding the RXR. Thus, it is proposed that TBT exposure influences the Rxr:Ppara heterodimer, and the genes in this signaling pathway.

5.8 Genes related to the steroid biosynthesis were downregulated by TBT

Two genes assessed in this thesis, *sqlea* and *ebp,* are involved in the steroid biosynthesis pathway. *sqlea* encodes squalene epoxidase a| (also known as squalene monooxidase). This is an enzyme which facilitates the first step of steroid oxygenation (Gill et al., 2011). Exposure of TBT to zebrafish eleutheroembryos and to adult male rare minnow have led to an increase in the expression of these two proteins (Martínez et al., 2020; Zhang et al., 2017). In this thesis, a significant decrease in gene expression for both genes were reported, with lower mRNA synthesized with increasing TBT concentrations. In vertebrates and fungi, a decrease in squalene epoxidase results in a decrease in steroids, in particular the synthesis of cholesterol and ergosterol (Belter et al., 2011). *ebp* encodes EBP delta isomerase, another enzyme involved in steroid synthesis. This enzyme lies further down in the steroid biosynthesis pathway and deals with the conversions of precursors of cholesterol and Vitamin D3 (Martínez et al., 2020;

Zhang et al., 2017). Cholesterol is an important precursor for bile acid biosynthesis and steroid hormone metabolism (Martínez et al., 2020; Tokarz et al., 2013; Zhang et al., 2017). Several processes are thus affected by downregulation of cholesterol, depleting the precursor for further metabolism and processes.

5.9 Elucidating differences in gene expression from this study and other studies

The expression of *rbp2* was upregulated, while the expression of *sqlea* and *ebp* were downregulated upon TBT exposure in this thesis. These results displayed opposite trends to what has previously been described for similar genes and pathways in other teleost fish (Martínez et al., 2020; Zhang et al., 2017). Differences in gene expression observed from other studies might be due to the nature of the experiment and species-specific differences. Martinez et al. employed zebrafish embryos while Zhang et.al employed male rare minnow for their experiments (2020; 2017). In this thesis, juvenile Atlantic cod was used and there was no differentiation between genders. To do so, the sample size should be bigger, as in this experiment two females and two males were selected at random. When Chen et al. were performing their TBT exposure experiments on juvenile Japanese medaka, they found adipocyte areas to decrease over time, despite this being an opposite trend of what has been observed by others (K. Chen et al., 2021). They made the assumption that this is due to the decomposition of fat during juvenile development (K. Chen et al., 2021). Sexual differential expression patterns caused by TBT exposure has previously been described (Lyssimachou et al., 2015; McGinnis & Crivello, 2011). In addition, this study employed *ex vivo* studies using PCLS, in which the cultures were exposed to TBT in a 48 h time span, whilst the studies mentioned here consisted of fish that were exposed to waterborne TBT in their tanks. Martinez et al. exposed zebrafish embryos from 2–5 dpf , while Zhang et al. exposed their rare minnows for 60 days (Martínez et al., 2020; Zhang et al., 2017), thus enabling more time for adverse effects to occur and allowing the study of TBT-mediated effects on whole organisms instead of only organs. Thus, the study here can be said to be valuable at the organ level and still of relevance as the liver is important for metabolism, detoxification and endocrine regulation, and can at times also reflect whole body metabolic disorders (Churcher et al., 2015; Lyssimachou et al., 2015).

6 CONCLUSION

The first objective of this thesis was to characterize the binding of the custom-made pAbs to gmRxr. The antibodies were anticipated to be good candidates for binding all gmRxr subtypes, due to the strong aa similarities in the region of gmRxra used as an immunogen, as well as the polyclonal nature of the antibodies causing them to recognize several epitopes. The antibodies were able to bind to gmRxrb1, hence, showing a specificity towards Rxr. However, the specificity of the pAbs towards other subtypes were not explored in this thesis, as the focus was solely on the most prominent immunoreactive band in cod liver tissue.

In this thesis the antibodies only recognized gmRxrb1 when it was in a denatured condition. From the results obtained in this thesis the antibodies were not able to capture any gmRxr in their native states with a standard IP technique. However, this can be due to numerous different parameters, such as low binding strength between the antibodies and gmRxrb1 in the conformation present under non-denaturing conditions, the complex environment of the homogenates causing interferences with antibody binding, non-optimal buffer conditions, or other reasons not explored.

The second aim of the thesis was to explore differential gene expression in liver tissues from PCLS after a 48 h exposure to 9-cis-RA and TBT. No significant decrease in viability was observed, thus strengthening the results of the gene expression analysis. Of the genes tested, only *pparg* displayed differential expression by being upregulated when liver tissues were exposed to 9-cis-RA. For most genes a similar trend in gene expression pattern was observed with both TBT and 9-cis-RA, but TBT produced greater differential expression than 9-cis-RA. This could suggest that the affinity of TBT for Rxr is stronger than that for 9-cis-RA. TBT exposure resulted in upregulation of *pparg* and *rbp2*. These genes are connected to lipogenesis and retinoid metabolism. On the other hand, TBT exposure resulted in a downregulation of *sqlea* and *ebp*, which are important enzymes in the steroid biosynthesis pathway. Thus, in this thesis, three signal pathways were shown to be affected through TBT exposure in Atlantic cod. The alterations of the signaling pathways observed here are likely to cause lipid accumulation, more uptake of retinols and disturbed homeostasis in Atlantic cod. However, these effects can only be speculated, and need to be investigated in an *in vivo* exposure experiment, preferably using early life stages of Atlantic cod.

7. FUTURE PERSPECTIVES

This thesis deals with primary investigation of antibody specificity as this was the first time these antibodies were tested on cod samples. Reporting the quality of the antibodies using different immunochemical techniques, as described in this thesis, is important for antibody validation (Pillai-Kastoori et al., 2020). In hindsight though, it could be a good idea to use antibodies that have already been established to work for the immunoassays planned for. For instance, several ChIP procedures using antibodies from Santa Cruz biotechnology have been mentioned in the discussion. As shown in this thesis, the sequence of hRXRa and gmRxra are very similar and it is possible that antibodies designed against hRXRa also could have worked for Atlantic cod.

In this thesis, a peptide sequence from gmRxra was used to generate polyclonal antibodies and the quality of the synthesized antibodies was assessed. The peptide was chosen from an area of high similarity between the Rxr subtypes in Atlantic cod. Here, the immunoprecipitation was unsuccessful. Further studies with the antibodies should attempt to find the reason as to why this was. Optimization of the IP could thus be performed. For instance, by modifying the steps in the protocol, such as reducing wash steps or changing buffer conditions. The antibodies should also be tested using different homogenates from other tissues, and even from cod cell lines. This will generate a larger validation library.

In relation to the Immunoprecipitation, interference in the homogenate was proposed as a possible reason for why IP might not have functioned. Although several controls were included in the assay, one important control should have been included. This is the immunogen control, which had been used throughout the western blotting procedure. If IP was performed with homogenate that had some of the immunogen control added to it, the immunogen control would be in the same environment as the native Rxr in the liver homogenates, and if the immunogen control showed up in the resulting western blot, this could disclaim the assumption above, whereas no band would strengthen this claim. Thus, more thought should be placed into the controls prior to starting the IP procedures, and to spend time modifying the procedure.

In this thesis, only a subset of genes within a signaling pathway was assessed. This gives an indication of possible consequences of TBT exposure; however, it does not give clear indications of the effects on the entire signaling pathways. Relevant ideas for further studies could be to focus on more genes in the adipogenesis and lipogenesis, steroid biosynthesis, and retinol metabolism pathways investigated in this thesis. Particularly since there is little

information on this topic in many teleost fish, apart from model organisms. Studies on adverse effects on Atlantic cod exposed to TBT could also be conducted by performing *in vivo* exposure studies, for instance during development, over time, in order to get an indication of the actual effects caused by TBT on the organism level. This is important, since TBT and other OTCs are still prevalent in the aquatic environment and adverse health effects on aquatic organisms such as fish from these pollutants are therefore still highly relevant.

Rxr functions as a heterodimeric partner with several other NRs, and a general toxicity trend of TBT has been proposed based on heterodimerization with other NRs and because of the vast array of DEGs found in zebrafish after TBT exposure (Martínez et al., 2020). In addition, since RXR/Rxr has mostly been studied in relation to heterodimers, the role of RXR/Rxr homodimers remains largely elusive. Thus, there is far more to learn about effects of TBT exposure on gene expression in Atlantic cod and other animals. Furthermore, RXR/Rxr is widely expressed in several tissues and has multiple roles in the development of organs. There is thus concern regarding disruption of development of multiple organ functions from exposure to environmental pollutants, such as OTCs (Shoucri et al., 2017). The results presented in this thesis thus present only the tip of the iceberg, with far more genes to be tested and evaluated. Further approaches for this could be through high throughput next generation sequencing (NGS), such as mRNA-seq and ChIP-seq (K. Chen et al., 2021; Martínez et al., 2020).

7 REFERENCES

Alharbi, O. M. L., Basheer, A. A., Khattab, R. A., & Ali, I. (2018). Health and environmental effects of persistent organic pollutants. *Journal of Molecular Liquids, 263*, 442-453. doi:https://doi.org/10.1016/j.molliq.2018.05.029

Alzieu, C. L., Sanjuan, J., Deltreil, J. P., & Borel, M. (1986). Tin contamination in Arcachon Bay: Effects on oyster shell anomalies. *Marine Pollution Bulletin, 17*(11), 494-498. doi:https://doi.org/10.1016/0025-326X(86)90636-3

Antizar-Ladislao, B. (2008). Environmental levels, toxicity and human exposure to tributyltin (TBT)-contaminated marine environment. A review. *Environment International, 34*(2), 292-308. doi:https://doi.org/10.1016/j.envint.2007.09.005

Arnold, S. L. M., Amory, J. K., Walsh, T. J., & Isoherranen, N. (2012). A sensitive and specific method for measurement of multiple retinoids in human serum with UHPLC-MS/MS. *Journal of Lipid Research, 53*(3), 587-598. doi:https://doi.org/10.1194/jlr.D019745

Bass, J. J., Wilkinson, D. J., Rankin, D., Phillips, B. E., Szewczyk, N. J., Smith, K., & Atherton, P. J. (2017). An overview of technical considerations for Western blotting applications to physiological research. *Scand J Med Sci Sports, 27*(1), 4-25. doi:10.1111/sms.12702

Beinsteiner, B., Markov, G. V., Bourguet, M., McEwen, A. G., Erb, S., Patel, A. K. M., . . . Billas, I. M. L. (2022). A novel nuclear receptor subfamily enlightens the origin of heterodimerization. *BMC Biology, 20*(1), 217. doi:10.1186/s12915-022-01413-0

Belter, A., Skupinska, M., Giel-Pietraszuk, M., Grabarkiewicz, T., Rychlewski, L., & Barciszewski, J. (2011). Squalene monooxygenase – a target for hypercholesterolemic therapy. *392*(12), 1053-1075. doi:doi:10.1515/BC.2011.195

Berg, E., & Albert, O. T. (2003). Cod in fjords and coastal waters of North Norway: distribution and variation in length and maturity at age. *ICES Journal of Marine Science, 60*(4), 787-797. doi:10.1016/s1054-3139(03)00037-7

Beyer, A., Mackay, D., Matthies, M., Wania, F., & Webster, E. (2000). Assessing Long-Range Transport Potential of Persistent Organic Pollutants. *Environmental Science & Technology, 34*(4), 699-703. doi:10.1021/es990207w

Beyer, J., Song, Y., Tollefsen, K. E., Berge, J. A., Tveiten, L., Helland, A., . . . Schøyen, M. (2022). The ecotoxicology of marine tributyltin (TBT) hotspots: A review. *Marine Environmental Research, 179*, 105689. doi:https://doi.org/10.1016/j.marenvres.2022.105689

Birgisdottir, B. E., Brantsæter, A. L., Kvalem, H. E., Knutsen, H. K., Haugen, M., Alexander, J., . . . Meltzer, H. M. (2012). Fish liver and seagull eggs, vitamin D-rich foods with a shadow: Results from the Norwegian Fish and Game Study. *Molecular Nutrition & Food Research, 56*(3), 388-398. doi:https://doi.org/10.1002/mnfr.201100395

Blaber, S. J. M. (1970). The Occurence of a Penis-like Outgrowth Behind the Right Tentacle in Spent Females of Nucella Lapillus (L.). *Journal of Molluscan Studies, 39*(2-3), 231-233. doi:10.1093/oxfordjournals.mollus.a065097

Blaner, W. S., Brun, P.-J., Calderon, R. M., & Golczak, M. (2020). Retinol-binding protein 2 (RBP2): biology and pathobiology. *Critical Reviews in Biochemistry and Molecular Biology, 55*(2), 197-218. doi:10.1080/10409238.2020.1768207

Borge, A. V. (2021). Identification and characterization of retinoid X receptors (RXR) in Atlantic cod (Gadus morhua) and their response to organic tin exposure. In: The University of Bergen.

Borghi, V., & Porte, C. (2002). Organotin Pollution in Deep-Sea Fish from the Northwestern Mediterranean. *Environmental Science & Technology, 36*(20), 4224-4228. doi:10.1021/es025725c

Borgå, K., Fisk, A. T., Hoekstra, P. F., & Muir, D. C. G. (2004). Biological and chemical factors of importance in the bioaccumulation and trophic transfer of persistent organochlorine contaminants in arctic marine food webs. *Environmental Toxicology and Chemistry, 23*(10), 2367-2385. doi:https://doi.org/10.1897/03-518

Bridgham, J. T., Eick, G. N., Larroux, C., Deshpande, K., Harms, M. J., Gauthier, M. E. A., . . . Thornton, J. W. (2010). Protein Evolution by Molecular Tinkering: Diversification of the Nuclear Receptor Superfamily from a Ligand-Dependent Ancestor. *PLOS Biology, 8*(10), e1000497. doi:10.1371/journal.pbio.1000497

Brtko, J., & Dvorak, Z. (2015). Triorganotin compounds - ligands for "rexinoid" inducible transcription factors: Biological effects. *Toxicology Letters, 234*(1), 50-58. doi:https://doi.org/10.1016/j.toxlet.2015.02.009

Brtko, J., & Dvorak, Z. (2020). Natural and synthetic retinoid X receptor ligands and their role in selected nuclear receptor action. *Biochimie, 179*, 157-168. doi:10.1016/j.biochi.2020.09.027

Capitão, A. M. F., Lopes-Marques, M. S., Ishii, Y., Ruivo, R., Fonseca, E. S. S., Páscoa, I., . . . Castro, L. F. C. (2018). Evolutionary Exploitation of Vertebrate Peroxisome Proliferator-Activated Receptor γ by Organotins. *Environmental Science & Technology, 52*(23), 13951-13959. doi:10.1021/acs.est.8b04399

Casas, F., Daury, L., Grandemange, S., Busson, M., Seyer, P., Hatier, R., . . . Wrutniak-Cabello, C. (2003). Endocrine regulation of mitochondrial activity: involvement of truncated RXRα and c-Erb Aαl proteins. *The FASEB Journal, 17*(3), 426-436. doi:https://doi.org/10.1096/fj.02-0732com

Casini, M., Hjelm, J., Molinero, J.-C., Lövgren, J., Cardinale, M., Bartolino, V., . . . Kornilovs, G. (2009). Trophic cascades promote threshold-like shifts in pelagic marine ecosystems. *Proceedings of the National Academy of Sciences, 106*(1), 197-202. doi:doi:10.1073/pnas.0806649105

Casini, M., Lövgren, J., Hjelm, J., Cardinale, M., Molinero, J. C., & Kornilovs, G. (2008). Multi-level trophic cascades in a heavily exploited open marine ecosystem. *Proc Biol Sci, 275*(1644), 1793-1801. doi:10.1098/rspb.2007.1752

Chatagnon, A., Veber, P., Morin, V., Bedo, J., Triqueneaux, G., Sémon, M., . . . Benoit, G. (2015). RAR/RXR binding dynamics distinguish pluripotency from differentiation associated cis-regulatory elements. *Nucleic Acids Res, 43*(10), 4833-4854. doi:10.1093/nar/gkv370

Chen, K., Iwasaki, N., Qiu, X., Xu, H., Takai, Y., Tashiro, K., . . . Oshima, Y. (2021). Obesogenic and developmental effects of TBT on the gene expression of juvenile Japanese medaka (Oryzias latipes). *Aquatic Toxicology, 237*, 105907. doi:https://doi.org/10.1016/j.aquatox.2021.105907

Chen, Q., Fang, W., Cui, K., Chen, Q., Xiang, X., Zhang, J., . . . Ai, Q. (2021). Endoplasmic reticulum stress induces hepatic steatosis by transcriptional upregulating lipid droplet protein perilipin2. *The FASEB Journal, 35*(10), e21900. doi:https://doi.org/10.1096/fj.202100739RR

Chiu, M. L., Goulet, D. R., Teplyakov, A., & Gilliland, G. L. (2019). Antibody Structure and Function: The Basis for Engineering Therapeutics. *Antibodies, 8*(4), 55. Retrieved from https://www.mdpi.com/2073-4468/8/4/55

Cho, Y.-M., Yang, A.-H., Kim, B.-Y., & Han, Y.-H. (2010). The cleavage fragment of retinoid X receptor-α ligand binding domain inhibits radiosensitization by retinoic acid. *Oncol Rep, 23*(6), 1715-1720. doi:10.3892/or_00000816

Chormare, R., & Kumar, M. A. (2022). Environmental health and risk assessment metrics with special mention to biotransfer, bioaccumulation and biomagnification of environmental pollutants. *Chemosphere, 302*, 134836. doi:https://doi.org/10.1016/j.chemosphere.2022.134836

Churcher, A. M., Pujolar, J. M., Milan, M., Huertas, M., Hubbard, P. C., Bargelloni, L., . . . Canário, A. V. M. (2015). Transcriptomic profiling of male European eel (Anguilla anguilla) livers at sexual maturity. *Comparative Biochemistry and Physiology Part D: Genomics and Proteomics, 16*, 28-35. doi:https://doi.org/10.1016/j.cbd.2015.07.002

Convention, S. (2019). The POPs. Retrieved from https://chm.pops.int/TheConvention/ThePOPs/tabid/673/Default.aspx

Dale, K., Yadetie, F., Müller, M. B., Pampanin, D. M., Gilabert, A., Zhang, X., . . . Goksøyr, A. (2020). Proteomics and lipidomics analyses reveal modulation of lipid metabolism by perfluoroalkyl substances in liver of Atlantic cod (Gadus morhua). *Aquatic Toxicology, 227*, 105590. doi:https://doi.org/10.1016/j.aquatox.2020.105590

de Lera, Á. R., Krezel, W., & Rühl, R. (2016). An Endogenous Mammalian Retinoid X Receptor Ligand, At Last! *ChemMedChem, 11*(10), 1027-1037. doi:https://doi.org/10.1002/cmdc.201600105

Di Martino, O., Ferris, M. A., Hadwiger, G., Sarkar, S., Vu, A., Menéndez-Gutiérrez, M. P., . . . Welch, J. S. (2022). RXRA DT448/9PP generates a dominant active variant capable of inducing maturation in acute myeloid leukemia cells. *Haematologica, 107*(2), 417-426. doi:10.3324/haematol.2021.278603

Drinkwater, K. F. (2005). The response of Atlantic cod (Gadus morhua) to future climate change. *ICES Journal of Marine Science, 62*(7), 1327-1337. doi:10.1016/j.icesjms.2005.05.015

Dunn, N. (2022, 18.05.2022). ZFIN Zebrafish Nomenclature Conventions.

Eide, M., Goksøyr, A., Yadetie, F., Gilabert, A., Bartosova, Z., Frøysa, H. G., . . . Karlsen, O. A. (2023). Integrative omics-analysis of lipid metabolism regulation by peroxisome proliferator-activated receptor a and b agonists in male Atlantic cod. *Front Physiol, 14*, 1129089. doi:10.3389/fphys.2023.1129089

Eide, M., Rydbeck, H., Tørresen, O. K., Lille-Langøy, R., Puntervoll, P., Goldstone, J. V., . . . Karlsen, O. A. (2018). Independent losses of a xenobiotic receptor across teleost evolution. *Sci. Rep., 8*(1), 10404.

Eide, M., Zhang, X., Karlsen, O. A., Goldstone, J. V., Stegeman, J., Jonassen, I., & Goksøyr, A. (2021). The chemical defensome of five model teleost fish. *Scientific Reports, 11*(1), 10546. doi:10.1038/s41598-021-89948-0

Ellingsen, K. E., Anderson, M. J., Shackell, N. L., Tveraa, T., Yoccoz, N. G., & Frank, K. T. (2015). The role of a dominant predator in shaping biodiversity over space and time in a marine ecosystem. *Journal of Animal Ecology, 84*(5), 1242-1252. doi:https://doi.org/10.1111/1365-2656.12396

Evans, R. M., & Mangelsdorf, D. J. (2014). Nuclear Receptors, RXR, and the Big Bang. *Cell, 157*(1), 255-266. doi:10.1016/j.cell.2014.03.012

Fernández-Llamazares, Á., Garteizgogeascoa, M., Basu, N., Brondizio, E. S., Cabeza, M., Martínez-Alier, J., . . . Reyes-García, V. (2020). A State-of-the-Art Review of Indigenous Peoples and Environmental Pollution. *Integrated Environmental Assessment and Management, 16*(3), 324-341. doi:https://doi.org/10.1002/ieam.4239

Frank, K. T., Petrie, B., Choi, J. S., & Leggett, W. C. (2005). Trophic cascades in a formerly cod-dominated ecosystem. *Science, 308*(5728), 1621-1623. doi:10.1126/science.1113075

Frigo, Daniel E., Bondesson, M., & Williams, C. (2021). Nuclear receptors: from molecular mechanisms to therapeutics. *Essays in Biochemistry, 65*(6), 847-856. doi:10.1042/ebc20210020

Gill, S., Stevenson, J., Kristiana, I., & Brown, Andrew J. (2011). Cholesterol-Dependent Degradation of Squalene Monooxygenase, a Control Point in Cholesterol Synthesis beyond HMG-CoA Reductase. *Cell Metabolism, 13*(3), 260-273. doi:https://doi.org/10.1016/j.cmet.2011.01.015

Gore, A. C., Chappell, V. A., Fenton, S. E., Flaws, J. A., Nadal, A., Prins, G. S., . . . Zoeller, R. T. (2015). EDC-2: The Endocrine Society's Second Scientific Statement on Endocrine-Disrupting Chemicals. *Endocrine Reviews, 36*(6), E1-E150. doi:10.1210/er.2015-1010

Grun, F., & Blumberg, B. (2006). Environmental obesogens: organotins and endocrine disruption via nuclear receptor signaling. *Endocrinology, 147*(Suppl 6), S50.

Grun, F., Watanabe, H., Zamanian, Z., Maeda, L., Arima, K., Cubacha, R., . . . Blumberg, B. (2006). Endocrine-disrupting organotin compounds are potent inducers of adipogenesis in vertebrates. *Mol. Endocrinol., 20*(9), 2141.

Grün, F., & Blumberg, B. (2009). Endocrine disrupters as obesogens. *Mol Cell Endocrinol, 304*(1-2), 19-29. doi:10.1016/j.mce.2009.02.018

Guliy, O. I., Evstigneeva, S. S., & Dykman, L. A. (2023). Recombinant antibodies by phage display for bioanalytical applications. *Biosensors and Bioelectronics, 222*, 114909. doi:https://doi.org/10.1016/j.bios.2022.114909

Haug, T., Falk-Petersen, S., Greenacre, M., Hop, H., Lindstrøm, U., Meier, S., . . . Wold, A. (2017). Trophic level and fatty acids in harp seals compared with common minke whales in the Barents Sea. *Marine Biology Research, 13*(9), 919-932. doi:10.1080/17451000.2017.1313988

Heyman, R. A., Mangelsdorf, D. J., Dyck, J. A., Stein, R. B., Eichele, G., Evans, R. M., & Thaller, C. (1992). 9-cis retinoic acid is a high affinity ligand for the retinoid X receptor. *Cell, 68*(2), 397-406. doi:https://doi.org/10.1016/0092-8674(92)90479-V

Hiller-Sturmhöfel, S., & Bartke, A. (1998). The endocrine system: an overview. *Alcohol Health Res World, 22*(3), 153-164.

Hoch, M. (2001). Organotin compounds in the environment — an overview. *Applied Geochemistry, 16*(7), 719-743. doi:https://doi.org/10.1016/S0883-2927(00)00067-6

Huang, W., Xu, F., Li, J., Li, L., Que, H., & Zhang, G. (2015). Evolution of a novel nuclear receptor subfamily with emphasis on the member from the Pacific oyster Crassostrea gigas. *Gene, 567*(2), 164-172. doi:https://doi.org/10.1016/j.gene.2015.04.082

Hutchinson, T. H., Lyons, B. P., Thain, J. E., & Law, R. J. (2013). Evaluating legacy contaminants and emerging chemicals in marine environments using adverse outcome pathways and biological effects-directed analysis. *Mar Pollut Bull, 74*(2), 517-525. doi:10.1016/j.marpolbul.2013.06.012

Jin, L., & Li, Y. (2010). Structural and functional insights into nuclear receptor signaling. *Advanced Drug Delivery Reviews, 62*(13), 1218-1226. doi:https://doi.org/10.1016/j.addr.2010.08.007

Jones, J. W., Pierzchalski, K., Yu, J., & Kane, M. A. (2015). Use of Fast HPLC Multiple Reaction Monitoring Cubed for Endogenous Retinoic Acid Quantification in Complex Matrices. *Analytical Chemistry, 87*(6), 3222-3230. doi:10.1021/ac504597q

Karl, H., Kammann, U., Aust, M.-O., Manthey-Karl, M., Lüth, A., & Kanisch, G. (2016). Large scale distribution of dioxins, PCBs, heavy metals, PAH-metabolites and radionuclides in cod (Gadus morhua) from the North Atlantic and its adjacent seas. *Chemosphere, 149*, 294-303. doi:https://doi.org/10.1016/j.chemosphere.2016.01.052

Kelly, B. C., Ikonomou, M. G., Blair, J. D., Morin, A. E., & Gobas, F. A. P. C. (2007). Food Web□Specific Biomagnification of Persistent Organic Pollutants. *Science, 317*(5835), 236-239. doi:doi:10.1126/science.1138275

Khan, S. H., & Okafor, C. D. (2022). Interactions governing transcriptional activity of nuclear receptors. *Biochemical Society Transactions, 50*(6), 1941-1952. doi:10.1042/bst20220338

Krężel, W., Rühl, R., & de Lera, A. R. (2019). Alternative retinoid X receptor (RXR) ligands. *Molecular and Cellular Endocrinology, 491*, 110436. doi:https://doi.org/10.1016/j.mce.2019.04.016

Kyte, J., & Doolittle, R. F. (1982). A simple method for displaying the hydropathic character of a protein. *Journal of Molecular Biology, 157*(1), 105-132. doi:https://doi.org/10.1016/0022-2836(82)90515-0

Lal, A., Haynes, S. R., & Gorospe, M. (2005). Clean Western blot signals from immunoprecipitated samples. *Mol Cell Probes, 19*(6), 385-388. doi:10.1016/j.mcp.2005.06.007

Langston, W. J., Pope, N. D., Davey, M., Langston, K. M., O' Hara, S. C. M., Gibbs, P. E., & Pascoe, P. L. (2015). Recovery from TBT pollution in English Channel environments: A problem solved? *Marine Pollution Bulletin, 95*(2), 551-564. doi:https://doi.org/10.1016/j.marpolbul.2014.12.011

le Maire, A., Grimaldi, M., Roecklin, D., Dagnino, S., Vivat-Hannah, V., Balaguer, P., & Bourguet, W. (2009). Activation of RXR-PPAR heterodimers by organotin environmental endocrine disruptors. *EMBO Rep., 10*(4), 367.

le Maire, A., Rey, M., Vivat, V., Guée, L., Blanc, P., Malosse, C., . . . Bourguet, W. (2022). Design and in vitro characterization of RXR variants as tools to investigate the biological role of endogenous rexinoids. *Journal of Molecular Endocrinology, 69*(3), 377-390. doi:10.1530/jme-22-0021

Lechtzier, V., Hutoran, M., Levy, T., Kotler, M., Brenner, T., & Steinitz, M. (2002). Sodium dodecyl sulphate-treated proteins as ligands in ELISA. *Journal of Immunological Methods, 270*(1), 19-26. doi:https://doi.org/10.1016/S0022-1759(02)00214-4

Lipman, N. S., Jackson, L. R., Trudel, L. J., & Weis-Garcia, F. (2005). Monoclonal Versus Polyclonal Antibodies: Distinguishing Characteristics, Applications, and Information Resources. *ILAR Journal, 46*(3), 258-268. doi:10.1093/ilar.46.3.258

Lyssimachou, A., Santos, J. G., Andre, A., Soares, J., Lima, D., Guimaraes, L., . . . Santos, M. M. (2015). The Mammalian "Obesogen" Tributyltin Targets Hepatic Triglyceride Accumulation and the Transcriptional Regulation of Lipid Metabolism in the Liver and Brain of Zebrafish. *PLOS ONE, 10*(12), e0143911.

Ma, S., & Zhang, Y. (2020). Profiling chromatin regulatory landscape: insights into the development of ChIP-seq and ATAC-seq. *Molecular Biomedicine, 1*(1), 9. doi:10.1186/s43556-020-00009-w

MacPhee, D. J. (2010). Methodological considerations for improving Western blot analysis. *Journal of Pharmacological and Toxicological Methods, 61*(2), 171-177. doi:https://doi.org/10.1016/j.vascn.2009.12.001

Mangelsdorf, D. J., Borgmeyer, U., Heyman, R. A., Zhou, J. Y., Ong, E. S., Oro, A. E., . . . Evans, R. M. (1992). Characterization of three RXR genes that mediate the action of 9-cis retinoic acid. *Genes Dev, 6*(3), 329-344. doi:10.1101/gad.6.3.329

Mangelsdorf, D. J., & Evans, R. M. (1995). The RXR heterodimers and orphan receptors. *Cell, 83*(6), 841-850. doi:https://doi.org/10.1016/0092-8674(95)90200-7

Martínez, R., Codina, A. E., Barata, C., Tauler, R., Piña, B., & Navarro-Martín, L. (2020). Transcriptomic effects of tributyltin (TBT) in zebrafish eleutheroembryos. A functional benchmark dose analysis. *Journal of Hazardous Materials, 398*, 122881. doi:https://doi.org/10.1016/j.jhazmat.2020.122881

Matschiner, M., Barth, J. M. I., Tørresen, O. K., Star, B., Baalsrud, H. T., Brieuc, M. S. O., . . . Jentoft, S. (2022). Supergene origin and maintenance in Atlantic cod. *Nature Ecology & Evolution, 6*(4), 469-481. doi:10.1038/s41559-022-01661-x

McGinnis, C. L., & Crivello, J. F. (2011). Elucidating the mechanism of action of tributyltin (TBT) in zebrafish. *Aquatic Toxicology, 103*(1), 25-31. doi:https://doi.org/10.1016/j.aquatox.2011.01.005

Meftahi, G. H., Bahari, Z., Zarei Mahmoudabadi, A., Iman, M., & Jangravi, Z. (2021). Applications of western blot technique: From bench to bedside. *Biochemistry and Molecular Biology Education, 49*(4), 509-517. doi:https://doi.org/10.1002/bmb.21516

Mishra, M., Tiwari, S., & Gomes, A. V. (2017). Protein purification and analysis: next generation Western blotting techniques. *Expert Review of Proteomics, 14*(11), 1037-1053. doi:10.1080/14789450.2017.1388167

Morais, S., Bell, J. G., Robertson, D. A., Roy, W. J., & Morris, P. C. (2001). Protein/lipid ratios in extruded diets for Atlantic cod (Gadus morhua L.): effects on growth, feed utilisation, muscle composition and liver histology. *Aquaculture, 203*(1), 101-119. doi:https://doi.org/10.1016/S0044-8486(01)00618-4

Mortensen, A. S., & Arukwe, A. (2007). Modulation of xenobiotic biotransformation system and hormonal responses in Atlantic salmon (Salmo salar) after exposure to tributyltin (TBT). *Comparative Biochemistry and Physiology Part C: Toxicology & Pharmacology, 145*(3), 431-441. doi:https://doi.org/10.1016/j.cbpc.2007.01.013

Mukha, A., Kalkhoven, E., & van Mil, S. W. C. (2021). Splice variants of metabolic nuclear receptors: Relevance for metabolic disease and therapeutic targeting. *Biochimica et Biophysica Acta (BBA) - Molecular Basis of Disease, 1867*(10), 166183. doi:https://doi.org/10.1016/j.bbadis.2021.166183

Nagaya, T., Murata, Y., Yamaguchi, S., Nomura, Y., Ohmori, S., Fujieda, M., . . . Seo, H. (1998). Intracellular Proteolytic Cleavage of 9-cis-Retinoic Acid Receptor α by Cathepsin L-type Protease Is a Potential Mechanism for Modulating Thyroid Hormone Action*. *Journal of Biological Chemistry, 273*(50), 33166-33173. doi:https://doi.org/10.1074/jbc.273.50.33166

Nam, K. N., Mounier, A., Fitz, N. F., Wolfe, C., Schug, J., Lefterov, I., & Koldamova, R. (2016). RXR controlled regulatory networks identified in mouse brain counteract deleterious effects of Aβ oligomers. *Scientific Reports, 6*(1), 24048. doi:10.1038/srep24048

Napoli, J. L. (2016). Functions of Intracellular Retinoid Binding-Proteins. *Subcell Biochem, 81*, 21-76. doi:10.1007/978-94-024-0945-1_2

Nasiri, H., Valedkarimi, Z., Aghebati-Maleki, L., Abdolalizadeh, J., Kazemi, T., Esparvarinha, M., & Majidi, J. (2017). Production and purification of polyclonal antibody against F(ab')2 fragment of human immunoglobulin G. *Vet Res Forum, 8*(4), 307-312.

Nielsen, R., Pedersen, T. A., Hagenbeek, D., Moulos, P., Siersbaek, R., Megens, E., . . . Stunnenberg, H. G. (2008). Genome-wide profiling of PPARgamma:RXR and RNA polymerase II occupancy reveals temporal activation of distinct metabolic pathways and changes in RXR dimer composition during adipogenesis. *Genes Dev, 22*(21), 2953-2967. doi:10.1101/gad.501108

Oliveira, D. D. d., Rojas, E. G., & Fernandez, M. A. d. S. (2020). Should TBT continue to be considered an issue in dredging port areas? A brief review of the global evidence. *Ocean & Coastal Management, 197*, 105303. doi:https://doi.org/10.1016/j.ocecoaman.2020.105303

Omae, I. (2003). Organotin antifouling paints and their alternatives. *Applied Organometallic Chemistry, 17*(2), 81-105. doi:https://doi.org/10.1002/aoc.396

Ono, K., Knutsen, H., Olsen, E. M., Ruus, A., Hjermann, D. Ø., & Chr. Stenseth, N. (2019). Possible adverse impact of contaminants on Atlantic cod population dynamics in coastal ecosystems. *Proceedings of the Royal Society B: Biological Sciences, 286*(1908), 20191167. doi:doi:10.1098/rspb.2019.1167

Oostindie, S. C., Lazar, G. A., Schuurman, J., & Parren, P. W. H. I. (2022). Avidity in antibody effector functions and biotherapeutic drug design. *Nature Reviews Drug Discovery, 21*(10), 715-735. doi:10.1038/s41573-022-00501-8

Parmar, M. B., Shams, R., & Wright, J. M. (2013). Genomic organization and transcription of the medaka and zebrafish cellular retinol-binding protein (rbp) genes. *Marine Genomics, 11*, 1-10. doi:https://doi.org/10.1016/j.margen.2013.04.001

Philip, S., Castro, L. F. C., da Fonseca, R. R., Reis-Henriques, M. A., Vasconcelos, V., Santos, M. M., & Antunes, A. (2012). Adaptive evolution of the Retinoid X receptor in vertebrates. *Genomics, 99*(2), 81-89. doi:https://doi.org/10.1016/j.ygeno.2011.12.001

Pillai-Kastoori, L., Heaton, S., Shiflett, S. D., Roberts, A. C., Solache, A., & Schutz-Geschwender, A. R. (2020). Antibody validation for Western blot: By the user, for the user. *J Biol Chem, 295*(4), 926-939. doi:10.1074/jbc.RA119.010472

Prebensen, A. (2023). Activation of Atlantic cod (Gadus morhua) retinoid X receptors by organic tin compounds. In: The University of Bergen.

Rantakokko, P., Main, K. M., Wohlfart-Veje, C., Kiviranta, H., Airaksinen, R., Vartiainen, T., . . . Virtanen, H. E. (2014). Association of placenta organotin concentrations with growth and ponderal index in 110 newborn boys from Finland during the first 18 months of life: a cohort study. *Environmental Health, 13*(1), 45. doi:10.1186/1476-069X-13-45

Rasheed, T., Bilal, M., Nabeel, F., Adeel, M., & Iqbal, H. M. N. (2019). Environmentally-related contaminants of high concern: Potential sources and analytical modalities for detection, quantification, and treatment. *Environment International, 122*, 52-66. doi:https://doi.org/10.1016/j.envint.2018.11.038

Rathi, B. S., Kumar, P. S., & Vo, D.-V. N. (2021). Critical review on hazardous pollutants in water environment: Occurrence, monitoring, fate, removal technologies and risk assessment. *Science of The Total Environment, 797*, 149134. doi:https://doi.org/10.1016/j.scitotenv.2021.149134

Ruiz, J. M., Bachelet, G., Caumette, P., & Donard, O. F. X. (1996). Three decades of tributyltin in the coastal environment with emphasis on Arcachon Bay, France. *Environmental Pollution, 93*(2), 195-203. doi:https://doi.org/10.1016/0269-7491(96)00029-2

Sarvas, T. H., & Fevolden, S. E. (2005). Pantophysin (Pan I) locus divergence between inshore v. offshore and northern v. southern populations of Atlantic cod in the north-east Atlantic. *Journal of Fish Biology, 67*(2), 444-469. doi:https://doi.org/10.1111/j.0022-1112.2005.00738.x

Schmittgen, T. D., & Livak, K. J. (2008). Analyzing real-time PCR data by the comparative CT method. *Nature Protocols, 3*(6), 1101-1108. doi:10.1038/nprot.2008.73

Schøyen, M., Green, N. W., Hjermann, D. Ø., Tveiten, L., Beylich, B., Øxnevad, S., & Beyer, J. (2019). Levels and trends of tributyltin (TBT) and imposex in dogwhelk (Nucella lapillus) along the Norwegian coastline from 1991 to 2017. *Marine Environmental Research, 144*, 1-8. doi:https://doi.org/10.1016/j.marenvres.2018.11.011

Scott, G. R., & Sloman, K. A. (2004). The effects of environmental pollutants on complex fish behaviour: integrating behavioural and physiological indicators of toxicity. *Aquatic Toxicology, 68*(4), 369-392. doi:https://doi.org/10.1016/j.aquatox.2004.03.016

Sever, R., & Glass, C. K. (2013). Signaling by Nuclear Receptors. *Cold Spring Harbor Perspectives in Biology, 5*(3). doi:10.1101/cshperspect.a016709

Sharma, S., Shen, T., Chitranshi, N., Gupta, V., Basavarajappa, D., Sarkar, S., . . . Gupta, V. (2022). Retinoid X Receptor: Cellular and Biochemical Roles of Nuclear Receptor with a Focus on Neuropathological Involvement. *Mol Neurobiol, 59*(4), 2027-2050. doi:10.1007/s12035-021-02709-y

Shoucri, B. M., Martinez, E. S., Abreo, T. J., Hung, V. T., Moosova, Z., Shioda, T., & Blumberg, B. (2017). Retinoid X Receptor Activation Alters the Chromatin Landscape To Commit Mesenchymal Stem Cells to the Adipose Lineage. *Endocrinology, 158*(10), 3109-3125. doi:10.1210/en.2017-00348

Shulman, A. I., & Mangelsdorf, D. J. (2005). Retinoid X Receptor Heterodimers in the Metabolic Syndrome. *New England Journal of Medicine, 353*(6), 604-615. doi:10.1056/NEJMra043590

Smith, B. S. (1971). Sexuality in the American Mud Snail , Nassarius Obsoletus Say. *Journal of Molluscan Studies, 39*(5), 377-378. doi:10.1093/oxfordjournals.mollus.a065117

Sousa, A. C. A., Pastorinho, M. R., Takahashi, S., & Tanabe, S. (2014). History on organotin compounds, from snails to humans. *Environmental Chemistry Letters, 12*(1), 117-137. doi:10.1007/s10311-013-0449-8

Star, B., Nederbragt, A. J., Jentoft, S., Grimholt, U., Malmstrøm, M., Gregers, T. F., . . . Jakobsen, K. S. (2011). The genome sequence of Atlantic cod reveals a unique immune system. *Nature, 477*(7363), 207-210. doi:10.1038/nature10342

Stossi, F., Dandekar, R. D., Johnson, H., Lavere, P., Foulds, C. E., Mancini, M. G., & Mancini, M. A. (2019). Tributyltin chloride (TBT) induces RXRA down-regulation and lipid accumulation in human liver cells. *PLOS ONE, 14*(11), e0224405. doi:10.1371/journal.pone.0224405

Strøm, J. F., Bøhn, T., Skjæraasen, J. E., Gjelland, K. Ø., Karlsen, Ø., Johansen, T., . . . Olsen, E. M. (2023). Movement diversity and partial sympatry of coastal and Northeast Arctic cod ecotypes at high latitudes. *Journal of Animal Ecology, n/a*(n/a). doi:https://doi.org/10.1111/1365-2656.13989

Sugawara, A., Yen, P. M., Qi, Y., Lechan, R. M., & Chin, W. W. (1995). Isoform-specific retinoid-X receptor (RXR) antibodies detect differential expression of RXR proteins in the pituitary gland. *Endocrinology, 136*(4), 1766-1774. doi:10.1210/endo.136.4.7895689

Suzuki, T., Hidaka, T., Kumagai, Y., & Yamamoto, M. (2020). Environmental pollutants and the immune response. *Nature Immunology, 21*(12), 1486-1495. doi:10.1038/s41590-020-0802-6

Szanto, A., Narkar, V., Shen, Q., Uray, I. P., Davies, P. J. A., & Nagy, L. (2004). Retinoid X receptors: X-ploring their (patho)physiological functions. *Cell Death & Differentiation, 11*(2), S126-S143. doi:10.1038/sj.cdd.4401533

Takai, Y., Takamura, T., Enoki, S., Sato, M., Kato-Unoki, Y., Qiu, X., . . . Oshima, Y. (2020). Transcriptome analysis of medaka (Oryzias latipes) exposed to tributyltin. *Japanese Journal of Environmental Toxicology, 23*(1), 10-21. doi:10.11403/jset.23.10

Tallafuss, A., Hale, L. A., Yan, Y.-L., Dudley, L., Eisen, J. S., & Postlethwait, J. H. (2006). Characterization of retinoid-X receptor genes rxra, rxrba, rxrbb and rxrg during zebrafish development. *Gene Expression Patterns, 6*(5), 556-565. doi:https://doi.org/10.1016/j.modgep.2005.10.005

Tate, J., & Ward, G. (2004). Interferences in immunoassay. *Clin Biochem Rev, 25*(2), 105-120.

Tokarz, J., Möller, G., Hrabě de Angelis, M., & Adamski, J. (2013). Zebrafish and steroids: What do we know and what do we need to know? *The Journal of Steroid Biochemistry and Molecular Biology, 137*, 165-173. doi:https://doi.org/10.1016/j.jsbmb.2013.01.003

Toporova, L., & Balaguer, P. (2020). Nuclear receptors are the major targets of endocrine disrupting chemicals. *Molecular and Cellular Endocrinology, 502*, 110665. doi:https://doi.org/10.1016/j.mce.2019.110665

Trefts, E., Gannon, M., & Wasserman, D. H. (2017). The liver. *Curr Biol, 27*(21), R1147-r1151. doi:10.1016/j.cub.2017.09.019

Trivedi, R., Tripathi, J. K., Knopf, B., Manocha, G. D., & Jurivich, D. A. (2021). A simplified and sensitive immunoprecipitation approach for the analysis of HSF1 in murine liver tissue. *MethodsX, 8*, 101478. doi:https://doi.org/10.1016/j.mex.2021.101478

Waldock, M. J., & Thain, J. E. (1983). Shell thickening in Crassostrea gigas: Organotin antifouling or sediment induced? *Marine Pollution Bulletin, 14*(11), 411-415. doi:https://doi.org/10.1016/0025-326X(83)90445-9

Watanabe, M., & Kakuta, H. (2018). Retinoid X Receptor Antagonists. *Int J Mol Sci, 19*(8). doi:10.3390/ijms19082354

Weikum, E. R., Liu, X., & Ortlund, E. A. (2018). The nuclear receptor superfamily: A structural perspective. *Protein Science, 27*(11), 1876-1892. doi:https://doi.org/10.1002/pro.3496

Weller, M. G. (2018). Ten Basic Rules of Antibody Validation. *Anal Chem Insights, 13*, 1177390118757462. doi:10.1177/1177390118757462

Windsor, F. M., Pereira, M. G., Morrissey, C. A., Tyler, C. R., & Ormerod, S. J. (2020). Environment and food web structure interact to alter the trophic magnification of persistent chemicals across river ecosystems. *Science of The Total Environment, 717*, 137271. doi:https://doi.org/10.1016/j.scitotenv.2020.137271

Xu, Y.-C., Pantopoulos, K., Zheng, H., Zito, E., Zhao, T., Tan, X.-Y., . . . Luo, Z. (2023). Phosphorus Overload Promotes Hepatic Lipolysis by Suppressing GSK3β-Dependent Phosphorylation of PPARα at Ser84 and Thr265 in a Freshwater Teleost. *Environmental Science & Technology, 57*(6), 2351-2361. doi:10.1021/acs.est.2c06330

Yang, C., Song, H., Wang, Y., Peng, F., & Wei, Q. (2007). A new approach for producing polyclonal antibodies using impure antigens. *Journal of Biochemical and Biophysical Methods, 70*(4), 613-618. doi:https://doi.org/10.1016/j.jbbm.2007.02.001

Zahavi, D., & Weiner, L. (2020). Monoclonal Antibodies in Cancer Therapy. *Antibodies, 9*(3), 34. Retrieved from https://www.mdpi.com/2073-4468/9/3/34

Zhang, J., Zhang, C., Sun, P., Huang, M., Fan, M., & Liu, M. (2017). RNA-sequencing and pathway analysis reveal alteration of hepatic steroid biosynthesis and retinol metabolism by tributyltin exposure in male rare minnow (Gobiocypris rarus). *Aquatic Toxicology, 188*, 109-118. doi:https://doi.org/10.1016/j.aquatox.2017.03.015

Zhao, Y., Zhang, K., Giesy, J. P., & Hu, J. (2015). Families of nuclear receptors in vertebrate models: characteristic and comparative toxicological perspective. *Sci Rep, 5*, 8554. doi:10.1038/srep08554

8. APPENDIX

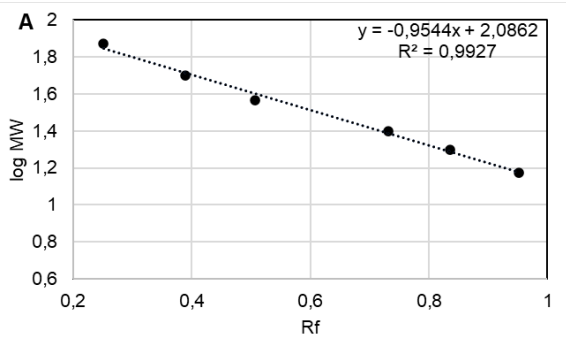
A
y = -0,9544x + 2,0862
R² = 0,9927
log MW
Rf

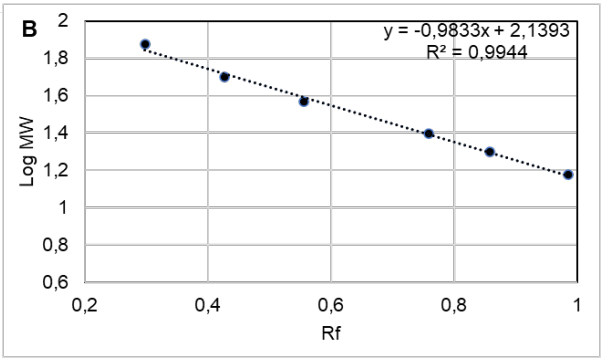
B
y = -0,9833x + 2,1393
R² = 0,9944
Log MW
Rf

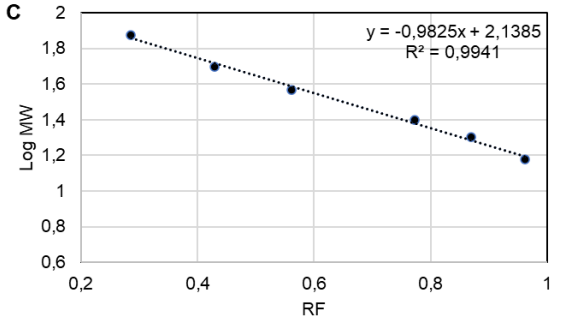
C
y = -0,9825x + 2,1385
R² = 0,9941
Log MW
RF

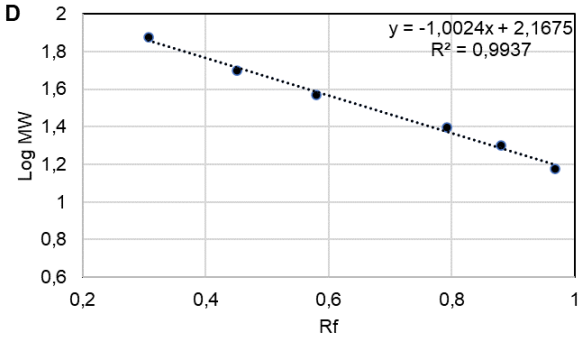
D
y = -1,0024x + 2,1675
R² = 0,9937
Log MW
Rf

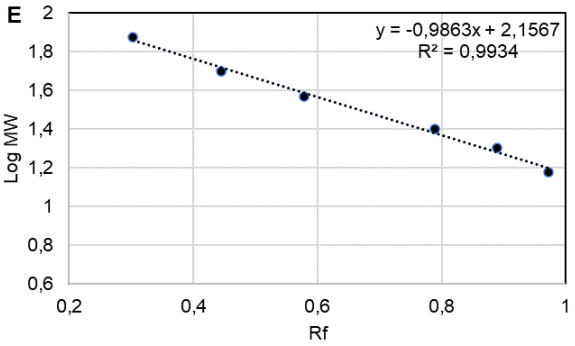
E
y = -0,9863x + 2,1567
R² = 0,9934
Log MW
Rf

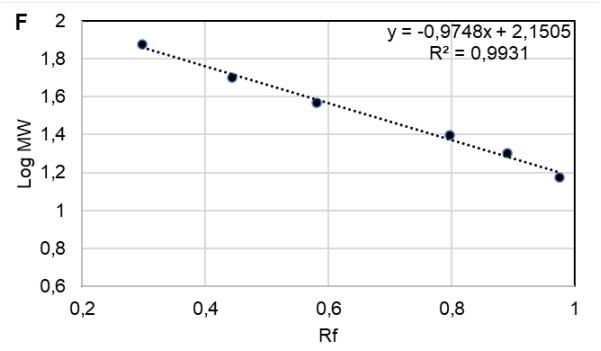
F
y = -0,9748x + 2,1505
R² = 0,9931
Log MW
Rf

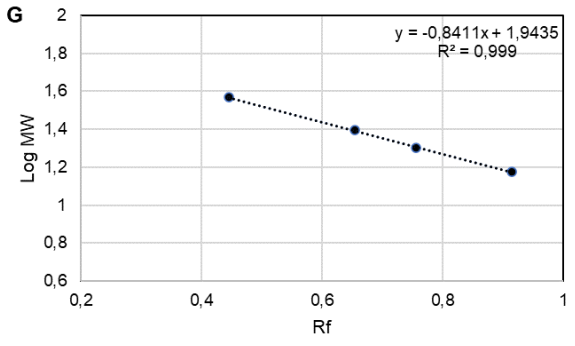
G
y = -0,8411x + 1,9435
R² = 0,999
Log MW
Rf

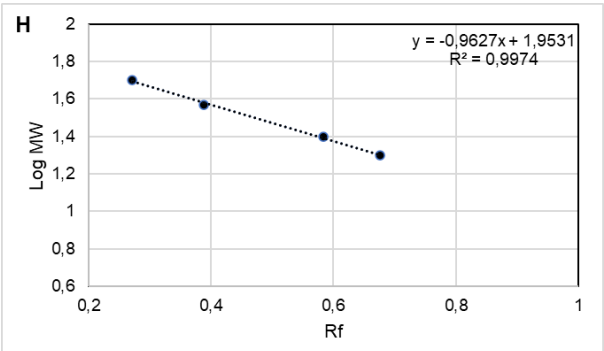
H
y = -0,9627x + 1,9531
R² = 0,9974
Log MW
Rf

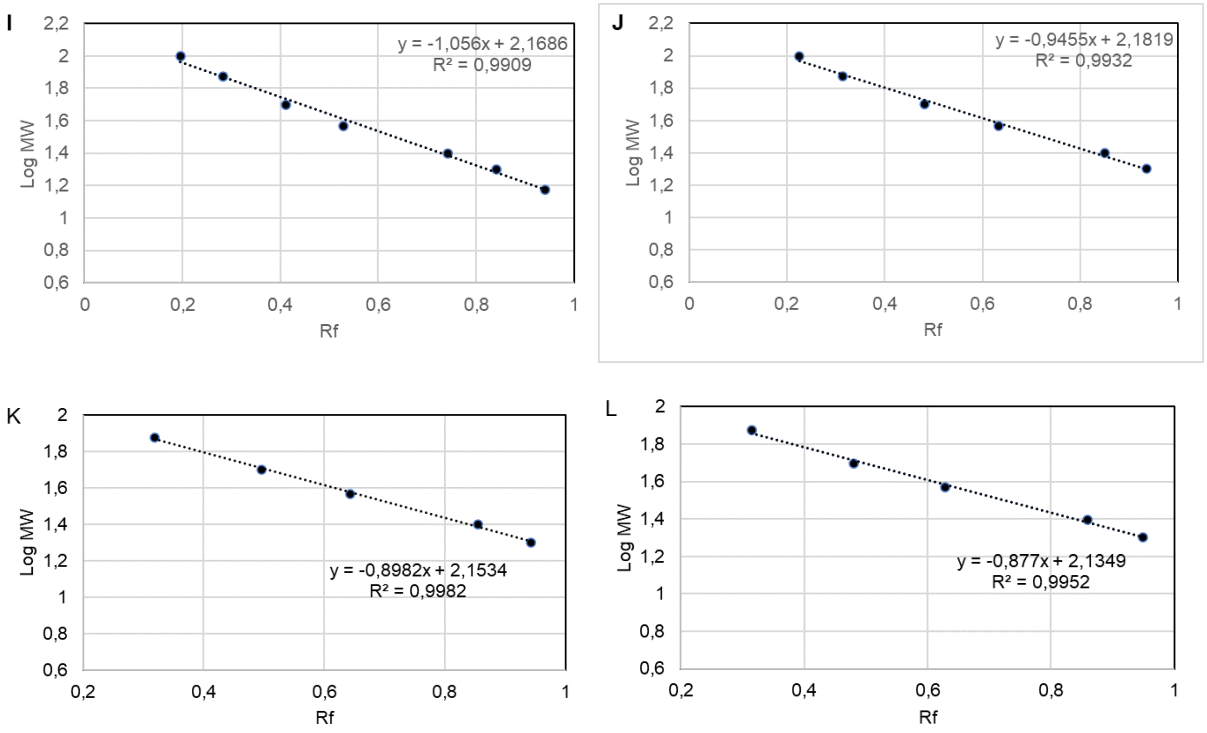

Figure A1 Standard curve for MW determination. Extreme points were removed from the plot, to generate linear curves with R^2 values as close to 1.00 as possible, for accurate prediction of MW of proteins in gels and membranes. Rf values indicate the migration distance of the proteins divided by the migration of the gel fronts. The standard curves were prepared for the following gels and western blot membranes with Atlantic cod (*Gadus morhua*) tissues: Membrane with different tissues incubated with pAb # 5789 **(A)** and p8Ab # 5859 **(B)**, Membrane with liver tissues incubated with pAb #5789 **(C)**, pre-immune serum of pAb #5789 **(D)**, pAb #5859 **(E)**, pre-immune serum of pAb #5859 **(F)**. Membrane from two-dimensional polyacrylamide gel electrophoresis (2D-PAGE) **(G)**. Imperial™ Protein-stained membrane from 2D-PAGE **(H)**. Membranes from the immunoprecipitation (IP) procedure incubated with pAb #5789 **(I)** and pAb #5859 **(J).** Membrane with the unbound fractions from the IP procedure incubated with pAb #5789 **(K)** and pAb # 5859 **(L)**.

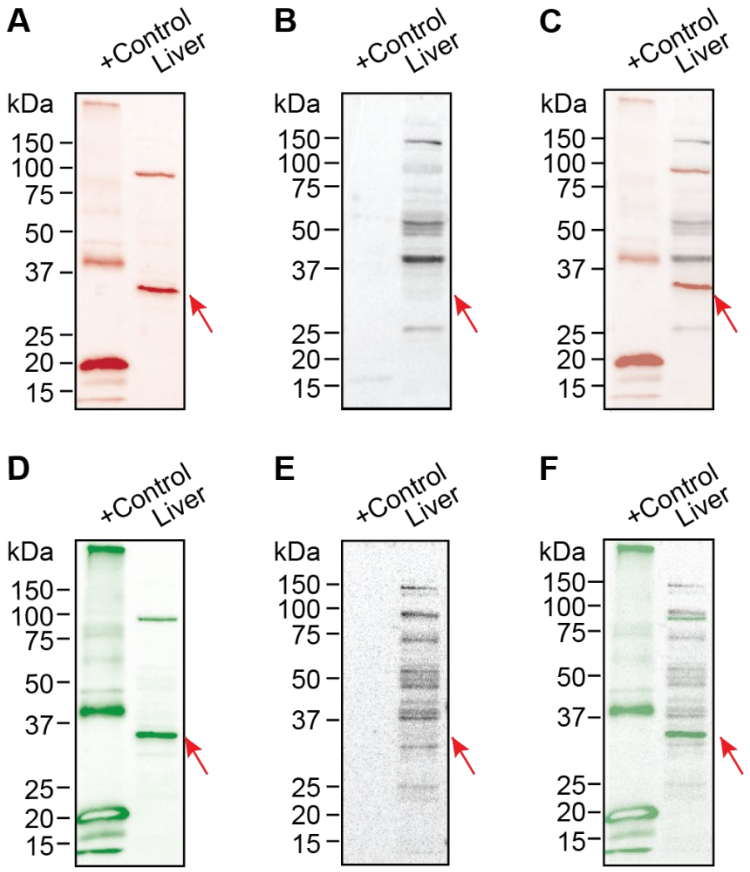

Figure A2. Comparison of immunoreactive proteins in liver by incubation with antibodies and pre-immune serum in western blot analyses. 15 µg liver tissue homogenates were separated in 12 % SDS-PA gels, as well as 0.335 µg of immunogen control (provided by GenScript), against. The nitrocellulose membranes were cut in half, to a total of 4 membranes. The membranes were incubated O/N with 1 µg/µL of **A**) pAb #5789, **B**) Pre-immune serum of pAb #5789, **C**) **A** and **B** computationally merged. **D**) 1 µg/µL pAb #5859, **E**) Pre-immune serum of pAb #5859, and **F**) **D** and **E** computationally merged. Immunoreactive bands were visualized with Super Signal™ West Pico Plus Chemiluminescent Substrate kit. Images were taken with Bio-Rad's ChemiDoc™ XRS+ imaging system. Precision Plus Protein™ All blue standards molecular weight markers are indicated on the left of each subfigure. Arrows are included to indicate the presence or absence of the band of interest at 35 kDa.

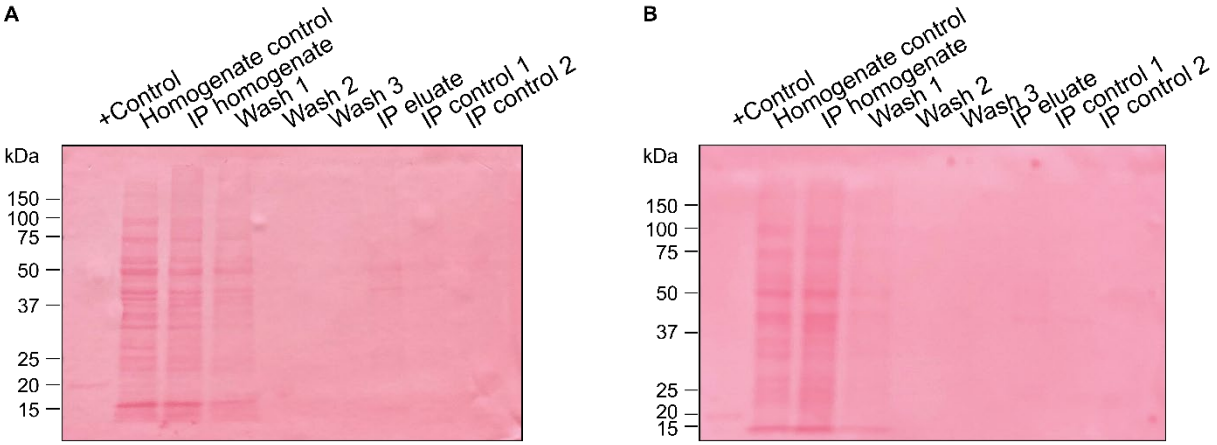

Figure A3. Immunoprecipitated (IP) liver homogenates shown in Ponceau S-stained western blot (WB) prior to antibody incubations. 1 mL liver homogenates were immunoprecipitated with Protein G agarose beads (Roche, Ca. no. 11 243 233 001). Immunoprecipitation was performed with both **A)** pAb #5789 and **B)** pAb #5859. Two IP controls were included, one consisting of beads and homogenate, but no antibody added ("IP control 1"), and one consisting of beads and antibody, but no homogenate ("IP control 2"). Western blot analysis was performed with the IP eluates and the IP controls, 0.335 µg immunogen control, 15 µg liver homogenates tested previously ("Homogenate control"), as well as against the homogenate used in IP ("IP homogenate") and wash fractions ("Wash 1/2/3Molecular weight markers are indicated on the left of A) and B).

Table A1. Raw data from the Nanodrop measurement. Fish has been abbreviated to F. with the number of the fish next to it.

	Sample Name	Nucleic Acid(ng/uL)	A260/ A280	A260/ A230	Corrected (ng/uL)	Impurity 1	Impurity 1 A260
F 1	DMSO (0.2 %)	223,207	1,9	1,5			
	TBT (0.1 µM)	248,089	1,9	0,3			
	TBT (1 µM)	259,766	1,9	1,4			
	TBT (10 µM)	118,229	1,8	1,3			
	9-cis-RA (0.1 µM)	178,332	1,9	1,4	165,04	Guanadin e ITC	
	9-cis-RA (1 µM)	199,743	1,8	0,5	171,52	Guanadin e ITC	
	9-cis-RA (10 µM)	168,404	1,8	1,5			
F 2	DMSO (0.2 %)	251,654	1,8	1,8			
	TBT (0.1 µM)	221,16	1,9	0,7	207,28	Guanadin e ITC	
	TBT (1 µM)	209,452	1,9	0,7	185,76	Phenol	0,532
	TBT (10 µM)	210,621	1,9	0,9	198,96	Guanadin e ITC	
	9-cis-RA (0.1 µM)	235,534	1,9	0,4	195,84	Guanadin e ITC	

	9-cis-RA (1 µM)	229,794	1,9	0,6	204,24	Guanadine ITC
	9-cis-RA (10 µM),	198,992	1,9	0,9	192,56	Guanadine ITC
F3	DMSO (0.2 %)	244,276	1,9	1,3	234,12	Guanadine ITC
	TBT (0.1 µM)	252,224	1,9	1,1	238,64	Guanadine ITC
	TBT (1 µM)	175,458	1,9	0,6	155,32	Guanadine ITC
	TBT (10 µM)	205,986	1,9	0,4	188,68	Guanadine ITC
	9-cis-RA (0.1 µM)	292,245	2,0	1,0	283,16	Guanadine ITC
	9-cis-RA (1 µM)	238,94	1,9	0,9	229,76	Guanadine ITC
	9-cis-RA (10 µM)	229,519	1,9	0,7	210,88	Guanadine ITC
F4	DMSO (0.2 %)	398,6	2,0	1,4	395,72	Guanadine ITC
	TBT (0.1 µM)	367,645	2,0	1,4	366,8	Guanadine ITC
	TBT (1 µM)	251,004	1,9	2,0		
	TBT (10 µM)	328,611	2,0	1,3	325,32	Guanadine ITC
	9-cis-RA (0.1 µM)	232,469	1,9	1,8		
	9-cis-RA (1 µM)	244,22	1,9	2,1		
	9-cis-RA (10 µM)	263,718	1,9	1,7		
F5	DMSO (0.2 %)	372,866	1,9	1,5		
	TBT (0.1 µM)	195,962	1,9	0,7	191,88	Guanadine ITC
	TBT (1 µM)	287,554	1,9	0,6	271	Guanadine ITC
	TBT (10 µM)	168,818	1,9	0,5	153,8	Guanadine ITC
	9-cis-RA (0.1 µM)	261,211	1,9	1,6		
	9-cis-RA (1 µM)	342,469	2,0	1,3		
	9-cis-RA (10 µM)	312,987	1,9	1,7		